Dissertation zur Erlangung des Doktorgrades

der Fakultät für Chemie und Pharmazie

der Ludwig-Maximilians-Universität München

Structures and DNA-Binding Activities of the Hinge Domains from the Structural Maintenance of Chromosomes Proteins of *Pyrococcus furiosus* and the Mouse Condensin Complex

Julia Johanna Griese

aus

Erbach im Odenwald

2010

This thesis has been prepared from March 2007 to August 2010 in the laboratory of Professor Dr. Karl-Peter Hopfner at the Gene Center of the Ludwig-Maximilians-University of Munich (LMU).

Parts of this thesis have been published:

Griese, J.J., Witte, G. and Hopfner, K.P. (2010) Structure and DNA binding activity of the mouse condensin hinge domain highlight common and diverse features of SMC proteins. *Nucleic Acids Res.*, **38**, 3454-3465.

Griese, J.J. and Hopfner, K.P. (2010) Structure and DNA-binding activity of the *Pyrococcus furiosus* SMC Protein Hinge Domain. *Proteins: Struct. Funct. Bioinform., in press*.

Parts of this thesis have been presented at international conferences and workshops:

Poster presentation and talk at the 2nd EU-IP DNA Repair Workshop for Young Scientists, June 23-27, 2008 in Porto, Portugal.

Poster presentation and talk at the 3rd EU-IP DNA Repair Workshop for Young Scientists, February 19-21, 2009 in Taormina, Sicily, Italy.

Poster presentation at the Gordon Research Conference on Diffraction Methods in Structural Biology, July 18-23, 2010 in Lewiston, Maine, USA.

TABLE OF CONTENTS

TABLE OF FIGURES

1 SUMMARY

Structural Maintenance of Chromosomes (SMC) proteins are vital for a wide range of cellular processes including chromosome structure and dynamics, gene regulation, and DNA repair. Whereas prokaryotic genomes encode for only one SMC protein that exists as a homodimer, eukaryotes possess six different SMC proteins that form three distinct heterodimeric complexes, with the holocomplexes additionally containing several specific regulatory subunits. The prokaryotic SMC complex is required for chromosome condensation and segregation. In eukaryotes, this function is carried out by the condensin complex with SMC2 and SMC4 at its core. The complex containing SMC1 and SMC3, named cohesin, is responsible for sister chromatid cohesion during mitosis and meiosis. Cohesin is also employed in DNA double-strand break repair, whereas condensin participates in single-strand break repair. The as yet unnamed SMC5-SMC6 complex is involved in several DNA repair pathways as well as homologous recombination in meiosis.

SMC proteins consist of N and C-terminal domains that fold back onto each other to create an ATPase "head" domain, connected to a central "hinge" domain via long antiparallel coiled-coils. The hinge domain mediates dimerisation of SMC proteins and binds DNA, but it is not clear to what purpose this activity serves.

The aim of this work was therefore to characterise the structure and function of the SMC hinge domain in more detail. Specifically, the hinge domains of the *Pyrococcus furiosus* SMC protein and of mouse condensin were studied. Both their high-resolution crystal structures as well as low-resolution solution envelopes were determined, and their DNA-binding activity was analysed qualitatively and quantitatively.

While the SMC hinge domain fold is largely conserved from prokaryotes to eukaryotes, functionally relevant structural differences can be observed. Most importantly, the surface charge has been almost reversed throughout evolution. The data obtained confirm that of all three eukaryotic SMC complexes, condensin is most closely related to prokaryotic SMC proteins. Both the *P. furiosus* and the mouse condensin hinge domain preferentially bind single-stranded DNA, but the mouse condensin hinge displays a much higher affinity than its prokaryotic counterpart, suggesting that this function has been enhanced during the course of evolution. The single-stranded DNA-binding activity might be important for the function of the condensin complex in single-strand break repair, but probably plays a different role in prokaryotes, possibly in the DNA-loading process of the prokaryotic SMC complex during replication.

2 INTRODUCTION

2.1 The Discovery of Chromosomes

In 1880, Walther Flemming coined the term "chromatin", meaning "stainable material", to describe the substance in the nucleus that is strongly stained by aniline dyes (1):

> Mit Chromatin soll demnach nur bezeichnet sein: diejenige Substanz im Zellkern, welche bei den als Kerntinctionen bekannten Behandlungen mit Farbstoffen die Farbe aufnimmt.

Flemming also named nuclear division "mitosis" (from Greek *mitos*, thread) because of the threadlike metamorphosis of the nucleus during this process (2). Only afterwards, in 1888, did Heinrich Wilhelm Waldeyer then call the bodies that are formed from chromatin during mitosis and that Flemming had referred to as *Kernfäden* (nuclear threads) "chromosomes", "stainable bodies" (from Greek *chroma*, colour, and *soma*, body) (3).

With the limited means of his time, Flemming rendered a very accurate description of nuclear division. He realised that chromatin transforms into a number of separate threads (chromosomes) for cell division, and also found that these threads are split longitudinally so that each daughter cell obtains one half. He could only make these observations because of the condensed state that chromosomes assume during mitosis (Figure 2.1), as during interphase chromosomes are not discernible as separate entities.
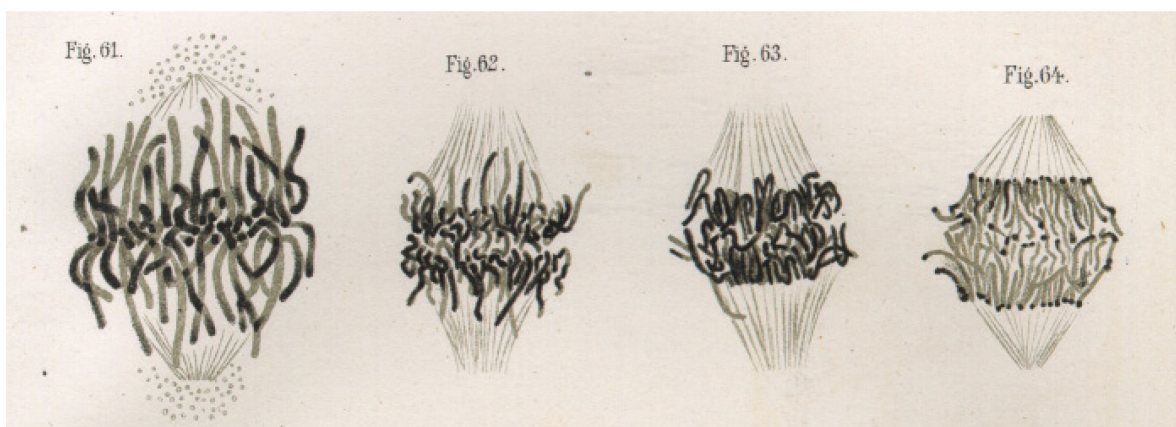
Figure 2.1. Drawings of chromosomes in anaphase of mitosis by Walther Flemming (2).

2.2   Structural Maintenance of Chromosomes Proteins

Before a cell divides, each chromosome is duplicated, and the resulting identical sister chromatids are distributed to the daughter cells in mitosis. During interphase the chromosomes are loosely packed to enable transcription and replication. They would become hopelessly entangled if they were to be partitioned in this form. Therefore, after replication, chromosomes have to be condensed into a "transportable" form before cell division is possible. To ensure that the two daughter cells both contain the full set of chromosomes, sister chromatids have to be kept together until they are properly aligned at the cell equator and attached to microtubules with opposing polarity, so that they can then be pulled apart towards opposite cell poles.

Throughout all domains of life, Structural Maintenance of Chromosomes (SMC) complexes are responsible for the faithful inheritance of genetic information. They are involved in a wide range of vital cellular processes including cell division, gene regulation and DNA repair, acting as global organisers and safeguards of the genome. Most prominently, SMC complexes are responsible for chromosome condensation and sister chromatid cohesion during cell division – processes whose importance was recognised very early on, but that nonetheless are only just beginning to be understood.

At the heart of the SMC complexes are SMC proteins. They are essential, highly conserved and very old proteins that arose even before histones (4) and have evolved to fulfil diverse functions in genome maintenance. Whereas prokaryotic genomes encode for only one SMC protein that exists as a homodimer, eukaryotes possess six different SMC proteins that form three distinct heterodimeric complexes. The prokaryotic SMC complex is required for chromosome condensation and segregation (5). In eukaryotes, this function is carried out by the condensin complex with SMC2 and SMC4 at its core, the closest relative of the prokaryotic SMC complex (6) (chapter 2.2.3). The complex containing SMC1 and SMC3, named cohesin, is responsible for sister chromatid cohesion during mitosis and meiosis (7) (chapter 2.2.2). The as yet unnamed SMC5-SMC6 complex is involved in several DNA repair pathways, telomere maintenance, and homologous recombination in meiosis, but its precise function is still poorly understood (8) (chapter 2.2.4). Both cohesin and condensin are also involved in gene regulation (9-14) and DNA repair (chapters 2.2.2.3 and 2.2.3.3).

2.2.1 Molecular Architecture of SMC Proteins and SMC Complexes

SMC proteins are large polypeptides, containing 1000 – 1300 residues. They have a striking domain architecture consisting of a ~50 nm long antiparallel coiled-coil region with globular domains at both ends (4,15) (Figure 2.2A). Their N and C terminus interact at one end of the coiled-coil to make up an ATP-binding cassette (ABC)-type ATPase "head" domain (chapter 2.2.1.1). The "hinge" domain at the other end of the coiled-coil mediates dimerisation of SMC proteins to form a V- or ring-shaped dimer (15-17) (chapter 2.2.1.2). This hinge domain is the feature that distinguishes SMC proteins from the closely related Rad50 family involved in DNA double-strand break (DSB) repair (18). Rad50 contains the same bipartite ABC-type ATPase domain with a long coiled-coil insertion, but instead of the globular hinge domain it uses a Cys-X-X-Cys motif for dimerisation (19). Two such "Zinc hook" motifs are dimerised by coordinating a Zinc ion between them (Figure 2.2B).

Interestingly, while prokaryotic SMC complexes display a wide variety of "arm" (coiled-coil) conformations in electron micrographs (16,20), the arms of condensin are always associated with each other, whereas cohesin arms are always spread apart (15,21). It is currently not known whether these different conformations have functional consequences.

In addition to the SMC protein dimer, SMC holocomplexes contain several specific regulatory non-SMC subunits that typically associate with the SMC ATPase domains (4). The conserved "kleisin" winged-helix domain (WHD) subunit bridges the two head domains in an SMC dimer, thus closing the SMC ring (hence the name kleisin, derived from the Greek word for closure) (15,22). The kleisin also links other non-SMC subunits to the complex (4,23) (Figure 2.2B). Most non-SMC subunits apart from the kleisin contain HEAT repeat domains that facilitate protein-protein interactions.

The prokaryotic SMC homodimer associates with the kleisin ScpA which forms a subcomplex with ScpB, a WHD protein that has no homologue in eukaryotes (24-30). The holocomplex presumably contains two copies of each subunit (31), or possibly even four copies of ScpB (30). The *Escherichia coli* MukB protein is a strongly divergent SMC protein, closer homologues of which exist only in other γ-proteobacteria (32). Its two non-SMC subunits are termed MukE and MukF, the latter being the kleisin (33,34). A $MukE_4MukF_2$ complex binds to the head domains of a MukB dimer (35-37).
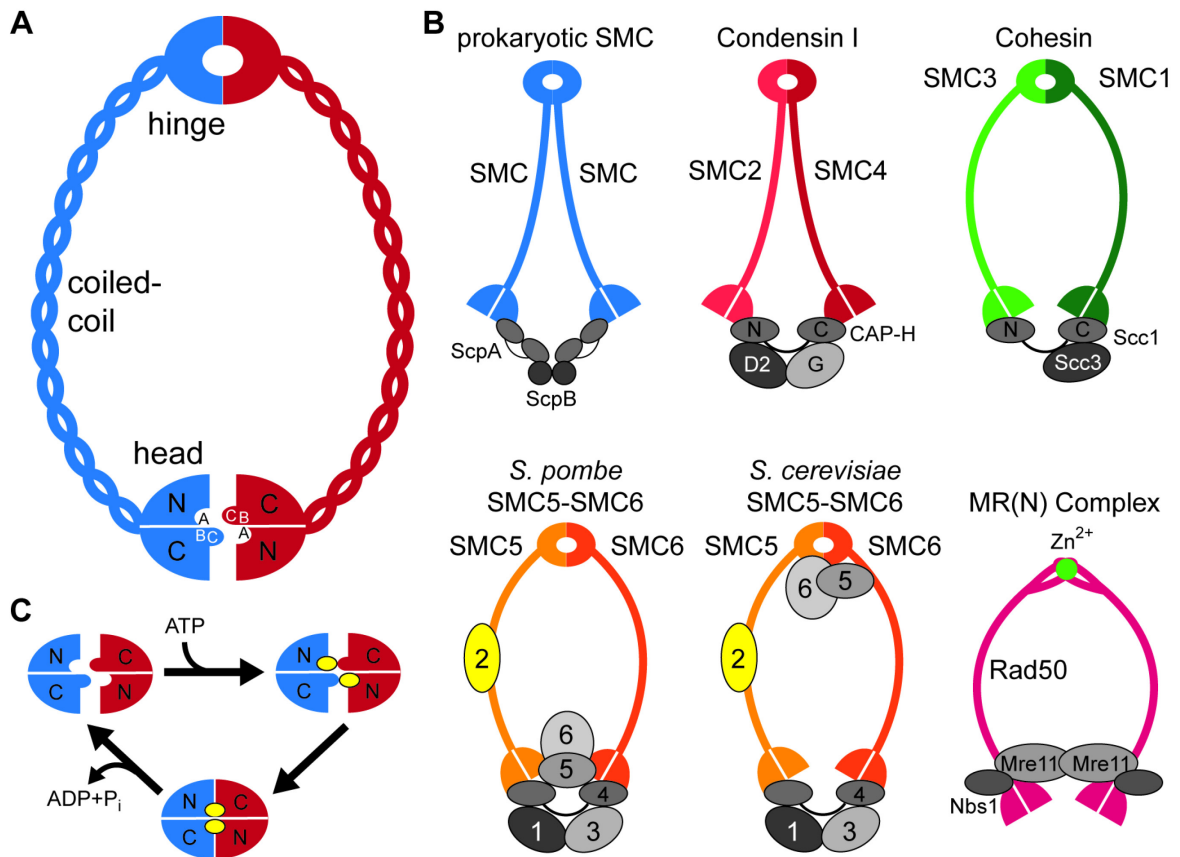
Figure 2.2. Molecular architecture of SMC proteins and SMC complexes. (**A**) Basic architecture of an SMC protein dimer. Each subunit consists of two globular domains connected to each other by a long antiparallel coiled-coil region. An ABC-type ATPase "head" domain is formed by the N and C terminus, with the Walker A motif located in the N-terminal half, and the Walker B and signature or C motifs in the C-terminal half. The central "hinge" domain mediates dimerisation of SMC proteins. (**B**) Prokaryotic and eukaryotic SMC complexes. The prokaryotic SMC complex is made up of an SMC homodimer and two copies each of two non-SMC subunits: the kleisin ScpA bridges the head domains and binds ScpB. Eukaryotes have three distinct SMC complexes, all containing only one copy of each subunit. The condensin complex consists of an SMC2-SMC4 heterodimer, a kleisin (CAP-H), and two HEAT repeat subunits (CAP-D2 and CAP-G). Cohesin contains an SMC1-SMC3 heterodimer and two non-SMC subunits, the kleisin Scc1, and the HEAT repeat subunit Scc3. The SMC5-SMC6 complex has up to six non-SMC subunits, Nse1-6. The kleisin Nse4 forms a subcomplex with Nse1 and Nse3. Nse2 associates with the coiled-coil region of SMC5. In fission yeast, Nse5-Nse6 are associated with the head domains, whereas in budding yeast they bind to the hinge domains. The MR(N) complex contains the Rad50 protein which is closely related to SMC proteins, but uses a Cys-X-X-Cys "Zinc hook" motif instead of the globular hinge domain to dimerise by coordinating a Zinc ion. The Mre11 subunit connects two Rad50 proteins at the ATPase domains. Nbs1 is only present in eukaryotes. (**C**) ATPase cycle of the SMC head domains. ATP binding leads to engagement of two head domains to form two shared ATPase active sites. Upon ATP hydrolysis, the head domains disengage again. ATP is symbolised by the yellow spheres. Figure adapted from references (4,18,38,39).

Unlike their prokaryotic ancestors, eukaryotic SMC complexes contain only one copy of each subunit (15,40,41). The single kleisin subunit binds one SMC head domain with its N-terminal helix-turn-helix domain and the other with its C-terminal WHD. Eukaryotic kleisins are grouped into four major classes, α, β, γ, and δ (38,42), β-kleisins only being found in higher eukaryotes.

α-Kleisins like budding yeast Scc1 associate with SMC1-SMC3 heterodimers and a HEAT repeat subunit such as Scc3 to form cohesin (43-49). In the complex, the N-terminal domain of Scc1 contacts the SMC3 head domain, and its C-terminal domain binds to the SMC1 head and Scc3 (15). A second HEAT repeat subunit termed Pds5 is less stably associated with cohesin and therefore not seen as integral part of the complex, but probably binds to Scc1 as well (50-52). In higher eukaryotes, there are two isoforms of SMC1, SMC1α and SMC1β (53). While the cohesin variant containing SMC1α is responsible for mitotic sister chromatid cohesion (46), the variant with SMC1β is involved in meiotic chromosome cohesion, dynamics, and recombination (53,54). However, even in lower eukaryotes that have only one SMC1 isoform, meiotic cohesin contains a special α-kleisin termed Rec8 and sometimes also a meiosis-specific HEAT repeat subunit (55-60).

Higher eukaryotes have two condensin complexes, condensin I and II, which share the same core subunits SMC2 and SMC4, but possess different sets of non-SMC subunits (40,41,61-63). Condensin I contains a γ-kleisin (CAP-H), whereas a β-kleisin (CAP-H2) is found in condensin II. Two HEAT repeat subunits associate with the kleisin, CAP-D2/D3 and CAP-G/G2 (41,64). The N-terminal domain of the kleisin links CAP-D2/D3 to SMC2, while its C-terminal domain connects CAP-G/G2 with SMC4 (41).

Lastly, the most divergent and most enigmatic eukaryotic SMC complex consists of an SMC5-SMC6 heterodimer and up to six non-SMC subunits termed non-SMC elements (Nse) (65-75). The δ-kleisin Nse4 forms a subcomplex with Nse1 and Nse3 (38,39,72,74). Nse3 contains a MAGE homology domain whose function is unknown (71). Nse1 has a RING-finger-like domain suggesting it may be an E3 ubiquitin ligase, but no activity has been observed so far (69,76). Instead, the RING domain seems to provide the link between Nse3 and Nse4 (76). Nse2 is a SUMO ligase (73,77,78) that associates with the coiled-coil region of SMC5 (39,72,74). The ARM/HEAT repeat proteins Nse5 and Nse6 have only been identified in yeast (70,73,74). In fission yeast, Nse5-Nse6 were found to be associated with the head and coiled-coil domains (38), whereas in budding yeast they have been

reported to bind to the hinge domains (39). However, fission and budding yeast Nse5-Nse6 are not homologous, and only the budding yeast orthologues are essential for cell viability.

2.2.1.1 The SMC Head Domain

The SMC ABC-type ATPase "head" domain has an unusual bipartite structure, being formed from the N and C-terminal domains which are separated by an ~900 residue coiled-coil insertion. While the N-terminal half of the ATPase domain contains the Walker A motif (also known as P loop), the Walker B motif and the signature or C motif are found in the C-terminal part (Figure 2.2A). The Walker A motif binds the α- and β-phosphate of ATP, while the γ-phosphate is bound by the signature motif. The Walker B motif contains the catalytic base for ATP hydrolysis, a glutamate that activates a water molecule for nucleophilic attack on the ATP γ-phosphate (4,79).

Structural and biochemical analyses of both prokaryotic and eukaryotic SMC head domains have shed more light on their mechanism. The crystal structure of the SMC head domain from the thermophilic archaeon *Pyrococcus furiosus* has been determined both in the nucleotide-free and the ATP-bound state (using a Walker B motif glutamate-to-glutamine mutation that prevents ATP hydrolysis, but not binding) (79), while the SMC head domain from the thermophilic bacterium *Thermotoga maritima* has been crystallised in the nucleotide-free state only (80). The structure of the *Haemophilus ducreyi* ATPγS-bound MukB head domain complexed with MukE and the middle and C-terminal domain of MukF has also been determined (81). Eukaryotic SMC proteins are represented by the head domain of SMC1 from *Saccharomyces cerevisiae* in complex with ATPγS and the C-terminal WHD of the Scc1 kleisin subunit (22).

Despite substantial sequence divergence, all four head domains are structurally very similar to each other and to the *P. furiosus* Rad50 ATPase domain (82). They also display a high structural similarity to a prototypic ABC ATPase (83), with the exception that they are composed of two parts. The N and C-terminal SMC domains form a single globular domain. A central β-sheet contains strands from both halves (Figure 2.3A).

In the absence of ATP, the *P. furiosus* SMC (PfuSMC) head domain is monomeric, but upon ATP binding it dimerises (79). In the dimer, the ATPase domains face each other, creating two composite active sites in the dimer interface in which two Mg^{2+}-ATP molecules are sandwiched (Figure 2.3A). Each ATP molecule binds to Walker A and B

motifs from one subunit and the signature motif from the other. The nucleophile for ATP hydrolysis is positioned and activated by residues from both subunits, confirming that only the head domain dimer is a functional ATPase (79). This suggests that ATP binding leads to engagement of the two head domains in an SMC dimer to close the SMC ring, while ATP hydrolysis opens it (Figure 2.2C).
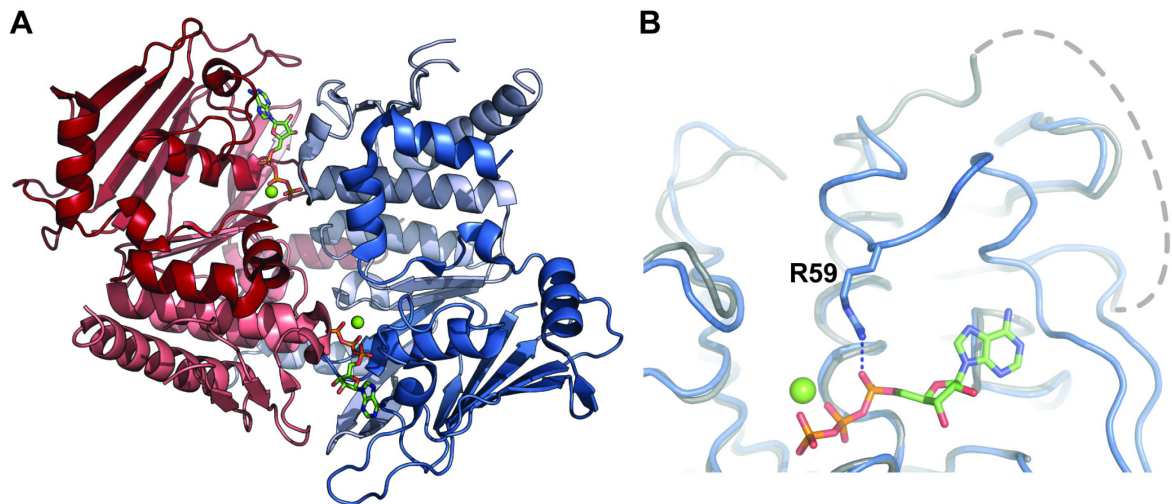
Figure 2.3. Crystal structure of the PfuSMC head domain. (**A**) Structure of the ATP-bound PfuSMC head domain dimer (pdb 1XEX) (79). Two Mg^{2+}-ATP molecules are sandwiched in the dimer interface. One monomer is coloured in shades of red, the other in shades of blue, with the N-terminal half of each monomer shown in the darker shade. Mg^{2+} is shown as green spheres, ATP as stick models with carbon atoms coloured green, nitrogen blue, oxygen red, and phosphorous orange. (**B**) The ATPase active site of the PfuSMC head domain in a superposition of the ATP-bound (blue; pdb 1XEX) and the nucleotide-free (grey; pdb 1XEW) state (Mg^{2+}-ATP shown as in (A)). Arginine 59 (stick model with carbon atoms coloured light blue and nitrogen dark blue) forms a hydrogen bond (dashed blue line) with the ATP α-phosphate. The loop containing R^{59} ("R loop") is rearranged and partially disordered in the nucleotide-free state (indicated by the dashed grey line).

Surprisingly, ATP binding and dimerisation do not cause major conformational changes in the PfuSMC head domain (79), indicating that SMC proteins are not motor proteins, as had initially been assumed due to their architectural similarity to myosin. Only a C-terminal helix rotates upon dimerisation to accommodate the other subunit and participate in the dimer interaction. Additionally, a surface loop containing a highly conserved arginine residue that contacts the ATP α-phosphate is rearranged and partially disordered in the absence of ATP (Figure 2.3B). This loop is located in the center of a basic patch on the inner surface of the SMC head domain (that is the surface from which the coiled-coils

emerge). Since the ATPase activity of condensin and prokaryotic SMC proteins is stimulated by DNA (16,17,79,84-86), the "R loop" is a likely candidate for a DNA sensor on the head domains. Indeed, mutation of the arginine residue does not affect basal ATPase activity, but completely abolishes its stimulation by DNA (79). In budding yeast, mutation of the arginine finger in both SMC1 and SMC3 leads to dramatically increased chromosome instability (87).

The binding of the C-terminal WHD (C-WHD) of Scc1 to the *S. cerevisiae* SMC1 head does not induce any conformational changes in the ATPase domain (22). The Scc1 C-WHD interacts with SMC1 in such a way as to prevent neither dimerisation nor ATP hydrolysis, although residues in the WHD recognition helix contact the Walker A motif, suggesting that Scc1 might have a regulatory effect on SMC1 ATPase activity. In fact, the C-terminal domain of Scc1 stimulates ATP hydrolysis at both SMC1-SMC3 active sites by promoting ATP binding to SMC1 (88). ATP can only be hydrolysed by either active site if it is bound to both, indicating that head domain engagement is a cooperative process driven by ATP binding.

As mentioned above, while in eukaryotes only one kleisin subunit bridges the head domains, prokaryotic SMC complexes contain two copies of the kleisin. Each MukB head domain therefore binds one MukF C-WHD (81). The MukF kleisin comprises four domains: an N-terminal WHD, a central helical domain that binds the MukE dimer, and a flexible linker segment connecting to the C-WHD. The interaction between the MukF C-WHD and the MukB head is similar to that between SMC1 and Scc1. However, upon ATP-induced head domain dimerisation, steric clashes between the two bound C-WHDs destabilise the head-WHD interaction and allow the flexible linker segment of one MukF subunit to competitively displace the C-WHD of the other MukF molecule. This displacement reaction is essential for the function of the MukBEF complex. It might be required for DNA loading (chapter 2.2.5).

2.2.1.2 The SMC Hinge Domain

The central hinge domain mediates dimerisation of SMC proteins. However, its function clearly exceeds that of a simple dimerisation domain, as it has been shown to bind DNA (17,31,86,89) as well as proteins (39,90). In case of the *Bacillus subtilis* SMC (BsuSMC) protein, ATP binding to the head domains stimulates DNA binding to the hinge domains (31), and this in turn stimulates ATP hydrolysis by the heads (16,17,86,91). This indicates

that the hinge domain is capable of transmitting structural changes along the coiled-coil region to the head domains and vice versa. FRET analysis and atomic force microscopy suggest that the coiled-coil can fold such that the hinge domain directly contacts the head domains (52,92).

Structures of two bacterial SMC hinge domains have been solved to date, these being the hinge domains of *T. maritima* SMC (TmaSMC) (15) and *E. coli* MukB (93,94) (discussed in detail in chapter 4.1.1.4). The MukB hinge domain is substantially smaller than that of the TmaSMC protein. Nonetheless the structures of the two hinge domains are quite similar. Two hinge domain monomers interact with each other via two interfaces to create a doughnut-shaped homodimer with two-fold symmetry. The coiled-coils are formed intramolecularly and emerge from the same face of the dimer (15,93,94).

2.2.2 The Function and Mechanism of Cohesin

Sister chromatid cohesion is crucial for proper chromosome segregation in mitosis and meiosis. Cohesion between sister chromatids enables the cell to attach sister kinetochores to microtubules with opposing polarity and subsequently resists the tendency of these microtubules to pull chromatids toward opposite spindle poles. An equilibrium between these two counteracting forces leads to the alignment of chromatid pairs on the metaphase plate (15).

Loss of cohesin function causes precocious loss of sister chromatid cohesion, defects in the biorientation of sister chromatids during mitosis, and at least temporary prometaphase arrest. Cohesion defects might be responsible for the high rates of meiosis I nondisjunction displayed by oocytes from older women, leading to trisomies such as Down's syndrome (23). Cohesin mutations have also been implicated in the Cornelia de Lange and Roberts/SC phocomelia genetic syndromes that cause slow growth, mental retardation, limb defects, and other abnormalities (95).

Cohesin is the most investigated and best understood of all SMC complexes and will therefore be discussed in some detail in the following.

2.2.2.1 Cohesin Function in Mitosis and Meiosis

While in yeast cohesin associates with chromatin near the G1-to-S phase transition (44,45), in vertebrates it binds to chromosomes during telophase (46,51,96). Loading of cohesin onto DNA requires the Scc2/Scc4 loading factor (47,48,97-102) which in vertebrates

(98,99), but apparently not in yeast (103), is recruited to chromatin by components of the prereplication complex. However, after loading, cohesin translocates along the chromosomes away from Scc2/Scc4 and towards sites of convergent transcriptional termination where it accumulates. Cohesin only occupies the entire length of genes if they are silent, suggesting that the complex is pushed along chromosomes by the transcription apparatus (104). During interphase, cohesin is dispersed every 10 – 20 kb along chromosome arms, but is more concentrated around centromeres (105-108). The enrichment of cohesin around centromeres depends on the *CEN*-sequence, proteins associated with this sequence like the centromere-specific histone H3 variant, and central kinetochore proteins (108-110).

Cohesion between sister chromatids is established during DNA replication (22,103). While the chromatin association of cohesin depends on its ATPase activity (111-113), establishment of cohesion does not (87). Lysine acetylation of SMC3 by an acetyl transferase named Eco1 is required for cohesion establishment (47,87,114-117) because it promotes the dissociation of an "antiestablishment" complex containing Pds5 and Wapl (118,119). Eco1 and two other proteins implicated in cohesion establishment, Ctf4 and Ctf18 (120,121), localise to replication forks (87). The DNA polymerase α-associated protein Ctf4 recruits Ctf18. The latter is part of a special replication factor C (RFC) complex that loads the proliferating cell nuclear antigen (PCNA) DNA-sliding clamp onto DNA (87,122). PCNA appears to be important for cohesin to be able to connect sister chromatids as they emerge from replication forks (114).

In vertebrates, but not in yeast, most of the cohesin bound to chromosome arms dissociates already during mitotic prophase (46,51). How and why cohesin is removed from chromosome arms in prophase is not understood, but the process is promoted by the phosphorylation of the Scc3 subunit by Polo-like kinase 1 (Plk1) (123-125). Condensin I (126) and Wapl (118,127,128) are also involved in prophase cohesin removal. At centromeres, cohesin is protected from phosphorylation by the protein shugoshin (Japanese for protector) (129-131) that associates with protein phosphatase 2A (PP2A) (132-134). Shugoshin promotes Aurora kinase complex localisation to the pericentromeric region to correct erroneous attachment of kinetochores. Ensuring bipolar attachment of kinetochores might in fact be the primary role of shugoshin, and the role of cohesin protection may have codeveloped to facilitate this process (135).

At the metaphase-to-anaphase transition, when all chromosomes have become bioriented, the separation of sister chromatids is triggered by the protease separase (48,136-144). For most of the cell cycle, separase activity is blocked by interaction with its inhibitory chaperone securin (145-149). During mitosis, the cyclin-dependent kinase 1 (Cdk1)-cyclin B complex phosphorylates and subsequently binds separase, thereby additionally inhibiting its activity (150,151). When the spindle assembly checkpoint is satisfied, the checkpoint protein Mad2 releases Cdc20 which in turn activates the ubiquitin protein ligase anaphase-promoting complex (APC) (152,153). Cdc20 recruits securin and cyclin B to the APC, leading to their ubiquitinylation and ensuing degradation, and hence to the release of separase (145,146,154,155). The now active protease cleaves the Scc1 kleisin subunit of chromatin-bound cohesin (48,142-144,156,157), and the C-terminal Scc1 cleavage product causes the SMC heads to dissociate (112), thus irreversibly dissolving sister chromatid cohesion and permitting chromosome segregation.

Phosphorylation of the kleisin by Plk1 enhances separase cleavage (125,158,159). Therefore Plk1 plays a role in both cohesin removal pathways. Separase cleavage, on the other hand, is not involved in cohesin removal during prophase (51). Indeed protection from separase cleavage might be the reason for prophase removal, as separase only cleaves chromatin-bound cohesin (156,157). The bulk of cohesin would thus not be destroyed in anaphase and be ready to reassociate with chromosomes in telophase to execute its interphase-specific functions. In yeast, on the other hand, cohesin can only reassociate with chromosomes after the kleisin has been resynthesised.

In meiosis I, the meiosis-specific kleisin Rec8 is protected around centromeres by meiotic shugoshin (160-165) so that the centromeres remain cohesed for the biorientation of dyad chromosomes at meiosis II, while from chromosome arms cohesin is removed by separase cleavage so that chiasmata can be resolved (137,166-169). Cleavage of Rec8, like that of its mitotic counterpart, is also enhanced by phosphorylation (170) which is counteracted by PP2A at centromeres due to shugoshin protection (171).

2.2.2.2 The Molecular Mechanism of Cohesin

Engineered cleavage of cohesin's coiled-coil region leads to dissociation of the complex from chromosomes and loss of sister chromatid cohesion (172). This argues that DNA is topologically entrapped inside the cohesin ring that encircles the chromosomes. The inner diameter of the cohesin complex is indeed wide enough to accommodate two strands of

DNA even when packed into chromatin. This "embrace" model has been strengthened further by the finding that even if cohesin is left intact, contact with DNA is lost if the DNA is cut into a small enough piece to slide out of the ring (173).

Cohesin complexes are still loaded onto DNA after replication, but they do not generate sister chromatid cohesion anymore (22,103). Therefore, there must be two ways for cohesin to bind to DNA, one that binds only individual chromatids, and one that connects sisters and is established during replication. If cohesin indeed forms a ring around DNA, cohesion might be generated by the replication fork moving through cohesin rings. Since the exact dimensions of the replication apparatus are unknown, it is not clear whether this would physically be possible. Alternatively, the cohesin ring might be temporarily opened to let the replication fork pass through, but maintained close to the fork by special cohesion establishment factors to enable reassociation of cohesin after fork passage (87). However, since cohesion establishment does not require ATP hydrolysis by cohesin (87), which is necessary to open cohesin rings, the first scenario appears more likely.

2.2.2.3 Cohesin Function in DNA Repair

The cohesin complex participates in DSB repair in mitotic (174-178) and meiotic (57,179,180) cells. Since cohesion establishment in S phase is necessary for efficient DSB repair in G2 (175), it was initially assumed that cohesin promotes DSB repair by homologous recombination (HR) simply because it already connects sister chromatids. However, cohesin is also specifically recruited to DSBs in postreplicative cells by the Mre11-Rad50-Nbs1 (MRN) complex (176,181,182) which detects DSBs and holds the DNA ends together (18,183). Induction of a single DSB indeed leads to genome-wide establishment of cohesion independently of DNA replication (184,185), cohesin thus acting like a safeguard of genome integrity. DNA-damage dependent cohesion establishment requires both *de novo* Eco1 activity and already existing cohesion (184,185). DSBs induce phosphorylation of Scc1 by Chk1 kinase, which in turn activates Scc1 acetylation by Eco1. This acetylation counteracts Wapl antiestablishment activity in G2/M phase (186,187). In contrast, in S phase Eco1 acetylates SMC3 to counteract Wapl and allow cohesion establishment (chapter 2.2.2.1). Therefore, Eco1 has different target sites in cohesin depending on the phase of the cell cycle.

2.2.3 The Function and Mechanism of Prokaryotic and Eukaryotic Condensins

Mutations in the *E. coli* MukBEF complex give rise to anucleate cells upon cell division (hence the name, derived from Japanese *mukaku*, anucleate) (32). The same phenotype was observed with *smc* and *scp* mutants in *B. subtilis* (24-28), leading to the conclusion that the prokaryotic SMC complex is required for chromosome partitioning.

The eukaryotic condensin complex has the same function. It is required, but not solely responsible for proper chromosome condensation and segregation during cell division (40,62,188-192). It seems to organise and maintain the chromosome scaffold rather than actually establishing it (192,193), but how it accomplishes this function is still unresolved.

2.2.3.1 Condensin Function in Mitosis

Condensin affects chromosome compaction, but it appears to have a structural rather than a catalytic role, stabilising rather than establishing the compacted state of the chromatin. Vertebrate chromosomes lacking condensin manage to compact almost normally, but prematurely lose their organised architecture during anaphase, when Cdk levels drop – unless the ensuing dephosphorylation of chromatin proteins is prevented (192-194). Hence, condensin seems to be necessary for the maintenance of the condensed chromatin state when the factors that have established it are dephosphorylated and thereby inactivated. Condensin is part of the non-histone "chromosome scaffold" (61). Depletion of the condensin subunit SMC2 results in mislocalisation of a number of scaffold components and ultimately solubilisation of the entire scaffold fraction (192,195), indicating that the chromosome scaffold is indeed a network of proteins that depends upon condensin for its assembly. Loss of condensin also leads to uncoordinated sister kinetochore movements, although the structure of the kinetochore itself is normal (192,194,196,197).

Whereas prokaryotic SMC proteins are recruited to replication origins (30,198,199), in vertebrates condensin I is confined to the cytoplasm during interphase and is loaded onto chromosomes at the end of prophase after nuclear envelope breakdown (NEBD). Condensin II is predominantly nuclear during interphase, but does not concentrate on chromatin until prophase either. Both condensin complexes dissociate from chromosomes by the end of telophase (126,194,200,201). Condensin I is targeted to chromosomes by A kinase-anchoring protein 95 (AKAP95) (202), while the tumour

suppressor protein Rbf1 is required for condensin II loading (203). Aurora B kinase additionally promotes chromatin loading of condensin I (191,204).

Vertebrate condensin I and II have distinct alternating patterns as well as some regions of overlap along chromosome arms (63,194,200). Both vertebrate condensins and yeast condensin are enriched at centromeres (63,194,200,205,206). In yeast, where condensin remains associated with chromatin throughout the cell cycle, it colocalises with the "cohesin loader" Scc2/Scc4 (206). The Scc2/Scc4 complex is not essential for condensin recruitment, but it promotes its association with chromatin and is required for chromosome condensation. Along chromosome arms, condensin is found at all RNA polymerase III genes together with transcription factor IIIC (TFIIIC) which is required for the recruitment of both Scc2/Scc4 and condensin. Cohesin and condensin chromatin association patterns are largely distinct from each other. Like cohesin, condensin is preferentially found between open reading frames (ORFs), but unlike cohesin it does not display a preference for convergent ORFs (206). Condensin binding to chromatin is also highly dynamic (194,201), in contrast to the rather stable binding of cohesin (207), although there is evidence that condensin binds to DNA in two different modes, one of which is very stable, while the other is not (208).

Like all cell cycle players, condensin is regulated by phosphorylation. In interphase, CK2 phosphorylates condensin I and thereby inhibits condensin activity. This inhibitory phosphorylation is removed during mitosis (209). Multiple kinases, including Cdk1, phosphorylate condensin I in mitosis. Cdk1 phosphorylation has a stimulatory effect on the DNA-supercoiling activity of condensin (191,210,211). The mitosis-specific phosphorylation sites in the condensin II kleisin are dephosphorylated by PP2A in anaphase (212).

Condensin II is required for chromosome condensation in early prophase, whereas condensin I appears to be dispensable at this stage. In contrast, condensin I is required for chromosome shortening and for normal timing of progression through prometaphase and metaphase, while condensin II is not necessary for these processes. After depletion of both condensin complexes, the onset of chromosome condensation is delayed until the end of prophase, but is then initiated rapidly before NEBD (126,194,200). Depletion of condensin I also results in a different chromosome appearance than depletion of condensin II (63), showing that condensin II and I associate with chromosomes sequentially and have distinct functions in mitotic chromosome assembly.

2.2.3.2 The Molecular Mechanism of Condensin

Condensin might not encircle chromosomes, but rather interact with DNA via its hinge domain. Unlike cohesin, condensin does not appear as a ring in electron micrographs, but instead forms a lollipop-like structure with both arms juxtaposed (21), and it has been observed sitting on DNA with its hinge domain (92). In contrast to cohesin, engineered cleavage of condensin arms did not release the complex from chromatin (195). However, condensin appears to be able to bind to DNA in two different modes *in vitro*, one that is salt-resistant, and one that is not (208). *In vitro*, the non-SMC subunits prevent DNA binding and reshaping by the SMC complex (31,36), whereas *in vivo* the non-SMC subcomplex stimulates SMC-induced chromatin compaction and is required for stable chromatin binding (64,213,214). These results are consistent with the non-SMC subunits blocking DNA entry into the SMC ring, but then locking the DNA-bound state once it has been established, possibly with the help of loading complexes.

ATP binding, but not hydrolysis, is required for the stable association of condensin with mitotic chromosomes in vertebrates (195), and for stable DNA binding by BsuSMC (31,86,91), whereas cohesin needs to bind *and* hydrolyse ATP (111-113). Possibly the head domain ATPase cycle is required for interaction with neighbouring condensin complexes, rather than for head domain engagement within the complex, to create a higher-order structure. With BsuSMC, intermolecular protein interactions are indeed detectable in the presence of DNA (16,31,86,91), and prokaryotic SMC proteins can form multimeric assemblies *in vitro* (30,35). To further support this hypothesis, a study with MukB demonstrated that DNA condensation occurs in a highly cooperative manner and results in the formation of large condensin clusters that can further interact with each other. ATP is required for the nucleation of these clusters, but not for their propagation (215).

Both prokaryotic and eukaryotic condensins have been shown to reshape and condense DNA *in vitro*, but results are conflicting as to whether this reshaping activity requires ATP hydrolysis or the non-SMC subunits (36,64,84,191,208,215-221). Condensin introduces positive supercoils into DNA in the presence of a type I topoisomerase, while producing positive trefoil knots in the presence of a type II topoisomerase. In single-molecule experiments, DNA can be reversibly compacted by condensin. Both during condensation and decondensation the step sizes are of variable length, indicating that condensin traps loops along the DNA (215,219).

The chromosome compaction and segregation defect of *mukB* or *smc* mutants can be suppressed by mutating or lowering the expression of the topoisomerase I gene (222,223), or by increasing the expression of topoisomerase IV (224). *Smc* mutant cells are also hypersensitive to inhibition of gyrase (223). Gyrase and topoisomerase IV increase the amount of negative supercoiling, while topoisomerase I lowers it. Hence condensin must somehow affect the formation of negative supercoils. It most likely does so by constraining the movement of DNA loops, leading to a torsion in the DNA that translates into negative supercoiling.

In conclusion, the currently available data indicate that condensin compacts DNA by stabilising DNA loops, acting as a "macromolecular clamp".

2.2.3.3 Condensin Function in DNA Repair

Studies in yeast have implied that condensin has an interphase-specific function in DNA repair, but they have not clarified which DNA repair pathway is affected (90,225). There are, however, indications that condensin is involved in DNA single-strand break (SSB) repair in higher eukaryotes (226). Human condensin I was shown to interact in an interphase-specific manner with the DNA nick-sensor poly(ADP-ribose) polymerase 1 (PARP1), and this interaction increased upon SSB damage induction. While nuclear retention of condensin was enhanced in the presence of SSBs, this was not the case for cohesin. Depletion of condensin I compromised SSB, but not DSB repair.

PARP1 detects SSBs and in response modifies itself, chromosomal and repair proteins with poly(ADP-ribose) (227). XRCC1 binds to poly(ADP-ribose) and provides a scaffold for the repair proteins. The DNA ends at a break site are usually damaged and have to be processed before the gaps can be filled and ligated. There are numerous types of damaged DNA ends, including 3'-phosphate and 5'-hydroxyl ends which are repaired by phosphatases and kinases, respectively. Other damaged ends are generally removed by endonucleases such as APE1, or the lyase activity of DNA polymerase β. The resulting single-nucleotide gaps are then repaired by the short-patch base-excision repair (BER) pathway, employing DNA polymerase β and DNA ligase IIIα. If the damage is too complicated to be removed directly, it is simply displaced by the polymerase in long-patch BER. This pathway requires the action of DNA polymerase δ/ε, flap endonuclease 1 (FEN1), and DNA ligase I, and is additionally stimulated by PARP1 and PCNA. The

polymerase fills in up to twelve nucleotides past the gap, and FEN1 then removes the displaced nucleotides, including the actual damage (227).

In addition to its interaction with PARP1, upon SSB damage induction condensin was found to interact with the scaffold protein XRCC1 as well as FEN1 and DNA polymerase δ/ε (226), indicating it is involved in long-patch BER.

The interaction between condensin and PARP1 was particularly strong in S phase, suggesting a function of condensin also in normal DNA replication (226). Indeed, condensin was found to accumulate at stalled replication forks in budding yeast (206), and was shown to be required for the replication checkpoint response after stalling replication by hydroxyurea treatment in fission yeast (225). Since it is not known whether condensin is also found at moving replication forks, its presence at stalled forks might either be due to its DNA repair function, or a function in undisturbed DNA replication.

2.2.4   The Function and Mechanism of the SMC5-SMC6 Complex

Due to its divergence from the other SMC proteins, the SMC5-SMC6 complex was the last SMC complex to be identified (65). To date, its precise function remains enigmatic. It is involved in several DNA repair pathways (65,66,68,69,71,77,78,228-233) and plays a role in resolving recombination intermediates during DNA repair and in meiosis (69,71,74,77,232-238).

Loading of the SMC5-SMC6 complex onto chromosomes occurs during DNA replication and requires the Scc2/Scc4 loading complex (239,240). At least in vertebrates the SMC5-SMC6 complex dissociates from chromatin again during mitosis (67,240). The complex concentrates at centromeres, telomeres and rDNA arrays, and colocalises with cohesin in intergenic regions (233,237,239). At rDNA arrays it appears to be required for efficient replication and consequently their correct segregation in mitosis (237,241).

The SMC5-SMC6 complex is recruited to DSBs by Mre11 and in turn recruits cohesin to the break site to promote recombination with the sister chromatid (239,242,243). The sumoylation activity of Nse2 is required for recruitment of both the SMC5-SMC6 complex and cohesin to DSBs, and Nse2 was shown to sumoylate several subunits of the SMC5-SMC6 complex (73,77,78) as well as the cohesin subunits Scc1 and Scc3 (243). Yet it is unclear whether the SMC5-SMC6 complex recruits cohesin directly or via other proteins, and it is also unclear if it directly facilitates sister chromatid recombination or does so only because it recruits cohesin. However, the SMC5-SMC6

complex also seems to control the localisation of DSBs and telomeres (73,241,244). Nse2 sumoylates telomere binding proteins in both yeast and human (73,244). This activity slows senescence in yeast by preventing aberrant recombination between sister telomeres (245). Relocalisation of break sites and telomeres might in fact promote accurate repair or telomere maintenance, respectively, simply by removing them from partially homologous sequences whose use as templates for recombination would lead to mutations.

2.2.5 The DNA-Loading Mechanism of SMC Complexes

If SMC complexes indeed encircle DNA, how does DNA enter the ring?

Cohesin needs to bind *and* hydrolyse ATP to stably associate with chromatin (111-113), whereas vertebrate condensin and BsuSMC only need to bind ATP (31,86,91,195). However, ATP-dependent head domain engagement (31) as well as their temporary disengagement (86) are required for stable DNA binding by BsuSMC. DNA stimulates the ATPase activity of condensin and prokaryotic SMC proteins (16,17,79,84,86,91). A DNA sensor loop on the PfuSMC head domain is required for DNA stimulation of ATP hydrolysis (79). In the BsuSMC protein, ATP binding to the head domains stimulates DNA binding to the hinge domains (31), and this in turn stimulates ATP hydrolysis by the head domains (16,17,86,91). These observations suggest that in the presence of DNA, the SMC ring is opened at the head domains by ATP hydrolysis, and closes again once the DNA has been encircled.

An opposing line of evidence suggests that DNA enters the SMC ring through the hinge domain (246). It was found that linking the hinge domains of budding yeast cohesin prevented its association with chromosomes, whereas linking the kleisin Scc1 to either or both head domains did not. However, these results were obtained by artificially fusing and crosslinking subunits of the cohesin complex and can therefore not be interpreted unambiguously.

With the available evidence, two opposing mechanisms for loading of SMC complexes onto DNA can be envisioned. The hinge-opening model (Figure 2.4A) is based entirely on the genetic engineering data of budding yeast cohesin (246). According to this model, the SMC complex first associates with DNA via its hinge domain. The hinge-hinge interface then opens and closes again once the DNA has passed through, thus trapping the DNA in the SMC ring.
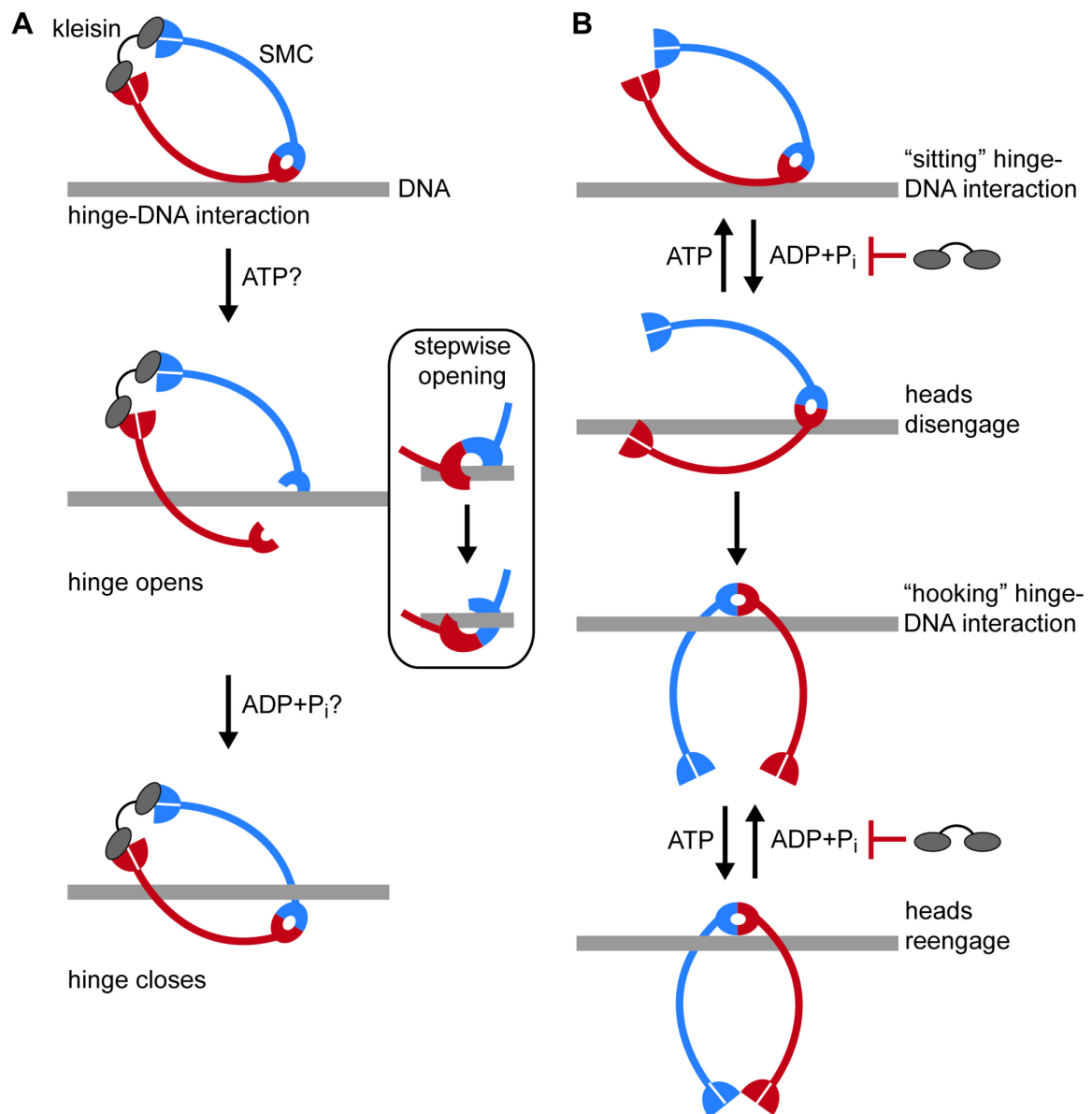
Figure 2.4. Models for the DNA-loading mechanism of SMC complexes. (**A**) Hinge-opening model, based on a study of budding yeast cohesin (246). The hinge domain mediates an initial interaction with the DNA and then opens up to let the DNA pass into the SMC ring. Because the hinge domain has two dimer interfaces, and the dimer interaction is very strong, it is more probable that the interfaces disengage sequentially. How this process would be coupled to the ATPase cycle of the head domains is unclear. (**B**) Head-opening model, based mostly on studies of BsuSMC (86). The hinge domain initially binds DNA in a loose, "sitting" mode. This stimulates ATP hydrolysis by the head domains so that they disengage, and the hinge domain can interact with DNA in a tighter "hooking" mode. The DNA passes between the head domains into the SMC ring, and the heads reengage after renewed ATP binding. The kleisin subunit suppresses ATP hydrolysis by BsuSMC and could therefore be envisioned to lock the DNA-bound state. Figure adapted from reference (247).

Hinge opening is anticipated to be coupled to the hinge-DNA interaction and to the ATPase cycle of the head domains, but it is unclear how this might be achieved mechanistically. Since the hinge-hinge interaction is very tight and mediated by two interfaces (15), it is more likely that the interfaces disengage and reengage sequentially.

In the second model, the hinge domain also plays a crucial role (Figure 2.4B). It interacts with DNA in two distinct modes (86). The initial loose, "sitting" mode of DNA binding stimulates ATP hydrolysis by the head domains so that they disengage. This promotes the tighter "hooking" mode of DNA binding via the hinge domain. The DNA enters the SMC ring through the interface between the two head domains that reengage after renewed ATP binding. The kleisin subunit ScpA suppresses ATP hydrolysis by BsuSMC (31). If the kleisin associated with the SMC complex only after it has been loaded onto DNA, it might thus inhibit dissociation of the complex from DNA. The Scc1 kleisin subunit of yeast cohesin and the bacterial MukEF complex, however, stimulate the ATPase activity of their respective SMC head domain partners (81,88). In this case, ATP hydrolysis might lead to a temporary disconnection of the kleisin subunit from the SMC heads that would be necessary for an opening of the ring. This scenario is supported by the findings that one of the two bound MukF C-WHDs is forced to detach from the MukB dimer upon ATP-mediated head domain engagement (81), and that only "unsaturated" MukBEF complexes (i.e. complexes with only one MukE$_2$F bound) are stable and able to bind DNA (36). Possibly the Scc2/Scc4 complex is required for DNA loading of cohesin because it promotes disconnection of the kleisin (111). Acetylation of SMC3 by Eco1 might inhibit renewed ATP binding or interaction with Scc2/Scc4, thus preventing dissociation of cohesin from chromatin (113).

2.3 Objectives

Whichever of the two DNA-loading models presented above is correct – if any –, it is obvious that the hinge domain plays a crucial role in the loading process. The hinge domain is clearly much more than just a simple dimerisation domain. Its DNA-binding activity is assumed to be essential for DNA loading of SMC proteins. However, there is evidence that – at least the prokaryotic – SMC hinge domains preferentially bind single-stranded DNA (ssDNA) rather than double-stranded DNA (dsDNA) (17,31,86,91). Since this activity is difficult to explain, it has so far been regarded as irrelevant for the physiological function of the SMC hinge domain.

Therefore the aim of this work was to analyse both prokaryotic and eukaryotic SMC hinge domains, and specifically their DNA-binding activity, in more detail. Because SMC proteins are such ancient proteins that have evolved to fulfil diverse cellular functions while maintaining a common architecture and high sequence similarity, comparison between hinge domains from different domains of life should also yield further insight into their evolution.

To this end, the hinge domains of the PfuSMC protein and of mouse condensin (mSMC2-mSMC4) were characterised structurally and biochemically. High-resolution crystal structures were combined with small-angle X-ray scattering data to clearly define the conformation of SMC hinge domains in solution. To learn more about the function of the DNA-binding activity of SMC hinge domains, this activity was analysed in detail both qualitatively as well as quantitatively.

3 MATERIALS AND METHODS

3.1 Materials

All chemicals used in this work were of the highest available grade obtained from Carl Roth, Merck, or Sigma-Aldrich, unless otherwise stated. Crystallisation screens and tools were from Hampton Research, NeXtal (QIAGEN), and Jena Bioscience. Oligonucleotide primers for polymerase chain reaction (PCR) were obtained in "high purity salt free" (HPSF®) form from Eurofins MWG Operon. RP-HPLC purified oligonucleotides for DNA-binding assays and crystallisation of protein-DNA complexes were purchased from Thermo Scientific. Enzymes for molecular biology were obtained from Fermentas, Finnzymes, or New England Biolabs.

3.2 Molecular Biology Methods

Common molecular biology procedures such as PCR, cleavage of phosphodiester bonds in DNA by restriction endonucleases, dephosphorylation of DNA ends by alkaline phosphatase, ligation of DNA ends, and separation of DNA fragments by agarose gel electrophoresis were carried out following standard protocols (248). Commercially available kits and enzymes were used according to the manufacturer's instructions.

Plasmid DNA was prepared using the QIAprep Spin Miniprep Kit (QIAGEN). The QIAquick Gel Extraction Kit (QIAGEN) was used to extract DNA from agarose gels. Whenever there were no undesired DNA molecules present in the sample, the QIAquick PCR Purification Kit (QIAGEN) was utilised to purify DNA. DNA sequencing was carried out by Eurofins MWG Operon.

3.2.1 Cloning and Site-Directed Mutagenesis

Constructs of SMC hinge domains for recombinant expression in *E. coli* were designed with the help of multiple sequence alignments of SMC proteins from various species generated with MultAlin or ClustalW2 (249,250), as well as coiled-coil predictions calculated by the COILS server (251), and secondary and tertiary structure predictions created by PSIPRED (252,253) and 3D-Jigsaw (254-256), respectively.

Oligonucleotide primers for PCR were designed with the help of GeneRunner (http://www.generunner.net/) and OligoCalc (257). PCR primers contained restriction sites

and, if desired, additional sequences encoding affinity tags for use in protein purification (Table 3.1).

Table 3.1. Oligonucleotide primers used for cloning and site-directed mutagenesis. Sequences are given in 5'-3' direction. The first sequence of each pair is the forward primer, the second the reverse primer. Recognition sites of restriction endonucleases are underlined. Bold nucleotides correspond to added sequences encoding affinity tags or stop codons, red nucleotides correspond to mutated codons. PfuSMC, *P. furiosus* SMC; mSMC, mouse SMC; aa, amino acid; N-Strep II, N-terminal Strep II tag.

Amplified gene fragment/ mutation	Sequence	Restriction site
PfuSMC aa 488-667	GGAATTCCATATGGAGTTAGAATCCTCAGAGAGA	NdeI
	CCGCTCGAGCCTAAGTTTCGTTGTATCTACTG	XhoI
mSMC2 aa 492-680 + N-Strep II	GGAATTCCATATG**TGGAGCCACCCGCAGTTCGAAAAG**CTAAAAG GAAAACATGAAGCT	NdeI
	GGAATTC**TCA**TTCTTGAAACTTGGTTAAAATC	EcoRI
mSMC2 aa 506-666	GGTATACCATATGCTTCAATTTGCTTACAAGGAC	NdeI
	CGAATTC**TCA**ACCTCCACTCAATGTTCCATG	EcoRI
mSMC4 aa 581-766	CATGCCATGGTTGAAGAAGCAAAGAGTTC	NcoI
	CCGCTCGAGGATAACCGAAGAGCCCA	XhoI
mSMC4 aa 595-752	CATGCCATGGGGAAAGTACTTGATGCAATAATTC	NcoI
	CCGCTCGAGACCGCCACTCATTGTACC	XhoI
PfuSMC K^{565}E	CTGAAAAGGCGATAGAATACTTGAAGGAGC	
	GCTCCTTCAAGTATTCTATCGCCTTTTCAG	
PfuSMC K^{605}E	GAGTATGATCAAGAAATAGAGAATGCTG	
	CAGCATTCTCTATTTCTTGATCATACTC	
mSMC2 K^{566}E	GAAGCTACTAGAAGAGGGGGAGTTGAAG	
	CTTCAACTCCCCCTCTTCTAGTAGCTTC	
mSMC2 K^{613}E	CTTTCCTTAGTTGACTATGAACCAGAACTTC	
	GAAGTTCTGGTTCATAGTCAACTAAGGAAAG	
mSMC4 K^{657}E	GTGTAAACTTCCTTGAAAAGCATAATATTGG	
	CCAATATTATGCTTTTCAAGGAAGTTTACAC	
mSMC4 K^{698}E	GATCTAGTTAAAGTGGAAAATGAGGAAATCCGCC	
	GGCGGATTTCCTCATTTTCCACTTTAACTAGATC	

The DNA fragments encoding the desired SMC hinge domain constructs were amplified from plasmids containing the sequences of interest (Table 3.2) using the Phusion® Flash High-Fidelity PCR Master Mix (Finnzymes) and cloned into the pET-21b vector

24

(Novagen). For heterodimeric SMC hinge domains, the DNA fragments were sequentially inserted into a modified bicistronic version of pET-21b (see Figure 7.1 for a map of this vector and Figure 7.2 for a depiction of the multiple cloning site).

Table 3.2. Plasmids containing full-length genes that were used as templates for the amplification of desired DNA fragments. Image plasmids are full-length cDNA clones.

Name	Vector	Gene	Obtained from
pPfuSMC	pET-21b	*P. furiosus smc*	Alfred Lammens
image ID 30543190	pYX-Asc	mouse *smc2*	imaGenes
image ID 6841276	pYX-Asc	mouse *smc4*	imaGenes

Point mutations were introduced into the vectors by site-directed mutagenesis following the QuikChange protocol (Stratagene), but employing the Phusion® Flash High-Fidelity PCR Master Mix (Finnzymes).

All constructs were verified by DNA sequencing. Constructs that were expressed and purified successfully and analysed further are listed in Table 3.3.

Table 3.3. Expression plasmids of SMC hinge domain constructs. PfuSMC, *P. furiosus* SMC; mSMC, mouse SMC; aa, amino acid; wt, wild-type; C-His$_6$, C-terminal hexahistidine tag; N-Strep II, N-terminal Strep II tag.

Name	Encoded fragment	Restriction sites	Tag	Vector
pPfuSMCh	PfuSMC aa 488-667 wt	NdeI/XhoI	C-His$_6$	pET-21b
pPfuSMCh^{K565E}	PfuSMC aa 488-667 K^{565}E	NdeI/XhoI	C-His$_6$	pET-21b
pPfuSMCh^{K605E}	PfuSMC aa 488-667 K^{605}E	NdeI/XhoI	C-His$_6$	pET-21b
pmSMC2h4h-l	mSMC2 aa 492-680 wt	NdeI/EcoRI	N-Strep II	bicistronic pET-21b
	mSMC4 aa 581-766 wt	NcoI/XhoI	C-His$_6$	
pmSMC2h^{K566E}4h-l	mSMC2 aa 492-680 K^{566}E	NdeI/EcoRI	N-Strep II	bicistronic pET-21b
	mSMC4 aa 581-766 wt	NcoI/XhoI	C-His$_6$	
pmSMC2h^{K566E}4h^{K657E}-l	mSMC2 aa 492-680 K^{566}E	NdeI/EcoRI	N-Strep II	bicistronic pET-21b
	mSMC4 aa 581-766 K^{657}E	NcoI/XhoI	C-His$_6$	
pmSMC2h^{K613E}4h^{K698E}-l	mSMC2 aa 492-680 K^{613}E	NdeI/EcoRI	N-Strep II	bicistronic pET-21b
	mSMC4 aa 581-766 K^{698}E	NcoI/XhoI	C-His$_6$	
pmSMC2h4h-s	mSMC2 aa 506-666 wt	NdeI/EcoRI		bicistronic pET-21b
	mSMC4 aa 595-752 wt	NcoI/XhoI	C-His$_6$	

3.3 Microbiology Methods

3.3.1 Transformation of *E. coli*

The *E. coli* strains used in this study are listed in Table 3.4. Chemically competent cells were prepared according to Hanahan (258). Cultures were grown in 200 ml LB medium supplemented with the appropriate antibiotics (Table 3.5) at 37°C to an optical density at 600 nm (OD_{600}) of ~0.5. Cells were harvested by centrifugation, resuspended in 30 ml of cold *TfB*I (Table 3.6), incubated on ice for 10 min, again pelleted by centrifugation and resuspended in 4 ml of cold *TfB*II (Table 3.6). The cells were aliquoted (75 µl), flash frozen in liquid nitrogen and stored at -80°C.

For transformation, ~100 ng of ligated DNA or 10 ng of plasmid DNA were added to 75 µl of competent cells and incubated on ice for 20 min. The cells were heat-shocked at 42°C for 30 s, cooled down on ice for 2 min, and after addition of 900 µl of LB medium, the cells were incubated for 45 – 60 min at 37°C under mild shaking. If a ligation reaction was transformed, the entire cell suspension was centrifuged briefly, most of the supernatant was removed, and the cell pellet was resuspended in the remaining medium and plated on LB-agar plates containing the appropriate antibiotics. If plasmid DNA was transformed, only 100 – 200 µl of the cell suspension were plated. The agar plates were incubated at 37°C overnight.

Table 3.4. *E. coli* strains used for cloning and recombinant protein production. The XL1-Blue strain was used for cloning, the Rosetta strains and the B834 strain were used for the production of native and selenomethionine-labelled proteins, respectively.

Strain	Genotype	Obtained from
XL1-Blue	*recA1 endA1 gyrA96 thi-1 hsdR17 supE44 relA1 lac* [F′ *proAB lacI^{q}ZΔM15* Tn*10* (Tet^R)]	Stratagene
Rosetta (DE3)	F$^-$ *ompT hsdS$_B$*(r$_B^-$ m$_B^-$) *gal dcm* (DE3) pRARE (Cam^R)	Novagen
Rosetta 2 (DE3)	F$^-$ *ompT hsdS$_B$*(r$_B^-$ m$_B^-$) *gal dcm* (DE3) pRARE2 (Cam^R)	Novagen
B834 (DE3) + pRARE	F$^-$ *ompT hsdS$_B$*(r$_B^-$ m$_B^-$) *gal dcm met* (DE3) pRARE (Cam^R)	Novagen

Table 3.5. Composition of LB medium (259) and antibiotic and IPTG stock solutions to be added to the medium in 1000-fold dilution. The recipe is for 1 L of medium. Agar was added to the medium to prepare LB-agar plates.

LB medium		Stock solutions		
Bacto-tryptone	10 g	ampicillin	100 mg/ml	in water
yeast extract	5 g	kanamycin	50 mg/ml	in water
NaCl	5 g	chloramphenicol	34 mg/ml	in ethanol
2 M NaOH	1.3 ml	tetracycline	10 mg/ml	in ethanol
± agar	15 g	IPTG	0.5 M	in water

Table 3.6. Buffers for the preparation of chemically competent *E. coli* cells.

*TfB*I		*TfB*II	
30 mM	potassium acetate	10 mM	MOPS
100 mM	KCl	10 mM	KCl
50 mM	$MnCl_2$	75 mM	$CaCl_2$
10 mM	$CaCl_2$	15% (v/v)	glycerol
15% (v/v)	glycerol	pH 7.0	adjusted with NaOH
pH 5.8	adjusted with acetic acid		

3.3.2 Recombinant Protein Production in *E. coli*

Proteins were produced recombinantly in *E. coli* Rosetta (DE3) or *E. coli* Rosetta 2 (DE3) (Novagen) in shaking cultures. For large scale expression, 3 L of LB medium supplemented with the appropriate antibiotics (Table 3.5) were inoculated 1:100 with an overnight culture in LB medium of the strain harbouring the expression vector. Cultures were grown at 37°C to an OD_{600} of ~0.7 – 0.8.

For the PfuSMC hinge domain constructs, expression of the recombinant gene was then induced with 0.5 mM IPTG (Table 3.5) and allowed to proceed for 5 h at 37°C.

For the mouse condensin hinge domain constructs, having reached an OD_{600} of ~0.7 – 0.8, cultures were cooled down to 18°C before expression was induced with 0.5 mM IPTG (Table 3.5) and allowed to proceed for 20 h at 18°C.

Cells were harvested by centrifugation, and the cell pellets were stored at -20°C until further use.

To obtain selenomethionine-labelled protein, constructs were expressed in the methionine auxotrophic strain *E. coli* B834 (DE3) additionally containing the pRARE plasmid (Novagen). 2.2 L of LeMaster's medium (Table 3.7) supplemented with the appropriate antibiotics and L-selenomethionine (45 mg/L; Calbiochem) were inoculated 1:100 with an overnight culture in LB medium of the methionine auxotrophic strain harbouring the expression vector. Expression was carried out as for the native proteins.

Table 3.7. Composition of LeMaster's medium (260). Solution A was autoclaved and combined with filter-sterilised solution B. The pH was adjusted to 7.5 with 10 M NaOH or concentrated HCl. 100 mg of L-selenomethionine (Calbiochem) were added per 2.2 L of medium.

Autoclavable solution A (g/2000 ml)			
L-alanine	1.000	L-serine	4.166
L-arginine hydrochloride	1.160	L-threonine	0.460
L-aspartic acid	0.800	L-tyrosine	0.340
L-cysteine	0.066	L-valine	0.460
L-glutamic acid	1.500	adenine	1.000
L-glutamine	0.666	guanosine	1.340
L-glycine	1.080	thymine	0.340
L-histidine	0.120	uracil	1.000
L-isoleucine	0.460	sodium acetate	3.000
L-leucine	0.460	succinic acid	3.000
L-lysine hydrochloride	0.840	ammonium chloride	1.500
L-phenylalanine	0.266	sodium hydroxide	1.700
L-proline	0.200	dibasic potassium phosphate	21.000

Non-autoclavable solution B (200 ml)	
glucose	20.0 g
magnesium sulfate heptahydrate	0.5 g
iron sulfate	8.4 mg
sulfuric acid (concentrated)	16.0 μl
thiamin	10.0 mg

3.4 Protein Biochemistry Methods

3.4.1 Purification of Recombinant Proteins

The PfuSMC hinge domain constructs were purified using heat denaturation of contaminating proteins, nickel chelate affinity chromatography and gel filtration. All purification steps were carried out at 8°C or on ice except for the affinity chromatography which was performed at room temperature. Cells from 2 – 3 L of culture were resuspended in buffer A (Table 3.8) and lysed by sonication. The lysate was incubated at 70°C for 10 min, then cleared by centrifugation, and applied to a gravity flow column containing Ni-NTA agarose beads (QIAGEN) equilibrated in buffer A. The beads were washed extensively with buffer A before protein was eluted with buffer B (Table 3.8). The eluate was concentrated in centrifugal filter units (Amicon Ultra, 10 000 MWCO, Millipore) and applied to a Superdex 200 pg 26/60 gel filtration column (GE Healthcare) equilibrated in buffer C (Table 3.8). Fractions containing only the homodimeric PfuSMC hinge domain were pooled, and the protein was concentrated to 50 – 100 mg/ml. Protein concentration was determined using a calculated extinction coefficient at 280 nm (261). The purification process was monitored by SDS-PAGE (chapter 3.4.2). Concentrated protein was aliquoted, flash frozen in liquid nitrogen and stored at -80°C until further use. Selenomethionine-labelled protein was purified analogously with the addition of 1 mM DTT to all buffers. TCEP was added to the concentrated protein to a final concentration of 1 mM to prevent oxidation of the selenomethionine residues.

Table 3.8. Buffers for protein purification.

Buffer A		Buffer B		Buffer C	
25 mM	Tris-HCl pH 8.0	25 mM	Tris-HCl pH 8.0	5 mM	Tris-HCl pH 8.0
300 mM	NaCl	300 mM	NaCl	100 mM	NaCl
20 mM	imidazole	250 mM	imidazole	0.1 mM	EDTA

The mouse condensin hinge domain constructs were purified according to the same protocol as the PfuSMC hinge domain, but omitting the heat denaturation step. All purification steps were carried out at 8°C or on ice. Fractions from the gel filtration that contained only the heterodimeric SMC2-SMC4 hinge domain were pooled and concentrated to 30 – 40 mg/ml.

3.4.2 Denaturing Polyacrylamide Gel Electrophoresis (SDS-PAGE)

Protein samples were analysed by SDS-PAGE according to Laemmli (262) using the vertical Mini-PROTEAN 3 System (BioRad). Depending on the molecular weight of the protein of interest, 1 mm thick gels containing 15% or 20% acrylamide in the separating gel were used. Before loading, samples were denatured in a reducing sample buffer by heating at 95°C for 5 min. Electrophoresis was performed at 200 – 250 V in running buffer. Gels were stained with a Coomassie Brilliant Blue R-250 (Carl Roth) solution and destained with deionised water. Gel and buffer compositions are listed in Table 3.9.

Table 3.9. Composition of denaturing polyacrylamide gels and the buffers and solutions required for SDS-PAGE. The volumes given are for one gel.

stacking gel	1.2 ml	3 M Tris-HCl pH 6.8, 0.4% (w/v) SDS
	0.6 ml	30% acrylamide-bisacrylamide 37.5:1
	3 ml	water
	4.8 µl	TEMED
	48 µl	10% (w/v) APS
15% acrylamide separating gel	3 ml	3 M Tris-HCl pH 8.5, 0.4% (w/v) SDS
	6 ml	30% acrylamide-bisacrylamide 37.5:1
	3 ml	water
	6 µl	TEMED
	78 µl	10% (w/v) APS
20% acrylamide separating gel	3 ml	3 M Tris-HCl pH 8.5, 0.4% (w/v) SDS
	8 ml	30% acrylamide-bisacrylamide 37.5:1
	1 ml	water
	6 µl	TEMED
	78 µl	10% (w/v) APS
4x sample buffer	110 mM	Tris-HCl pH 6.8
	16% (v/v)	glycerol
	4% (w/v)	SDS
	5% (v/v)	β-mercaptoethanol
	0.6% (w/v)	bromophenol blue
1x running buffer	192 mM	glycine
	25 mM	Tris
	0.1% (w/v)	SDS
staining solution	7% (v/v)	acetic acid
	50% (v/v)	ethanol
	0.2% (w/v)	Coomassie Brilliant Blue R-250

3.4.3 Analytical Size Exclusion Chromatography

In order to determine the oligomeric state and homogeneity of purified proteins, they were subjected to analytical gel filtration on a Superdex 200 10/300 GL column (GE Healthcare) in buffer C (Table 3.8). The column was calibrated with Gel Filtration Standard (BioRad) in the same buffer.

3.4.4 Dynamic Light Scattering Analysis

Dynamic light scattering (DLS) was employed to measure the hydrodynamic radius and particle size distribution of protein samples. The protein solution was diluted to a concentration of $1 - 10$ mg/ml and centrifuged for 5 min at 4°C and 13 200 rpm in an eppendorf 5415R centrifuge. A sample of 70 µl was transferred into a fluorescence ultra-micro cuvette (3×3 mm light path, type 105.251-QS, Hellma). DLS was measured in a Viscotek 802 DLS instrument. Ten measurements of 4 s each were conducted at 20°C. The OmniSIZE 3.0 software was used for instrument control and data analysis.

3.5 Structural Biology Methods

3.5.1 Background

The following chapter will briefly outline the fundamentals of X-ray crystallography and small-angle X-ray scattering (SAXS). A detailed description of the underlying theory would go far beyond the scope of this text and can be found elsewhere (263-266).

Both X-ray crystallography and SAXS exploit coherent (Thomson) scattering of X-rays: electrons oscillating in the electric field of an X-ray beam emit X-rays with the same wavelength as the incident beam, but 180° out of phase. In both cases, a collimated, monochromatic X-ray beam irradiates a sample, and the intensity of the X-rays that are scattered by the electrons in the sample is measured. The fundamental difference between X-ray crystallography and solution scattering lies in the relative organisation of the target molecules. In X-ray crystallography, the molecules are highly ordered within a crystal lattice. Diffraction from the crystal gives rise to discrete diffraction maxima that are caused by the convolution of the crystal lattice onto the continuous transform due to the atomic positions and that retain information about the specific orientations in the molecule. In solution scattering, on the other hand, the signals from all orientations of the target molecules relative to one another and the experimental apparatus are averaged.

Crystallography therefore provides significantly more information than SAXS, allowing structure determination to atomic resolution, whereas the maximum resolution of SAXS is 50 – 10 Å. However, crystallography requires diffraction-quality crystals that can often not be obtained. Moreover, crystal packing can force the macromolecules into non-physiological conformations. Therefore SAXS is best used as a complementary technique to X-ray crystallography – to ensure that the conformation captured in the crystal is the same that is adopted by the macromolecule in solution, or to obtain solution envelopes of complexes that fail to crystallise into which the crystal structures of their single components can then be docked.

3.5.2   X-ray Crystallography

3.5.2.1   *Crystallisation*

Proteins were crystallised by vapour diffusion at 20°C. Initial hits were obtained in commercial 96-well format sitting-drop screens. The Matrix Hydra II 96-channel microdispenser (Thermo Scientific) was used to dispense both the reservoir solution and the drops. The reservoir contained 50 µl solution, and drops were mixed from equal volumes of reservoir solution and protein (0.2+0.2 or 0.5+0.5 µl). The initial crystallisation conditions were optimised manually, originally with native and then with selenomethionine-labelled protein, in 24-well hanging-drop plates containing 300 µl reservoir solution with 2+2 µl drops. To optimise crystals, the composition of the reservoir solution as well as the precipitant and protein concentration were varied.

The refined crystallisation condition for the PfuSMC hinge domain contained 1.8 M ammonium sulphate, 0.2 M potassium-sodium tartrate, and 0.1 M trisodium citrate pH 6.0. The optimum protein concentration for crystal growth was 30 mg/ml. Crystals of a maximum size of ~0.4 × 0.2 × 0.2 mm appeared within two to three days. Cryoprotection was achieved by briefly soaking crystals in mother liquor supplemented with 15% (v/v) D(-)-2,3-butane diol, following which the crystals were immediately flash frozen in liquid nitrogen.

The best crystals of the short mouse condensin hinge domain construct mSMC2h4h-s were obtained in 15% (w/v) PEG 4000, 5% (v/v) isopropanol, 20% (v/v) glycerol, and 100 mM Tris-HCl pH 8.5, with a protein concentration of 40 mg/ml. Crystals

of a maximum size of ~0.5 × 0.2 × 0.1 mm appeared within one day. For data collection, crystals were flash frozen in liquid nitrogen without additional cryoprotection.

3.5.2.2 Data Collection

Data were collected at beamline PXI of the Swiss Light Source (SLS, Villigen, Switzerland) with the PILATUS hybrid pixel array detector. MOSFLM (267) was used to determine the optimum data collection strategy in order to achieve high redundancy and completeness. A fluorescence scan was performed with the selenomethionine-labelled protein crystals prior to data collection to determine the optimum wavelengths for the anomalous dispersion experiments.

3.5.2.3 Structure Determination, Model Building and Refinement

The crystals of the PfuSMC hinge domain belong to space group $C222_1$ and contain two molecules in the asymmetric unit (see Table 4.1 for crystallographic data, phasing and refinement statistics). The structure was determined by multiple wavelength anomalous dispersion (MAD) phasing. Data were indexed and integrated using the XDS package (268). Phases were calculated with AutoSHARP (269). One chain was built manually in Coot (270), and the second chain was then generated by molecular replacement using Phaser (271,272). The model was refined against the high remote wavelength dataset of the selenomethionine derivative. Non-crystallographic symmetry restraints were only applied in the first stages of refinement because the two chains present in the asymmetric unit are not completely identical. Initial refinement was carried out with CNS (273), followed by several rounds of refinement with phenix.refine (274) and rebuilding in Coot. Refinement included simulated annealing in initial cycles, individual atomic coordinate and isotropic B factor refinement, and bulk solvent corrections. Solvent molecules were added with phenix.refine and manually. The R_{free} factor was calculated from 10% of the data which were removed at random before the structure was refined. The structure was validated using MolProbity (275), RAMPAGE (276), and PROCHECK (277). The electrostatic surface potential was calculated with the Adaptive Poisson-Boltzmann Solver (APBS) (278). All figures were prepared with PyMOL (279). Coordinates and structure factors were deposited at the Protein Data Bank (PDB) with accession number 3NWC.

The short construct of the mouse condensin hinge domain mSMC2h4h-s crystallised in space group $P2_1$. The crystals contain one molecule each of the SMC2 and

SMC4 subunits in the asymmetric unit (see Table 4.2 for crystallographic data, phasing and refinement statistics). The structure was determined by single wavelength anomalous dispersion (SAD) phasing from a peak wavelength dataset of the selenomethionine-labelled protein crystals. The XDS package (268) was used to index and integrate the data. Phases were calculated with AutoSHARP (269). The model was largely automatically built with ARP/wARP (271,280,281) and completed by manual model building in Coot (270). Initial refinement was carried out with CNS (273), followed by several rounds of refinement with phenix.refine (274) and rebuilding in Coot. Refinement included simulated annealing in initial cycles, individual atomic coordinate and anisotropic B factor refinement, and bulk solvent corrections. Solvent molecules were added with phenix.refine and manually. The R_{free} factor was calculated from 10% of the data which were removed at random before the structure was refined. The structure was validated using MolProbity (275), RAMPAGE (276), and PROCHECK (277). The electrostatic surface potential was calculated with APBS (278). All figures were prepared with PyMOL (279). Coordinates and structure factors were deposited at the PDB with accession number 3L51.

3.5.3 Small-Angle X-ray Scattering of Protein Solutions

3.5.3.1 Sample Preparation

To prepare samples suitable for SAXS measurements, proteins were additionally purified via gel filtration on a Superdex 200 column (GE Healthcare), and concentrated to yield samples in concentration ranges from 2 to 20 mg/ml in buffer C (Table 3.8). The flowthrough of the concentration step was used as buffer reference for SAXS measurements. Immediately before the measurement, samples were centrifuged for 5 min at 4°C and 13 200 rpm in an eppendorf 5415R centrifuge.

3.5.3.2 Data Collection, Processing and Analysis

SAXS data were collected at beamline X33 at EMBL/DESY, Hamburg. All measurements were carried out at 20°C sample cell temperature. Scattering profiles of BSA and lysozyme were measured as reference for molecular mass determination.

The ATSAS package (282) was used to analyse data. Data were processed with PRIMUS (283). The radius of gyration (R_g) was derived by the Guinier approximation $[I(s) = I(0)\exp(-s^2 R_g^2/3)$ for $s\,R_g < 1.3]$. The molecular masses of the solutes were

determined by extrapolating the scattering intensities to zero angle, using BSA and lysozyme as reference. The pair-distance distribution function P(r) and the maximum dimension of the macromolecule D_{max} were computed with the program GNOM (284). Theoretical scattering profiles from atomic resolution models were calculated and fitted to measured profiles with CRYSOL (285).

Ab initio models of the PfuSMC hinge domain were reconstructed from the experimental data using the program GASBORi (286), initially without imposing any symmetry or other restrictions on possible models. Since all models were clearly two-fold symmetric, further models were calculated imposing two-fold symmetry. Eight independently reconstructed envelopes were aligned and averaged with SUPCOMB (287) and DAMAVER (288).

Ab initio models of the long mouse condensin hinge domain construct mSMC2h4h-l were reconstructed from the experimental data with GASBORp (286) without imposing any symmetry or other restrictions on possible models. Ten independently reconstructed envelopes were aligned and averaged with SUPCOMB (287) and DAMAVER (288).

Envelope representations were calculated using the Situs package (289,290), which was also used to dock atomic resolution models into the envelope.

3.6 *In Vitro* DNA-Binding Assays

3.6.1 Preparation of DNA Substrates

DNA oligonucleotide substrates carrying a 6-carboxyfluorescein (6-FAM) fluorescence label were used to monitor their binding to SMC hinge domains (Table 3.10). RP-HPLC-purified DNA oligonucleotides (Thermo Scientific) were dissolved in nuclease-free double distilled water. DNA concentration was determined using a calculated extinction coefficient at 260 nm (257). To anneal oligonucleotides, they were mixed with a 1.1-fold molar excess of the unlabelled oligonucleotide in annealing buffer (Table 3.11), incubated in a thermocycler (Biometra T personal) for 5 min at 95°C, and then cooled down to 4°C at a cooling rate of 0.1°C/s.

Table 3.10. Oligonucleotides used for DNA-binding assays.

Name	Oligonucleotide sequences
30-mer ssDNA	`5'-6-FAM-TTTTTTTTTTTTTTTTTTTTTTTTTTTTTT`
15-mer ssDNA	`5'-6-FAM-TTTTTTTTTTTTTTT`
30-mer dsDNA	strand 1: `5'-6-FAM-CCGGAAAGCATCTAGCATCCTGTCAGCTGC` strand 2: `5'-GCAGCTGACAGGATGCTAGATGCTTTCCGG`
30-mer ds-ssDNA-3'	strand 1: `5'-6-FAM-CATCCTGTCCGCTGC` strand 2: `5'-GCAGCGGACAGGATGTTTTTTTTTTTTTTT`
30-mer ds-ssDNA-5'	strand 1: `5'-6-FAM-CATCCTGTCCGCTGC` strand 2: `5'-TTTTTTTTTTTTTTTGCAGCGGACAGGATG`
45-mer ds-ss-dsDNA	strand 1: `5'-6-FAM-CATCCTGTCCGCTGC` strand 2: `5'-CCGGAGAGCATCTCG` strand 3: `5'-GCAGCGGACAGGATGTTTTTTTTTTTTTTTCGAGATGCTCTCCGG`

Table 3.11. Buffers for DNA-binding assays.

Annealing buffer	40 mM	Tris-HCl pH 7.5
	100 mM	NaCl
	10 mM	$MgCl_2$
1× PBS	137 mM	NaCl
	2.7 mM	KCl
	10 mM	Na_2HPO4
	1.8 mM	KH_2PO4
	pH 7.4	adjusted with NaOH or HCl
1× TB	90 mM	Tris
	90 mM	boric acid
	pH 8	without adjustment

3.6.2 Electrophoretic Mobility Shift Assays

To qualitatively assess DNA binding by SMC hinge domains, the electrophoretic mobility shift assay (EMSA) was used. The assay is based on the fact that in native gel electrophoresis a protein-DNA complex will migrate differently than the corresponding free DNA. The DNA is visualised via its fluorescence label.

Samples for EMSAs contained 12.5 nM of a DNA substrate and protein in a molar excess over the DNA as detailed in Table 3.12 in 1× PBS (Table 3.11) in a total volume of 20 µl. They were incubated at room temperature for 30 min before addition of 5 µl 50% (v/v) glycerol. The samples were then loaded onto an 0.5% (w/v) agarose gel in 1× TB

buffer (Table 3.11) and separated for 2 h at 4 V/cm and 8°C. Gels were scanned on a Typhoon 9400 fluorescence scanner (GE Healthcare) using the blue laser (488 nm wavelength) for excitation and the 520 BP 40 emission filter (photomultiplier tube voltage 600 V, normal sensitivity, focal plane +3 mm, pixel size 50 μm, 200 dots/cm).

Table 3.12. Samples for electrophoretic mobility shift assays (EMSAs). The molar excess of protein over DNA and the corresponding final protein concentration in the 20-μl samples are given.

Protein and DNA substrates	mSMC2h4h-s and mSMC2h4h-l with all DNA substrates		PfuSMCh with ssDNA substrates		PfuSMCh with dsDNA substrates	
Sample	[protein]/ [DNA]	[protein] (nM)	[protein]/ [DNA]	[protein] (nM)	[protein]/ [DNA]	[protein] (μM)
1	0	0	0	0	0	0
2	1	12.5	10	125.0	100	1.25
3	2	25.0	25	312.5	500	6.25
4	10	125.0	50	625.0	1000	12.50
5	25	312.5	100	1250.0	2500	31.25
6	50	625.0	250	3125.0	5000	62.50
7	100	1250.0	500	6250.0	10 000	125.00
8	250	3125.0	1000	12 500.0	25 000	312.50
9	500	6250.0	2500	31 250.0	50 000	625.00
10	1000	12 500.0	5000	62 500.0	100 000	1250.00

3.6.3 Fluorescence Quenching Titrations

Fluorescence quenching titrations were employed to quantitatively analyse the DNA-binding activity of SMC hinge domains, exploiting the fact that binding of 6-FAM-labelled DNA to proteins can lead to quenching of 6-FAM fluorescence.

The titrations were performed in a Horiba Jobin Yvon FluoroMax-P fluorimeter, using a 1.5-ml fluorescence cuvette (10×4 mm light path, type 119.004F-QS, Hellma) equipped with a magnetic stirring bar, at 20°C under constant stirring. The titration solution contained 25 nM 6-FAM-labelled DNA substrate (Table 3.10) in 1× PBS (Table 3.11) in a starting volume of 800 μl. Protein was added successively from a concentrated stock solution. After each addition of protein, the mixture was allowed to reach equilibrium for 1 min before measuring fluorescence. 6-FAM fluorescence was excited at 495 nm, and measured at the experimentally determined emission maximum of the DNA

substrate (between 515 and 518 nm) with an integration time of 1 s. Excitation and emission slit width were adjusted so that the signal was in the linear range of the photon counting multiplier (maximum 1.5×10^6 CPS). All measurements were performed in triplicate.

Data were normalised and fitted in Microsoft Excel$^®$ using a non-linear least squares fit algorithm with a single-site binding model,

$$K_\mathrm{d} = \frac{[P][D]}{[P \times D]}$$

(where K_d is the dissociation constant, $[P]$ is the concentration of protein, $[D]$ is the concentration of DNA, and $[P \times D]$ is the concentration of the complex). Dissociation constants are the result of global fits to triplicates, errors are the standard deviations of dissociation constants resulting from independent fits to the three measurements.

4 RESULTS

4.1 Crystal and Solution Structures of SMC Hinge Domains

4.1.1 The *Pyrococcus furiosus* SMC Hinge Domain

4.1.1.1 Cloning, Purification and Biochemical Characterisation

An expression construct of the PfuSMC protein was designed that spans the entire hinge domain including short stretches of the coiled-coil region (residues 488-667 of PfuSMC). The DNA fragment encoding the desired hinge domain construct was PCR-amplified from a pET-21b vector containing the full-length *P. furiosus smc* gene (kindly provided by Alfred Lammens) and inserted into the NdeI/XhoI sites of pET-21b, to be expressed with the vector-encoded C-terminal hexahistidine tag. The protein was produced recombinantly in *E. coli* and purified via heat denaturation of contaminating proteins, nickel chelate affinity chromatography, and gel filtration.

The purified protein was analysed by analytical size exclusion chromatography, SDS-PAGE, and dynamic light scattering (DLS) (Figure 4.1A-C). The protein is ≥95% pure as judged by SDS-PAGE analysis (Figure 4.1B). It elutes from the analytical gel filtration column in two peaks: a minor peak corresponding to ~4% of the total peak volume and a molecular weight of 100 kDa according to the calibration of the column, and a major peak corresponding to a molecular weight of 45 kDa (Figure 4.1A). Since the theoretical molecular weight of the PfuSMC hinge domain construct is 21 kDa, the major peak most likely consists of homodimeric PfuSMC hinge domain, while the minor peak might be a tetramer or hexamer or an undefined larger aggregate. However, the fraction of this larger species is so small that it cannot be resolved by DLS: the intensity distribution reveals only one peak at a hydrodynamic radius of 3.4 nm with a relative standard deviation of 26%, indicating that the protein is reasonably homogeneous and monodisperse (Figure 4.1C).
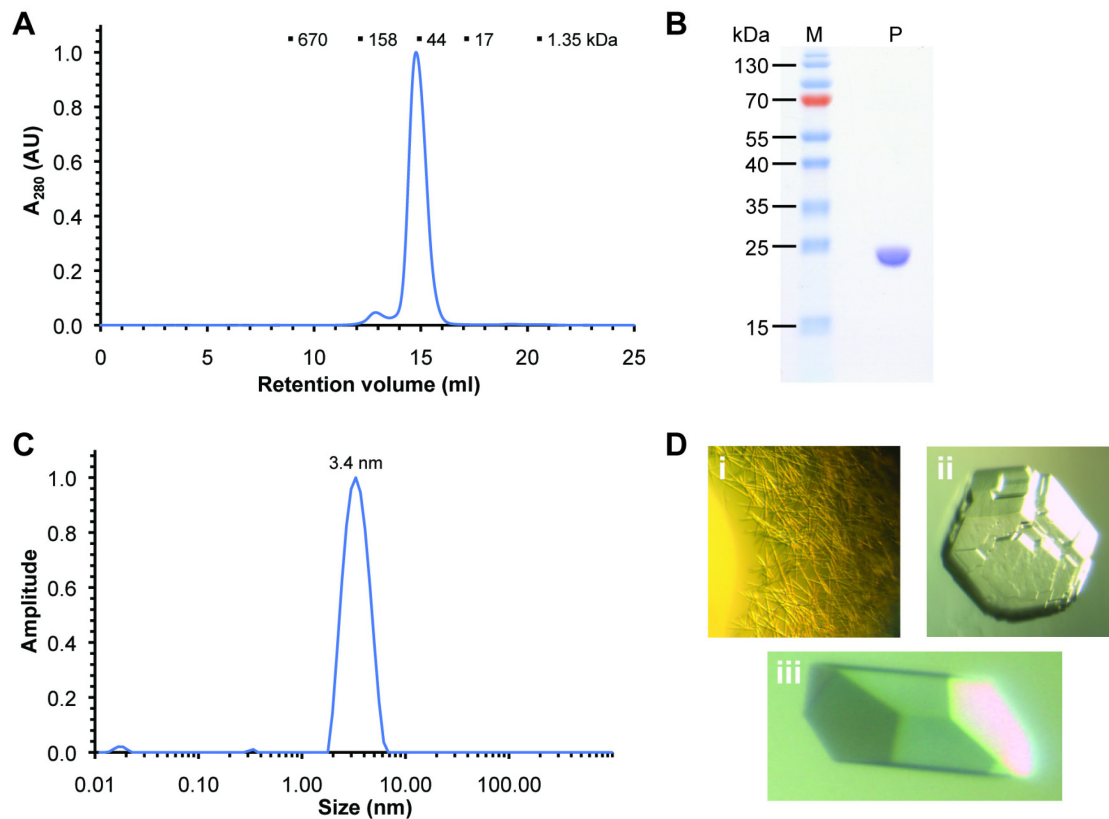
Figure 4.1. Purification and crystallisation of the PfuSMC hinge domain. (**A**) Analytical size exclusion chromatogram of the purified protein. 100 µl of 1 mM protein were separated on a Superdex 200 10/300 GL column (GE Healthcare) in 5 mM Tris-HCl pH 8.0, 100 mM NaCl, 0.1 mM EDTA. Above the chromatogram, the elution volumes of standard proteins are indicated with their molecular weights. (**B**) SDS-PAGE analysis of the purified protein. The sample was separated on a 15% SDS polyacrylamide gel and stained with Coomassie Brilliant Blue R-250 (Carl Roth). M, molecular weight marker; P, PfuSMC hinge domain. The molecular weight of selected marker bands is indicated. (**C**) Intensity distribution determined from dynamic light scattering analysis of the purified protein at a concentration of 5 mg/ml. The hydrodynamic radius of the major peak is indicated. (**D**) Crystals of the PfuSMC hinge domain: (**i**) initial crystals obtained in a commercially available screen (condition: 2 M ammonium sulphate, 0.1 M sodium acetate pH 4.6); (**ii**) multiple intergrown crystals obtained initially upon optimisation (condition: 2.2 M ammonium sulphate, 0.1 M sodium citrate, 7% (v/v) glycerol); (**iii**) crystal obtained in the final refined condition (1.8 M ammonium sulphate, 0.2 M potassium-sodium tartrate, 0.1 M trisodium citrate pH 6.0).

4.1.1.2 Crystallisation and Structure Determination

In initial screens, the PfuSMC hinge domain crystallised in several similar conditions containing ammonium sulphate and sodium citrate or acetate (Figure 4.1D i). However, upon optimisation most conditions did not yield single crystals but multiple intergrown crystals that could not be separated (Figure 4.1D ii). These crystals diffracted to 1.7 Å

resolution, but due to the superposition of diffraction patterns from multiple crystal lattices the data could not be integrated. Finally, a crystallisation condition was identified that yielded regular single crystals (Figure 4.1D iii). The condition was optimised with selenomethionine-labelled protein which proved to crystallise more readily than native protein. Selenomethionine derivative crystals belong to space group $C222_1$ with two molecules in the asymmetric unit and diffracted to 1.7 Å resolution at beamline PXI of the Swiss Light Source (SLS) (Figure 4.2A). Phases were determined from a MAD dataset. The resulting electron density map was easily interpretable (Figure 4.2B). The model was built manually and refined against the high remote wavelength dataset of the selenomethionine derivative. After several cycles of model building and refinement, the final R factors were 19.4% for R_{work} and 23.5% for R_{free}. In the final model, one chain spans residues 488 – 667, while the other chain encompasses residues 488 – 662. The geometry of both chains is well within acceptable range. Crystallographic data, phasing and refinement statistics are summarised in Table 4.1. An example of the initial and refined electron density can be found in Figure 4.2C.
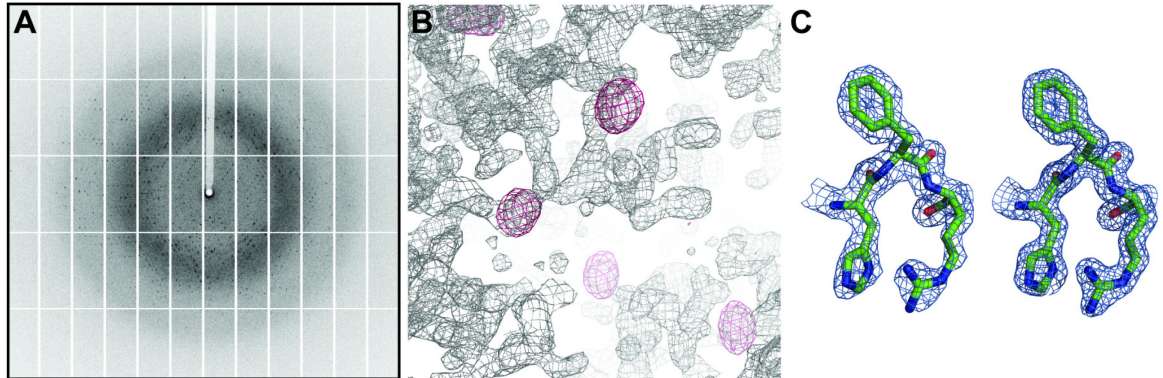
Figure 4.2. Diffraction pattern and electron density of the PfuSMC hinge domain crystals. (**A**) Diffraction pattern of the PfuSMC hinge domain crystals. An exemplary image from the high remote wavelength dataset of the selenomethionine derivative crystals recorded at SLS beamline PXI is shown. (**B**) Section of the experimental electron density map contoured at 1.5 σ (grey mesh) with anomalous difference density contoured at 3.5 σ (pink mesh). (**C**) Electron density around residues H^{653}-F^{654}-R^{655} of PfuSMC in the crystal structure of the PfuSMC hinge domain (residues 488 – 667 of PfuSMC). Left panel: experimental electron density contoured at 1.5 σ; right panel: final $2F_o$-F_c electron density contoured at 1.5 σ. Residues are shown as stick models with carbon atoms coloured green, nitrogen blue, and oxygen red.

Table 4.1. Crystallographic data, phasing and refinement statistics for the PfuSMC hinge domain structure. Data were collected at beamline PXI of the SLS. The values given in parentheses are for the highest resolution shell. Friedel mates were treated as independent reflections. The high remote wavelength dataset was used for refinement. The R_{free} factor was calculated from 10% of the data which were removed at random before the structure was refined. Ramachandran statistics were calculated with RAMPAGE (276).

Dataset	peak	inflection	high remote
wavelength (Å)	0.9788	0.9794	0.9778
space group	C222$_1$	C222$_1$	C222$_1$
unit cell dimensions (Å, a/b/c)	69.79 / 118.88 / 82.83	69.87 / 119.06 / 83.00	69.71 / 118.65 / 82.64
unit cell angles (°, α/β/γ)	90.0 / 90.0 / 90.0	90.0 / 90.0 / 90.0	90.0 / 90.0 / 90.0
redundancy	6.8 (6.6)	6.8 (6.6)	6.7 (6.5)
R_{sym} (%)	4.7 (34.9)	5.2 (44.1)	4.6 (33.4)
resolution (Å)	35.0-1.8 (1.9-1.8)	35.0-1.8 (1.9-1.8)	35.0-1.7 (1.8-1.7)
completeness (%)	99.1 (95.5)	99.0 (94.9)	99.3 (96.8)
I/σI	24.18 (4.77)	21.73 (3.91)	24.09 (4.73)
phasing power (acentric-anomalous)	2.161	0.832	1.776
R_{Cullis} (acentric-anomalous)	0.60	0.88	0.65
Figure of merit (acentric)	0.42		

Refinement

Dataset	high remote
number of reflections used in refinement	38 167
resolution (Å)	34.0-1.7
Model R_{work}/R_{free} (%)	19.4 / 23.5
protein nonhydrogen atoms	2840
water molecules	251
overall B factor (Å^2)	
all atoms	29.5
protein main and side chains	29.0
water	36.1
rms deviation from ideal geometry	
bonds (Å)	0.006
angles (°)	0.991
Ramachandran statistics (%) most favoured/allowed/disallowed regions	97.7 / 2.3 / 0.0

4.1.1.3 Crystal Structure of the **P. furiosus** *SMC Hinge Domain*

The PfuSMC hinge domain comprises two pseudo-two-fold-symmetric subdomains, each consisting of a three- or four-stranded mixed β-sheet sandwiched between α-helices. The subdomains interact such that a half-ring structure is created with an α-helical core, flanked by the β-sheets and one or two outer helices on both sides (Figure 4.3A and Figure 4.5A and B). A long ordered loop passing along the bottom face of the hinge domain, that is the face opposite the coiled-coil, links the two subdomains. As can be seen in a sequence alignment of SMC hinge domains from all three phylogenetic domains, this loop, located between β-strand 3 and α-helix F of the PfuSMC hinge, is the part of the hinge domain which displays the highest variability in both sequence and length (Figure 4.5A and B).
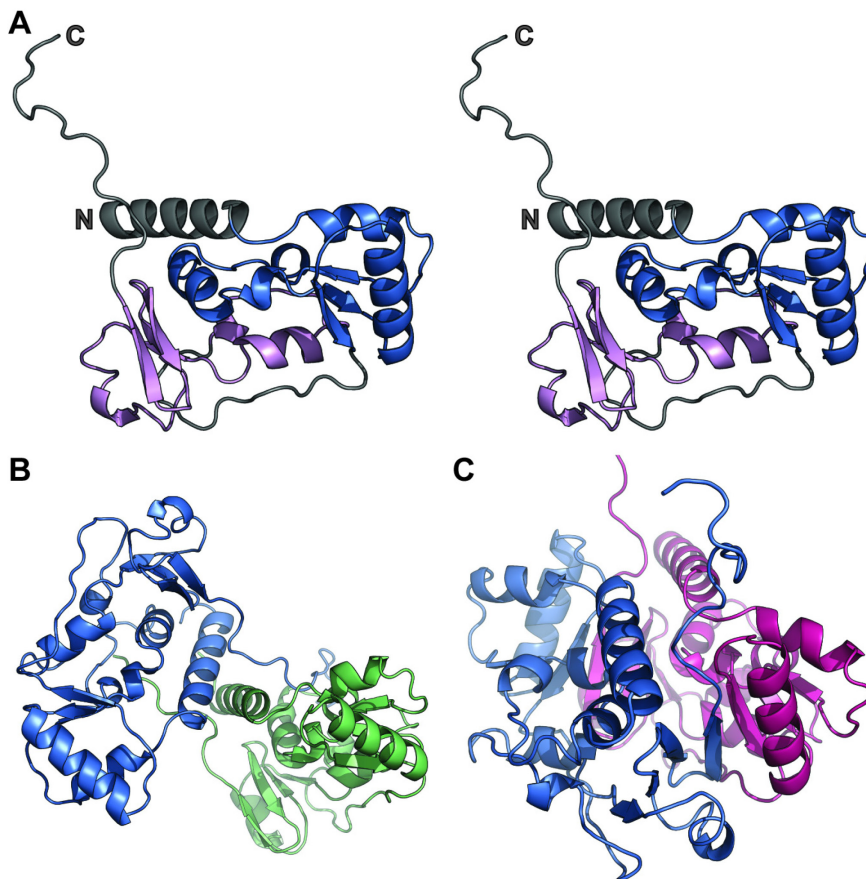
Figure 4.3. Crystal structure of the PfuSMC hinge domain. (A) Stereo view of the PfuSMC hinge domain monomer in cartoon representation, coloured by subdomains. The N-terminal subdomain is coloured blue, the C-terminal subdomain violet. The N and C-terminal segments predicted to belong to the coiled-coil region and the loop connecting the subdomains are coloured grey. **(B)** The dimer present in the asymmetric unit of the PfuSMC hinge domain crystals. Chain A is shown in blue, chain B in green. **(C)** The symmetry-generated dimer of the PfuSMC hinge domain. Chain A is shown in blue, chain A' in pink.

Unexpectedly, the predicted coiled-coil segments at the N and C terminus of the PfuSMC hinge do not join up into a coiled-coil. Instead, the N-terminal coiled-coil segment folds into a helix that is lying on top of the hinge domain core, while the C-terminal segment forms a long loop (Figure 4.3A). This conformation appears to be stabilised by crystal contacts: the N-terminal helices of both chains in the asymmetric unit contact each other, and the C-terminal coiled-coil segment of one chain loops around the other chain (Figure 4.3B). Since the coiled-coil segments are short – consisting of only four or five helical turns – the interaction between them is probably not very strong and therefore easily disrupted by crystal packing forces.

In crystals, the TmaSMC (15) and the *E. coli* MukB (93,94) hinge domains form two-fold-symmetric doughnut-shaped homodimers. The two chains present in the asymmetric unit of the PfuSMC hinge domain crystals assemble in a different manner, interacting via the predicted coiled-coil segments (Figure 4.3B), but the doughnut-shaped dimer is generated by symmetry operators (Figure 4.3C). In this symmetry-generated dimer, the two symmetrical interfaces between the monomers are formed largely by β-strand 3 of one monomer interacting with β6 and β7 of the other monomer to form two continuous mixed seven-stranded β-sheets (β1-3 + β4-7). Additional dimer interactions are contributed by helices αE and αH which flank the β-sheets on the outside (Figure 4.3C, Figure 4.4 and Figure 4.5A and B). The residues making up this dimer interface are among the most conserved residues in the hinge domains of SMC proteins from all three phylogenetic domains, suggesting that this dimeric assembly is the physiologically relevant oligomeric state of the SMC hinge domain (Figure 4.5A).
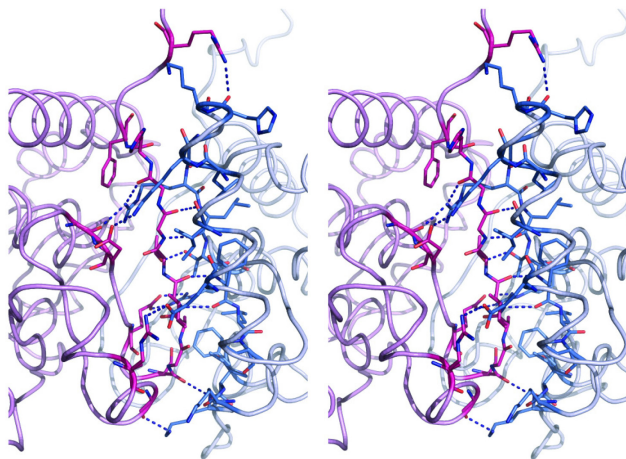
Figure 4.4. Stereo view of the dimer interface between the symmetry-related chains in the PfuSMC hinge domain crystal structure. Residues contributing to the subunit interaction are shown as stick models with carbon atoms coloured blue and pink for chain A and chain A', respectively, nitrogen dark blue, and oxygen light red. The protein backbone is depicted as ribbon model in light blue and violet for chain A and chain A', respectively. Hydrogen bonds are represented by dashed blue lines.

A

```
                   coil                          A              1     B              C          D      2
PfuSMCh    488      497       507       517       527       537       547
PfuSMCh    ELESSERELIAAEAQREVRGNRAAEEL..KRSGIGGIYGTLAELIKVKDEAYALAIEVALGNRADNVVVE
TmaSMCh    REIQFEKEMIERDMREYRGFSRAVRAVFEEKERFPGLVDVVSNLIEV.DEKYSLAVSVLLGGTAQNIVVR
BsuSMCh    QQARSKKDMLETMQGDFSGFYQGVKEVLKAKERLGGIRGAVLELIST.EQKYETAIEIALGASAQHVVTD
ScSMC2h    YQTCKNSEYLKRRVTNLEFNYTKPYPNF.EASFVHGVVGQLFQ.IDNDNIRYATALQTCAGGRLFNVVVQ
mSMC2h     NNLKGKHEALLAKFPNLQFAYKDPEKNW.NRNSVKGLVASLIN.VKDNST..ATALEVVAGERLYNVVVD
ScSMC4h    HRQRAMEARSSLSKAQNKSKVLTALSRLQKSGRINGFHGRLGD.LGVIDDSFDVAISTAC.PRLDDVVVD
mSMC4h     LFQKVEEAKSSLAMNRSRGKVLDAIIQEKKSGRIPGIYGRLGD.LGAIDEKYDIAISSCC.HALDYIVVD
consensus>50 .q...e.e.......n.................ri.Gi.g.l.#.i....de.y..Aiev..g.rldn!Vvd
```

```
TmaSMCh            coil                          A              1     B              C          D      2
                         E                    3                          E                 F          G
                   557       567       577       587                     597       607
PfuSMCh    DELVAEKAIKYLKEHKLGRLTFPLNKIKPKHV..........DSSVGLPAVDVIEY.DQKIENAVKF
TmaSMCh    NVDTAKAIVEFLKQNEAGRVTILPLDLIDGSFNRISGLEN.....ERGFVGYAVDLVKF.PSDLEVLGGF
BsuSMCh    DEQSARKAIQYLKQNSFGRATFLPLSVIRDRQLQSRDAETAAR..HSSFLGVASELVTF.DPAYRSVIQN
ScSMC2h    DSQTATQLLE..RGRLRKRVTIIPLDKIYTRPISSQVLDLAKK.IAPGKVELAINLIRF.DESITKAMEF
mSMC2h     TEVTAKKLLE..KGELKRRYTIIPLNKISARCIAPETLRVAQNLVGPDNVHVALSLVDY.KPELQKGMEF
ScSMC4h    TVECAQHCIDYLRKNKLGYARFILLDRLRQF..NLQPIST.....PENVPRLFDLVKPKNPKFSNAFYS
mSMC4h     SIDTAQECVNFLKKHNIGIATFIGLDKMTVWAKKMSKIQT.....PENTPRLFDLVKVKNEEIRQAFYF
consensus>50 d.dtA...ieylk.n..gr.tfipLdki...........e.....p...v..a.dl!.f.d.....a..f
```

```
                         E    *               3                          F          G
                   617       627       637       647       657       667
                       4               H         5       6       7
PfuSMCh    ALGDTVIVNSMEEA....RPHIGKVRMVTIEGELYERSGAITGGHFRARGLAVDTTKLR
TmaSMCh    LFGNSVVVETLDDAIRMKKKYRLNTRIATLDGELISGRGAITGGREERSSNVFERRIKL
BsuSMCh    LLGTVLITEDLKGANELAKLLGHRYRIVTLEGDVVNPGGSMTGGAVKKKNNSLLGRSRE
ScSMC2h    IFGNSLICEDPETAKKITFHPKIRARSITLQGDVYDPEGTLSGGSRNTSESLLVDIQKY
mSMC2h     VFGTTFVCNNMDNAKKVAFDKRIMTRTVTLGGDVFDPHGTLSGGARSQAASILTKFQEV
ScSMC4h    VLRDTLVAQNLKQANNVAYGK.KRFRVVTVDGKLIDISGTMSGGGNHVAKGLMKLGTNQ
mSMC4h     ALRDTLVANNLDQATRVAYQRDRRWRVVTLQGQIIEQSGTMSGGGSKVMRGRMGSSVID
consensus>50 .lgdtl!.#nldqA..vaf....r.RivTleGdvid..GtmsGG........l......
                       4               H         5       6       7                coil
```

B

C

Figure 4.5. Sequence alignment and topology diagram of the PfuSMC hinge domain. (**A**) Sequence alignment of the hinge domains of bacterial, archaeal and eukaryotic condensin SMC proteins. Pfu, *P. furiosus*; Tma, *T. maritima*; Bsu, *B. subtilis*; Sc, *S. cerevisiae*; m, *Mus musculus*. Numbering of residues is for PfuSMC. The secondary structure of the PfuSMC hinge domain is shown above the alignment, that of the TmaSMC hinge domain (pdb 1GXL) (15) be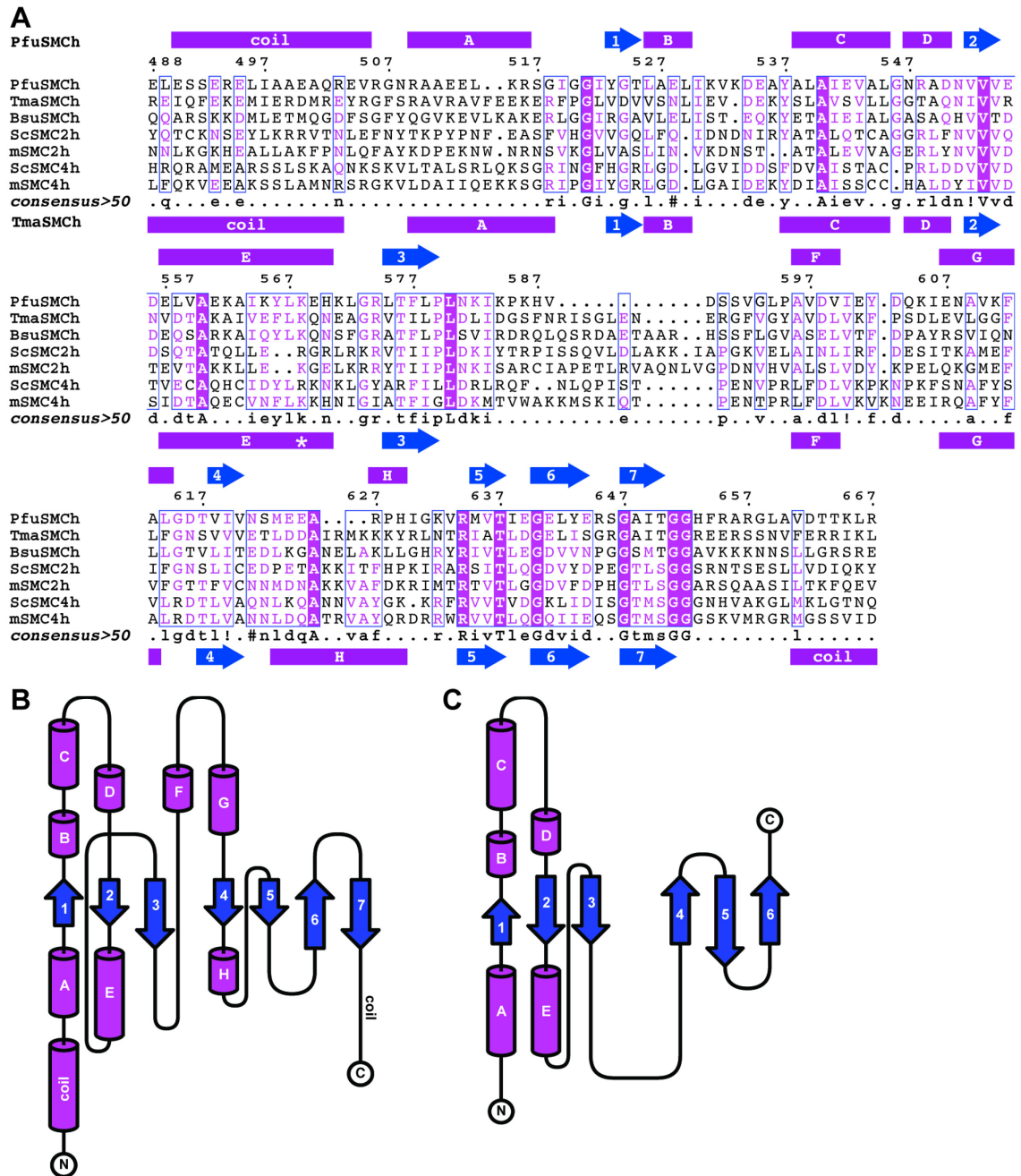low, with α-helices displayed as purple rectangles and β-strands as blue arrows. The asterisk marks the only lysine among many in the SMC hinge domain that is highly conserved (PfuSMC K[568]). In the consensus sequence, lower case letters are used ≥50%, upper case letters for ≥90% conservation; ! is any one of IV, and # is any one of NDQE. The alignment was generated with MultAlin (249). (**B**) Topology diagram of the PfuSMC hinge domain. (**C**) Topology diagram of the *E. coli* MukB hinge domain (pdb 2WMM) (93), omitting the N and C-terminal coiled-coil helices. In (B) and (C), α-Helices are depicted as purple barrels, β-strands as blue arrows. The diagrams were generated with TopDraw (291).

The doughnut-shaped dimer has a mostly negatively charged outer surface with a basic patch at the dimer interface, while the inner surface of the hinge domain dimer is mostly positively charged (Figure 4.6).
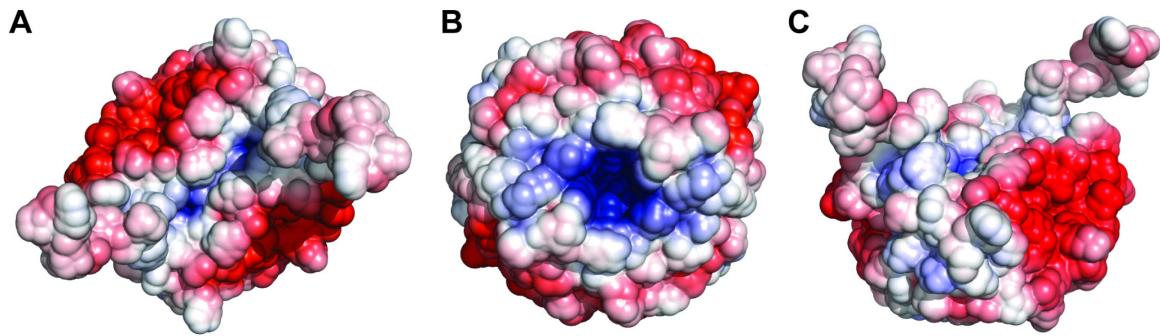

Figure 4.6. Electrostatic surface potential of the PfuSMC hinge domain dimer. Positively charged regions are coloured blue, negatively charged regions red, and neutral regions white. (**A**) View onto the top face, that is the side from which the coiled-coils emerge; (**B**) view onto the bottom face; (**C**) view from the side onto the dimer interface.

4.1.1.4 Similarity Between the P. furiosus and Other Prokaryotic SMC Hinge Domains

The tertiary structure of the archaeal PfuSMC hinge domain is very similar to that of the bacterial TmaSMC hinge (15) (Figure 4.7A). All secondary structure elements of the hinge domain core are conserved between bacteria and archaea (Figure 4.5A), and the rms deviation between the Cα traces of both proteins is 2.0 Å. Although the predicted coiled-coil segments of the PfuSMC and the TmaSMC hinge domain constructs are of the same length, they only form a coiled-coil in the TmaSMC hinge domain structure. As mentioned above, the unexpected conformation of the coiled-coil segments in the PfuSMC hinge domain crystals seems to be stabilised by crystal contacts. Since the intermolecular contacts in the TmaSMC hinge domain crystals were different, the coiled-coils could form in this case.

In both the PfuSMC and the TmaSMC hinge domain doughnut-shaped dimers there is a large central hole with a diameter of ~10 Å. In contrast, in the *E. coli* MukB hinge domain dimer there is no such central hole, and the entire hinge domain is significantly smaller than those of the PfuSMC and TmaSMC proteins (93,94). However, despite the substantial difference in size and large sequence divergence, the structure of the MukB hinge domain is quite similar to that of the PfuSMC hinge, as can be seen in their superposition in Figure 4.7B. The rms deviation between the Cα traces of both proteins is

3.0 Å. Interestingly, while the N-terminal subdomains of both hinges match almost perfectly, only the β-sheet of the C-terminal subdomain is present in the *E. coli* MukB hinge, but the α-helices are missing completely, being replaced by short loops, so that in fact no subdomains are discernible in the *E. coli* MukB hinge (see also the topology diagrams in Figure 4.5B and C).
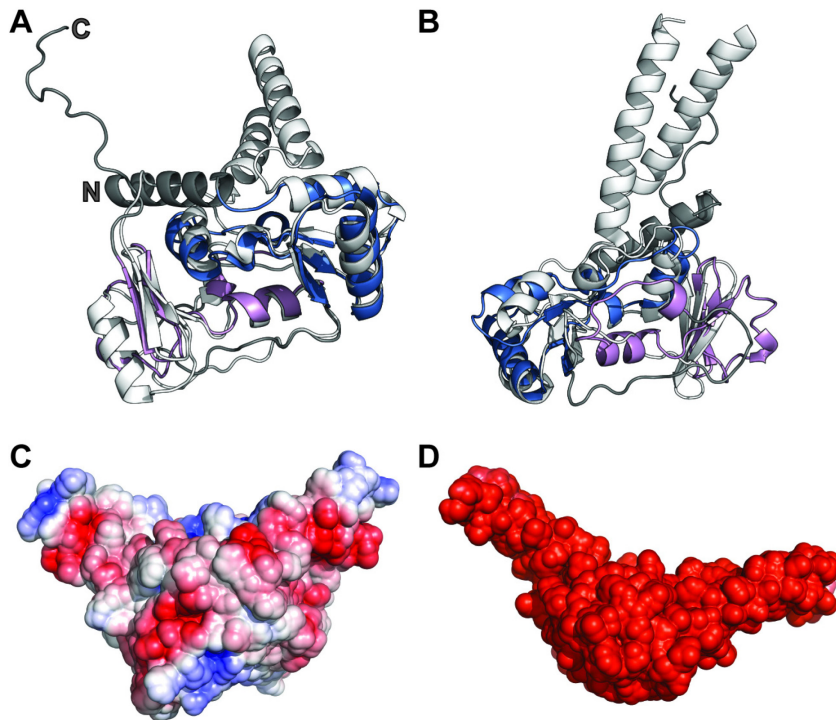
Figure 4.7. Comparison of the PfuSMC hinge domain structure with other prokaryotic SMC hinge domains. (**A**) Superposition of the PfuSMC hinge domain monomer with the TmaSMC hinge domain (pdb 1GXL) (15). The PfuSMC hinge domain is coloured by subdomains, with the N-terminal subdomain shown in blue, the C-terminal subdomain in violet, and the coiled-coil region and the loop connecting the subdomains coloured grey. The TmaSMC hinge domain is shown in white. (**B**) Superposition of the PfuSMC hinge domain monomer (coloured as in (A)) with the *E. coli* MukB hinge domain (shown in white; pdb 2WMM) (93). (**C**) Electrostatic surface potential of the TmaSMC hinge domain dimer (pdb 1GXL) (15), view onto the dimer interface. (**D**) Electrostatic surface potential of the *E. coli* MukB hinge domain dimer (pdb 2WMM) (93), view onto the dimer interface. In (C) and (D), positively charged regions are coloured blue, negatively charged regions red, and neutral regions white.

The surface charge distributions of the PfuSMC and TmaSMC hinge domains are similar, with a basic patch at the dimer interface surrounded by a mostly acidic outer surface (Figure 4.7C). However, the TmaSMC hinge domain is overall slightly more acidic, and the basic patch is also smaller than in the PfuSMC hinge and shifted more towards the

bottom face of the domain. The *E. coli* MukB hinge domain dimer on the other hand displays a completely negatively charged outer surface (Figure 4.7D). Although it is hard to believe that the MukB hinge is indeed as negatively charged as determined by APBS (278), its theoretical isoelectric point is 4.4, as compared to 5.9 and 5.5 for the PfuSMC and TmaSMC hinge domains, respectively (261).

4.1.1.5 Solution Scattering Analysis of the P. furiosus *SMC Hinge Domain*

To unambiguously determine whether the doughnut-shaped dimer of the SMC hinge domain is the biological assembly present in solution, SAXS experiments were performed with the PfuSMC hinge domain. The SAXS data are of very high quality, as the protein did not show any signs of aggregation even at concentrations of up to 20 mg/ml (Figure 4.8A).
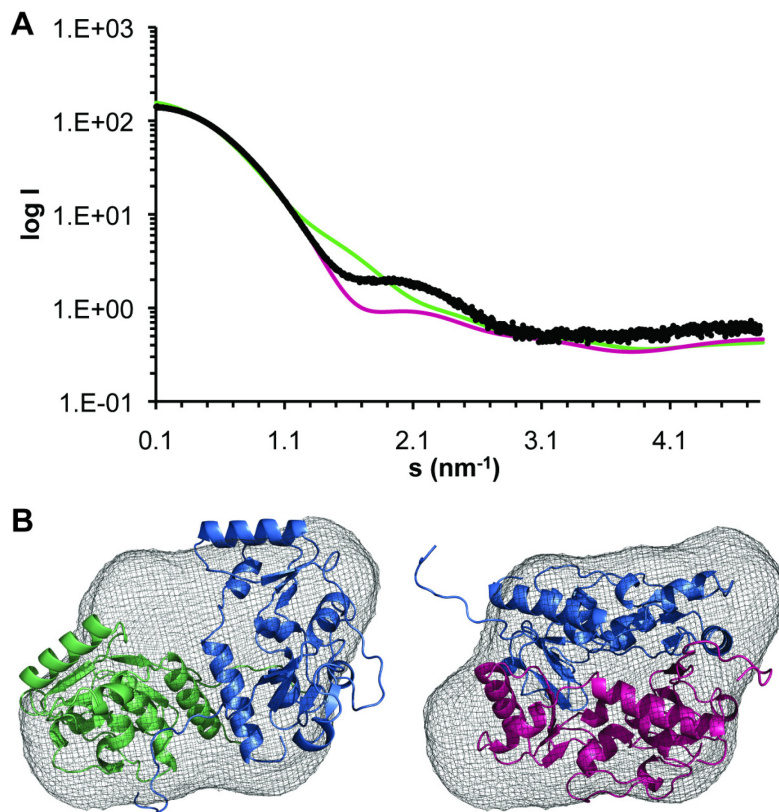
Figure 4.8. Solution scattering analysis of the PfuSMC hinge domain. (**A**) SAXS profiles of the PfuSMC hinge domain. The scattering profile of the protein in solution is shown in black, the theoretical scattering profiles of the dimer present in the asymmetric unit of the PfuSMC hinge domain crystals and the symmetry-generated dimer are shown in green and pink, respectively. (**B**) Solution envelope reconstruction of the PfuSMC hinge domain (grey mesh), superimposed with the dimer present in the asymmetric unit of the PfuSMC hinge domain crystals (left panel; chain A coloured blue, chain B green) and the symmetry-generated dimer (right panel; chain A coloured blue, chain A' pink).

The molecular mass determined from the scattering intensity extrapolated to zero angle confirms that the PfuSMC hinge domain exists as a homodimer in solution. The shape of the scattering profile indicates that this dimer has a globular conformation. To compare the solution to the crystal structure, theoretical scattering curves were calculated of both possible dimeric assemblies observed in the crystals (Figure 4.8A). The scattering profile of the dimer in the asymmetric unit does not fit the observed scattering profile at all; this dimer is more elongated than the dimer present in solution. The theoretical scattering profile of the symmetry-generated dimer, however, has the same shape as the observed profile, although the two profiles do not overlap completely. This is probably due to the conformation of the coiled-coil segments that is stabilised in the crystals, but likely to be flexible in solution, as would also be suggested by the solution envelope (see below, Figure 4.8B).

Initially, *ab initio* envelope reconstructions were calculated without imposing any symmetry. Since the resulting models were clearly two-fold symmetric, two-fold symmetry was then imposed to generate models of higher quality. Eight independent models were averaged to generate the final solution envelope model of the PfuSMC hinge domain into which both possible dimeric assemblies were docked (Figure 4.8B). The dimer present in the asymmetric unit is too narrow to fill the solution envelope completely and too long to completely fit into it. The symmetry-generated dimer however is docked into the SAXS model so that the hole in the ring coincides well with the depression in the envelope. Only the C-terminal coiled-coil segment does not fit into the envelope, which is not surprising, since it would be expected to be disordered in solution. The flexibility of the coiled-coil segments probably also accounts for the fact that the envelope is slightly bigger than the symmetry-generated dimer in the crystal structure. This agrees closely with the crystallographic results and is strong evidence that the biological assembly of the SMC hinge domain is indeed the doughnut-shaped dimer.

4.1.2 The Mouse Condensin Hinge Domain

4.1.2.1 *Cloning, Purification and Biochemical Characterisation*

Several mouse condensin hinge domain constructs of different lengths were created, two of which were analysed in detail. The longer of these two constructs, designated mSMC2h4h-l (residues 492 – 680 of SMC2, and 581 – 766 of SMC4), was designed to

contain a short stretch of coiled-coil at both ends, while the shorter one, mSMC2h4h-s (residues 506 – 666 of SMC2, and 595 – 752 of SMC4), does not contain any coiled-coil segments. DNA fragments encoding the desired hinge domain constructs were PCR-amplified from cDNA vectors and cloned into a modified bicistronic pET-21b vector. The *smc2* hinge fragment was inserted into the first cloning site directly downstream of the T7 promoter, and the *smc4* hinge fragment was cloned downstream of the second ribosome binding site to be expressed with the vector-encoded C-terminal hexahistidine tag (see Figure 7.1 for a vector map). In the long construct mSMC2h4h-l, the SMC2 subunit additionally carries an N-terminal Strep II tag added via the PCR primer. Both hinge domain constructs were produced recombinantly in *E. coli* and purified using nickel chelate affinity chromatography and gel filtration to yield stable heterodimeric SMC2-SMC4 hinge domains. Monomers were not observed during any stage of the purification of either construct, indicating that the dimer interaction is very strong.

The purified proteins were analysed by analytical size exclusion chromatography, SDS-PAGE, and DLS (Figure 4.9A-C). Both proteins are≥95% pure as judged by SDS -PAGE analysis (Figure 4.9B). While the two bands corresponding to the SMC2 and SMC4 subunits of the long construct mSMC2h4h-l are resolved on a 20% SDS polyacrylamide gel, both subunits of the short construct mSMC2h4h-s run at the same height. However, the retention volume on an analytical gel filtration column and the hydrodynamic radius of the protein determined by DLS (see below) strongly suggest that in mSMC2h4h-s both subunits are present at an equimolar ratio as well, and indeed they are both present in the crystals that were obtained of mSMC2h4h-s (chapter 4.1.2.2).

The long construct mSMC2h4h-l elutes from the analytical gel filtration column in two peaks, just like the PfuSMC hinge domain (chapter 4.1.1.1): a minor peak corresponding to ~15% of the total peak volume and a molecular weight of 60 kDa according to the calibration of the column, and a major peak corresponding to a molecular weight of 30 kDa (Figure 4.9A). The theoretical molecular weight of the mSMC2h4h-l heterodimer is 44 kDa, giving a ratio of observed to theoretical molecular weight of 0.7 for the major peak. Since this peak contains both the SMC2 and the SMC4 subunit, as revealed by SDS-PAGE analysis (Figure 4.9B), it most likely consists of the heterodimeric mouse condensin hinge domain, while the minor peak might be a tetramer or an undefined larger aggregate. However, the fraction of this larger species is too small to be resolved by DLS: the intensity distribution reveals only one peak at a hydrodynamic radius of 3.6 nm

with a relative standard deviation of 27%, indicating that the protein is reasonably homogeneous and monodisperse (Figure 4.9C).
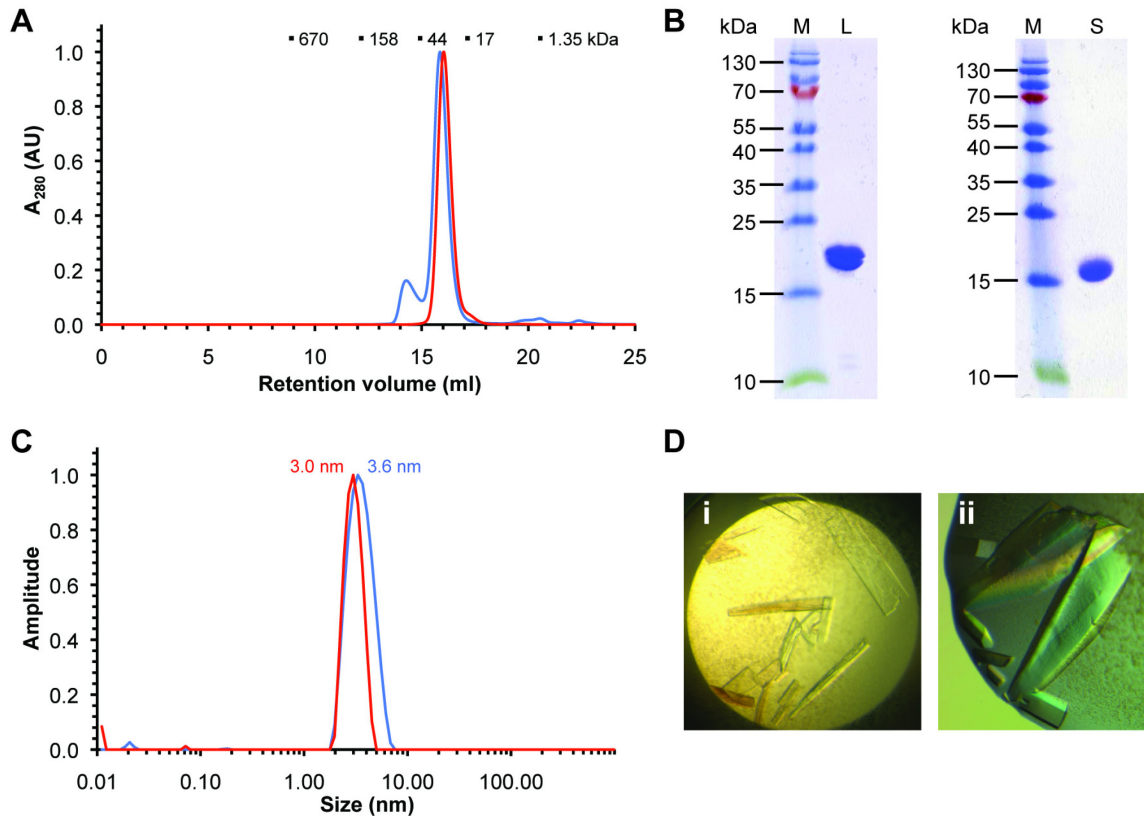

Figure 4.9. Purification and crystallisation of the mouse condensin hinge domain. (**A**) Analytical size exclusion chromatograms of the purified proteins mSMC2h4h-l (blue) and mSMC2h4h-s (red). 100 μl of 0.2 mM protein were separated on a Superdex 200 10/300 GL column (GE Healthcare) in 5 mM Tris-HCl pH 8.0, 100 mM NaCl, 0.1 mM EDTA. Above the chromatogram, the elution volumes of standard proteins are indicated with their molecular weights. (**B**) SDS-PAGE analysis of the purified proteins. The samples were separated on 20% SDS polyacrylamide gels and stained with Coomassie Brilliant Blue R-250 (Carl Roth). M, molecular weight marker; L, mSMC2h4h-l; S, mSMC2h4h-s. The molecular weight of selected marker bands is indicated. (**C**) Intensity distribution determined from dynamic light scattering analysis of the purified proteins mSMC2h4h-l (blue) and mSMC2h4h-s (red) at 5 mg/ml. The hydrodynamic radius of the major peak is indicated. (**D**) Crystals of the short mouse condensin hinge domain construct mSMC2h4h-s: (**i**) initial crystals obtained with native protein in a commercially available screen (condition: 20% (w/v) PEG 4000, 20% (v/v) isopropanol, 30% (v/v) glycerol, 0.1 M Tris-HCl pH 8.5); (**ii**) crystals obtained with selenomethionine-labelled protein in the final refined condition (15% (w/v) PEG 4000, 5% (v/v) isopropanol, 20% (v/v) glycerol, 0.1 M Tris-HCl pH 8.5).

The short construct mSMC2h4h-s elutes from the analytical gel filtration column in one peak with a retention volume only slightly bigger than that of the major peak of the longer

construct, corresponding to a molecular weight of 28 kDa (Figure 4.9A). The theoretical molecular weight of the mSMC2h4h-s heterodimer is 37 kDa, hence the ratio of observed to theoretical molecular weight is again 0.7, as for the long construct. Therefore this peak most likely consists of a heterodimer as well. DLS analysis shows one peak in the intensity distribution at a hydrodynamic radius of 3.0 nm with a relative standard deviation of 19%, implying that the short construct is not only smaller, but also more homogeneous and monodisperse than the long construct. However, when left at 20°C for longer periods of time, the short construct mSMC2h4h-s quickly started to aggregate, so that several peaks at large hydrodynamic radii appeared in the DLS intensity distribution, whereas the long construct mSMC2h4h-l remained stably monodisperse (data not shown).

The fact that the short construct is much more prone to aggregation than the long construct might explain why it crystallised so readily (chapter 4.1.2.2), while no crystals could be obtained of the long construct. In fact, the long construct mSMC2h4h-l is so soluble that even at concentrations of above 100 mg/ml the protein only precipitated in ~50% of screened crystallisation conditions. Protein concentrations from 10 to 110 mg/ml were tested in various sparse matrix and footprinting screens, but the protein either remained soluble or precipitated completely, and no crystalline precipitates were observed. Selenomethionine-labelled protein was screened as well since this derivative is often less soluble than native protein, and the construct contains eleven methionines. However, it behaved similarly to the native protein. Because of the large number of lysines in the protein (~8% of residues are lysines), reductive methylation of lysines (292) was also tried, but the small fraction of protein which did not precipitate during the methylation reaction behaved like native protein in crystallisation screens. Indeed, since the short construct mSMC2h4h-s contains a large number of lysines as well but crystallised readily, it was most likely not the lysines, but the flexible coiled-coil segments in mSMC2h4h-l which prevented crystal formation. Constructs with even longer coiled-coil segments tended to aggregate and be degraded during purification and behaved like mSMC2h4h-l in crystallisation screens and DNA-binding assays (chapter 4.2.1). They were therefore not analysed in detail.

Although all constructs bind DNA, cocrystallisation with double-stranded and single-stranded oligonucleotides of different lengths was unsuccessful, probably because DNA binding is not strong enough and not sequence specific (chapter 4.2.1).

4.1.2.2 Crystallisation and Structure Determination

In initial screens, the short construct mSMC2h4h-s crystallised in several similar conditions containing polyethylene glycol of different sizes and often isopropanol (Figure 4.9D i). Crystals could easily be reproduced and optimised both with native and selenomethionine-labelled protein (Figure 4.9D ii). The crystals belong to space group $P2_1$ with one heterodimer in the asymmetric unit. With a maximum resolution of 1.5 Å at beamline PXI of the SLS (Figure 4.10A), the selenomethionine derivative crystals diffracted to higher resolution than native ones and allowed phase determination by SAD. The resulting electron density map was of very high quality (Figure 4.10B) so that ~90% of the model could be built automatically. After several cycles of manual model building and refinement, the final R factors were 14.3% for R_{work} and 17.3% for R_{free}. The final model spans residues 506 – 660 of SMC2 and residues 595 – 752 of SMC4 including the entire hexahistidine tag, and has good geometry. Crystallographic data, phasing and refinement statistics are summarised in Table 4.2. An example of the initial and refined electron density can be found in Figure 4.10C.
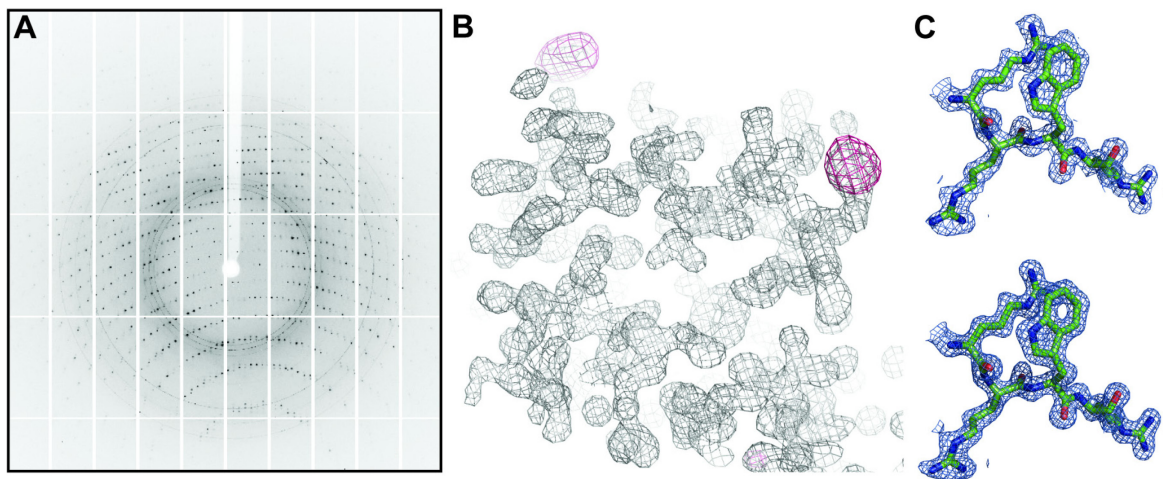
Figure 4.10. Diffraction pattern and electron density of the mouse condensin hinge domain crystals. (**A**) Diffraction pattern of the mSMC2h4h-s crystals. An exemplary image from the peak wavelength dataset of the selenomethionine derivative crystals recorded at SLS beamline PXI is shown. (**B**) Section of the experimental electron density map contoured at 1.5 σ (grey mesh) with anomalous difference density contoured at 3.5 σ (pink mesh). (**C**) Electron density around residues R^{731}-R^{732}-W^{733}-R^{734} of mSMC4 in the crystal structure of the mouse condensin hinge domain (residues 506 – 666 of mSMC2, and 595 – 752 of mSMC4). Top panel: experimental electron density contoured at 1.5 σ; bottom panel: final $2F_o$-F_c electron density contoured at 1.5 σ. Residues are shown as stick models with carbon atoms coloured green, nitrogen blue, and oxygen red.

Table 4.2. Crystallographic data, phasing and refinement statistics for the mouse condensin hinge domain structure. Data were collected at beamline PXI of the SLS. The values given in parentheses are for the highest resolution shell. Friedel mates were treated as independent reflections. The R_{free} factor was calculated from 10% of the data which were removed at random before the structure was refined. Ramachandran statistics were calculated with RAMPAGE (276).

wavelength (Å)	0.9776
space group	$P2_1$
unit cell dimensions (Å, a/b/c)	33.5 / 96.7 / 54.5
unit cell angles (°, $\alpha/\beta/\gamma$)	90.0 / 92.8 / 90.0
redundancy	3.3 (3.1)
R_{sym} (%)	3.9 (8.6)
resolution (Å)	29.13-1.51 (1.60-1.51)
completeness (%)	96.5 (90.6)
$I/\sigma I$	21.4 (11.7)
phasing power (acentric-anomalous)	1.58
R_{Cullis} (acentric-anomalous)	0.68
Figure of merit (acentric)	0.41
number of reflections used in refinement	53 947
Model R_{work}/R_{free} (%)	14.3 / 17.3
protein nonhydrogen atoms	2646
water molecules	379
glycerol molecules	6
overall B factor (Å^2)	
all atoms	17.1
protein main and side chains	15.1
water	28.9
glycerol	34.6
rms deviation from ideal geometry	
bonds (Å)	0.006
angles (°)	0.949
Ramachandran statistics (%) most favoured/allowed/disallowed regions	99.4 / 0.6 / 0.0

4.1.2.3 Crystal Structure of the Mouse Condensin Hinge Domain

The SMC2 and SMC4 hinge subunits assemble into a heterodimer. Each subunit forms a half-ring structure with an α-helical core that is bordered by a mixed β-sheet on both sides (Figure 4.11A). The β-sheets are then flanked on the outside by one or two α-helices. Like the PfuSMC (chapter 4.1.1.3) and the TmaSMC hinge domain (4), both subunits consist of two subdomains linked by a long but ordered loop that passes along the bottom face of the hinge, that is the face on the opposite side of the coiled-coil (Figure 4.11A).
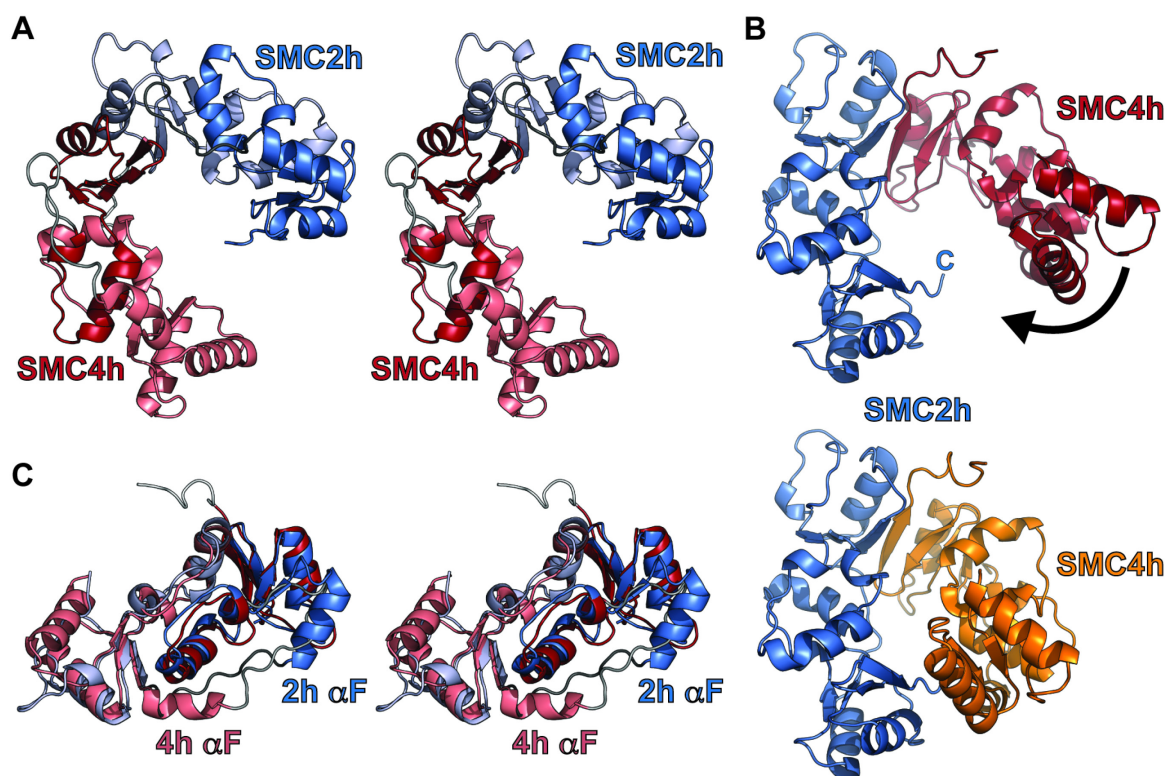
Figure 4.11. Crystal structure of the mouse condensin hinge domain. (**A**) Stereo view of the SMC2-SMC4 hinge domain, as seen from the bottom face, that is the face on the opposite side of the coiled-coil, coloured by subdomains. The SMC2 subunit is coloured in shades of blue, the SMC4 subunit in shades of red, with the N-terminal subdomain shown in the lighter shade. The long loop connecting the subdomains is shown in dark and light grey for SMC2 and SMC4, respectively. The hexahistidine tag on the C-terminus of the SMC4 hinge is coloured white. (**B**) The SMC2-SMC4 hinge domain heterodimer as seen from the top face, in the open and closed conformation. The top panel shows the open conformation found in the crystal structure, the bottom panel depicts the model of the closed conformation, generated by separately superposing the SMC2 and SMC4 subunits with the TmaSMC hinge domain dimer (pdb 1GXL) (15). The SMC2 subunit is shown in blue, the SMC4 subunit in red and orange for the open and closed conformation, respectively. (**C**) Superposition of the SMC2 and SMC4 subunit, shown in stereo. The colour scheme is the same as in (A).

This loop lies between β-strand 3 and α-helix F of the SMC2 hinge, and between helices F and G of the SMC4 hinge (see the sequence alignment and topology diagram in Figure 4.12).

The PfuSMC, the TmaSMC (15) and the *E. coli* MukB (93,94) hinge domains form two-fold-symmetric doughnut-shaped homodimers via two dimerisation interfaces. However, the SMC2 and SMC4 hinge dimerise via only one interface and thus do not adopt the expected doughnut-shape (Figure 4.11A and B). The subunit interface is made up largely by two interacting β-strands, namely mSMC2h β3 and mSMC4h β7, to form a continuous mixed seven-stranded β-sheet (mSMC2h β1-3 + mSMC4h β4-7). Additional dimer interactions are contributed by helices αE of mSMC2h and αI of mSMC4h which flank the β-sheet on the outside (Figure 4.11A and B, Figure 4.12).

At the opposite side of the half-rings, the SMC2 hinge has a four-stranded and the SMC4 hinge a three-stranded mixed β-sheet (mSMC2h β4-7, mSMC4h β1-3), but these do not interact in the crystals (Figure 4.11A and B). In fact, the angle between the two subunits is much wider than in the PfuSMC and TmaSMC hinge homodimer (15), the hinge being thus bent along the intact interface to open up the ring at the opposite side. Superposition with one of the prokaryotic SMC hinge homodimers reveals the probable reason for this partially open conformation: it seems that the SMC2 hinge is missing the last C-terminal β-strand that would be the one to interact with the outermost β-strand of the SMC4 hinge (β3) to form a pseudo-two-fold symmetric dimer. The residues that are predicted to make up this β-strand are part of the crystallised construct, but are evidently disordered. SAXS analysis (chapter 4.1.2.5) suggests that the SMC2-SMC4 hinge can also adopt a closed, doughnut-shaped structure which is presumably stabilised by the coiled-coil domains missing in the crystallised construct. There are no apparent crystal contacts that could have forced the hinge domain into this open conformation.

The expected "closed" conformation was modelled by separately superposing the SMC2 and SMC4 subunit of the mouse condensin hinge structure with the TmaSMC hinge domain dimer (Figure 4.11B). While this model produces some clashes at the intact interface and therefore obviously does not perfectly represent the biologically relevant closed conformation, it does show quite clearly that the C-terminal β-strand of the SMC2 hinge is indeed missing to close the ring. The structural similarity to the prokaryotic SMC hinge domains however strongly suggests that the subunit cores are correctly folded.
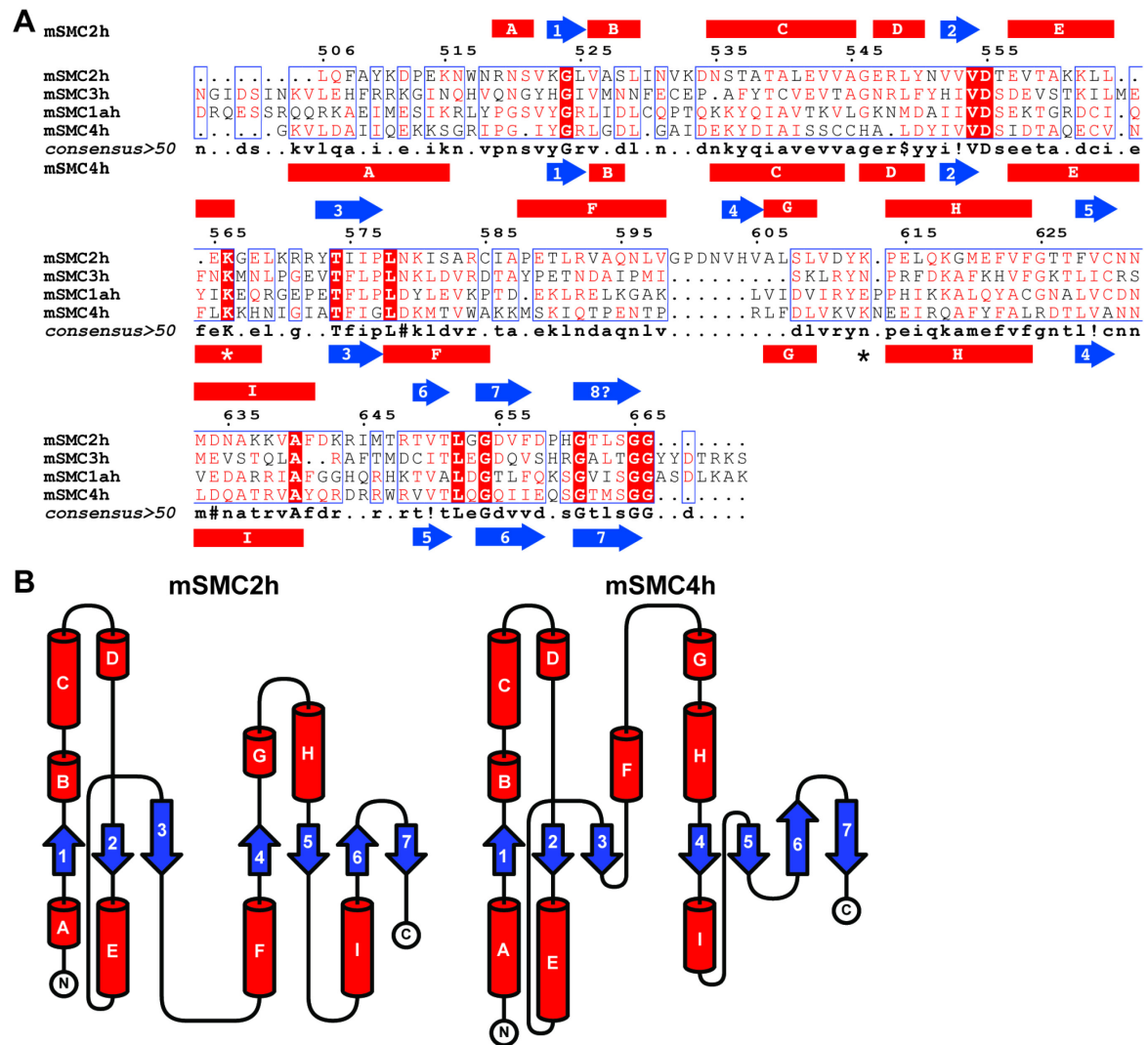
Figure 4.12. Sequence alignment and topology diagram of the mouse condensin hinge domain.
(**A**) Sequence alignment of the hinge domains of SMC1α, SMC2, SMC3, and SMC4 from mouse. Only residues present in the crystallised construct mSMC2h4h-s are shown for mSMC2 and mSMC4 (residues 506 – 666 of mSMC2, and 595 – 752 of mSMC4). Numbering of residues is for mSMC2. The secondary structure of the mSMC2 hinge domain is shown above the alignment, that of the mSMC4 hinge domain below the alignment. α-Helices are displayed as red rectangles, β-strands as blue arrows. The residues that probably form β8 of mSMC2 are invisible in the electron density. The asterisks mark mSMC2-K[566]/ mSMC4-K[657], and mSMC2-K[613]/ mSMC4-K[698]. In the consensus sequence, lower case letters are used for 50%, upper case letters for ≥90% conservatio n; ! is any one of IV, $ is any one of LM, and # is any one of NDQE. The alignment was generated with MultAlin (249). (**B**) Topology diagram of the mouse condensin hinge domain construct mSMC2h4h-s. α-Helices are depicted as red barrels, β-strands as blue arrows. The diagram was generated with TopDraw (291).

57

All rms deviations between the Cα traces of the PfuSMC, TmaSMC, and mSMC2 and mSMC4 hinge domains are below 3 Å (Table 4.3), and most secondary structure elements are conserved.

Table 4.3. Rms deviations between the Cα traces of the SMC hinge domains from *P. furiosus* (PfuSMCh), *T. maritima* (TmaSMCh; pdb 1GXL) (15), and mouse condensin (mSMC2h, mSMC4h).

	TmaSMCh	mSMC2h	mSMC4h
PfuSMCh	2.0 Å	1.4 Å	1.9 Å
TmaSMCh		2.2 Å	2.6 Å
mSMC2h			1.8 Å

While the mSMC2 hinge superimposes almost perfectly with the PfuSMC and TmaSMC hinge domains, the mSMC4 hinge domain displays notable differences in secondary structure as compared to its binding partner and the prokaryotic hinge domains (Figure 4.11C, Figure 4.12). In the mSMC2, PfuSMC and TmaSMC hinge domains, the N-terminal β-sheet merges directly into the long loop connecting the subdomains which terminates in a helix on the outside of the C-terminal β-sheet (mSMC2h αF). This helix is followed by a strand of the C-terminal β-sheet (mSMC2h β4). The mSMC2 and mSMC4 hinges have the same number of helices, but their F helices do not correspond to each other and are in completely different positions, flanking the C-terminal β-sheet in mSMC2h, and the helical core on the outside surface in mSMC4h. In the mSMC4 hinge, helix F lies between the N-terminal β-sheet and the connecting loop which terminates in helix G of the helical core, so that the C-terminal β-sheet of mSMC4h consists of one less strand than that of the mSMC2, PfuSMC and TmaSMC hinges (provided that the predicted C-terminal β-strand of mSMC2h is indeed formed).

Although the fold of the mouse condensin hinge is very similar to that of its prokaryotic counterparts, its surface charge distribution is strikingly different. The outer surface of the mouse condensin hinge is mostly basic to neutral (Figure 4.13), whereas prokaryotic SMC hinge domains have an acidic outer surface (Figure 4.6 and Figure 4.7C and D). The basic patch at the dimer interface is also much more pronounced in the condensin hinge than in the PfuSMC hinge domain.
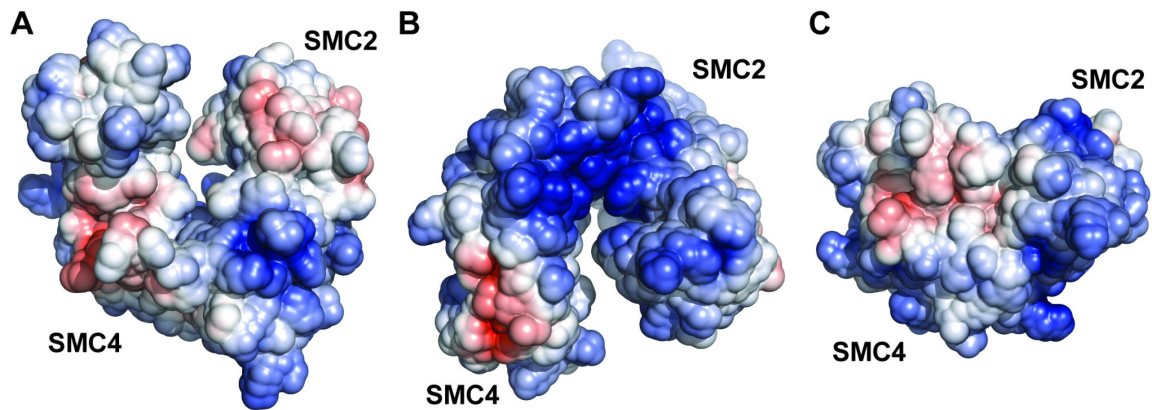
Figure 4.13. Electrostatic surface potential of the mouse condensin hinge domain. Positively charged regions are coloured blue, negatively charged regions red, and neutral regions white. (**A**) View onto the top face, that is the face from which the coiled-coils would emerge; (**B**) view onto the bottom face; (**C**) view from the side onto the closed interface.

4.1.2.4   Analysis of the SMC2-SMC4 Hinge Domain Interface

Most intersubunit contacts are formed by hydrophobic interactions, supported by few hydrogen bonds (Figure 4.14). It has long been unclear how eukaryotic SMC proteins specifically assemble into defined heterodimers (e.g. SMC1-SMC3, SMC2-SMC4), while prokaryotic SMC proteins form homodimers. Taking a closer look at the interface, the reason for dimerisation specificity is revealed. While most residues contributing to the interaction are conserved or replaced by similar residues within the subfamilies SMC2/SMC3 and SMC1α/SMC4 (293), the few non-conservative exchanges are apparently enough to make wrong pairing impossible.
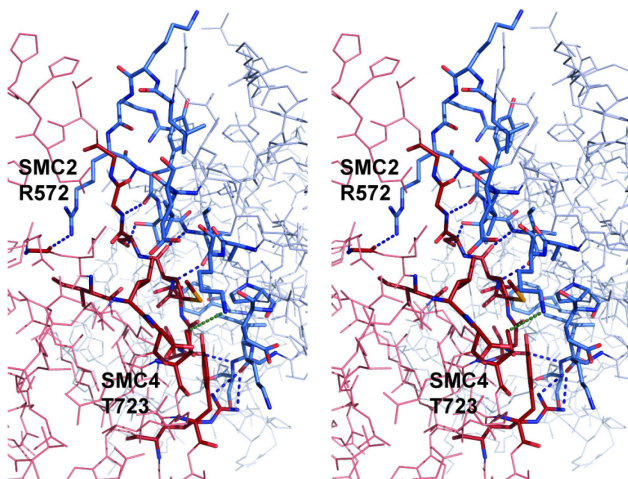
Figure 4.14. Stereo view of the interface between the mSMC2 and mSMC4 hinge. Residues contributing to the subunit interaction are shown as stick models with carbon atoms coloured blue and dark red for the SMC2 and SMC4 subunit, respectively, nitrogen dark blue, oxygen light red, and selenium orange. The surrounding residues are depicted as thin lines in light blue for SMC2, and rose for SMC4. Hydrogen bonds are represented by dashed blue lines. The 5.5 Å distance between SMC2-K^{561} and SMC4-T^{723} is indicated by a dashed green line.

For SMC2/SMC3, good candidate residues for dimerisation specificity within the N-terminal interface are $K^{570}R^{571}R^{572}$ of SMC2 which are replaced by $P^{582}G^{583}E^{584}$ in SMC3 (Figure 4.12A). These residues are placed in an otherwise conserved region, hence it is very likely that they are in similar positions in the SMC2 and SMC3 tertiary structures. Looking at the dimerisation interface, it is immediately obvious that the PGE sequence in SMC3 would not be able to form the same interactions with SMC4 as the KRR sequence in SMC2 (Figure 4.14). For example, SMC2-R^{572} forms a hydrogen bond with the backbone oxygen of SMC4-G^{740}. The shorter glutamate side chain in SMC3 could not support this interaction. Between the SMC4 and SMC1α C-terminal interface residues there is only one non-conservative exchange, namely SMC4-T^{723} for SMC1α-R^{626} (Figure 4.12A). Again, this residue is situated in an otherwise conserved region. Assuming that it therefore adopts a similar position in SMC1α as in SMC4, the arginine side chain would clash with K^{561} of SMC2, thus making it impossible for SMC1α to dimerise with SMC2. SMC3 on the other hand has a small threonine residue in place of SMC2-K^{561}, so that the SMC3 interface can accomodate the large side chain of SMC1α-R^{626}.

4.1.2.5   Solution Scattering Analysis of the Mouse Condensin Hinge Domain

To acquire structural information about the conformation of the mouse condensin hinge in solution, SAXS profiles were measured of both the short and the long hinge domain construct (Figure 4.15A). The best data were obtained with protein concentrations of 8 and 20 mg/ml for the short and long construct, respectively. While the short construct showed a slight tendency to aggregate at high concentrations, the long construct did not show any such signs even at 20 mg/ml, thus yielding data of very high quality with little noise even at larger angles. The molecular mass determined from the scattering intensity extrapolated to zero angle confirms that both constructs exist as heterodimers in solution. The scattering profiles were compared with SAXS profiles calculated from the crystal structure and the model of the closed conformation (Figure 4.15A). The observed profile of mSMC2h4h-s matches perfectly with the profile calculated from the crystal structure. This means that the crystallised construct mSMC2h4h-s adopts the same open conformation in solution as in the crystal. Hence, this conformation is not produced by crystal contacts.
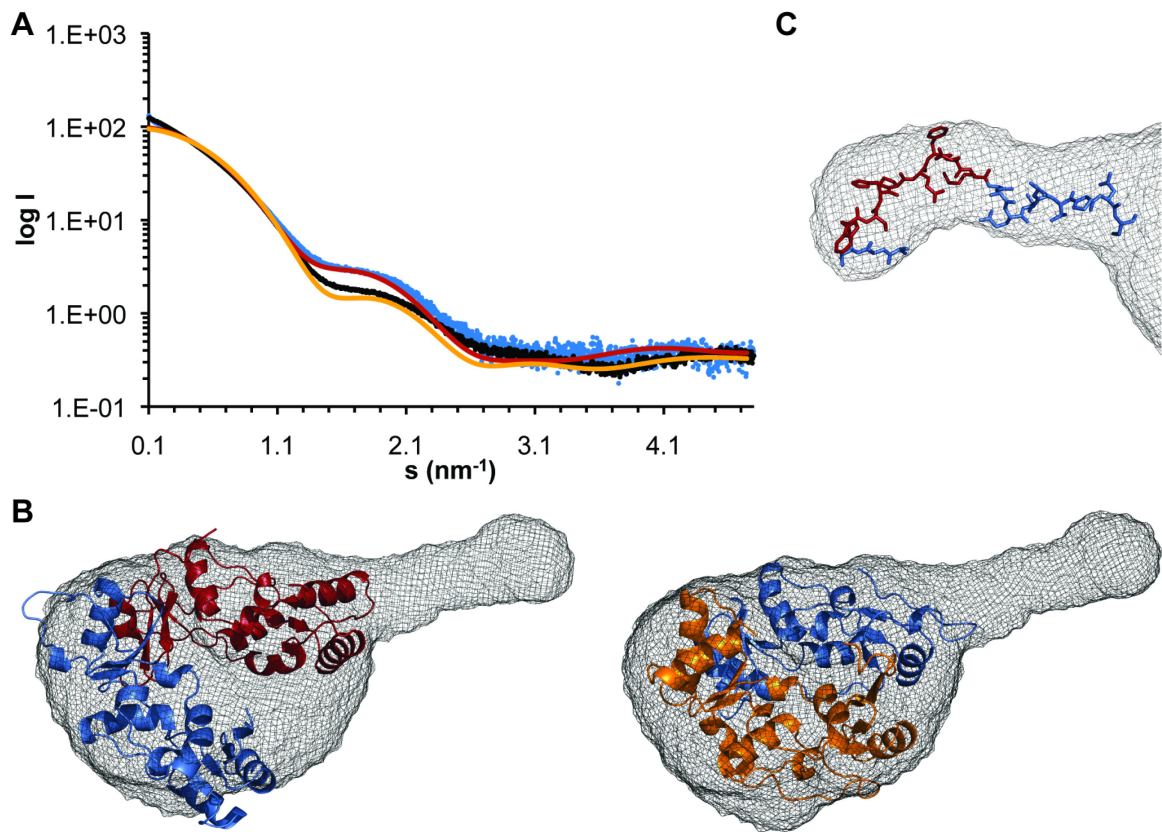
Figure 4.15. Solution scattering analysis of the mouse condensin hinge domain. (**A**) SAXS profiles of the short and long construct in solution in comparison with profiles calculated from atomic resolution models. The scattering profile of the long construct mSMC2h4h-l is shown in black, the profile of the short construct mSMC2h4h-s in blue. The calculated scattering profiles of the atomic resolution models of mSMC2h4h-s in the open and closed conformation are shown in red and orange, respectively. (**B**) Solution envelope reconstruction of the long construct mSMC2h4h-l (grey mesh), superimposed with the atomic resolution models of mSMC2h4h-s in the open (left panel; SMC2 subunit coloured blue, SMC4 red) and closed conformation (right panel; SMC2 blue, SMC4 orange). (**C**) Superposition of a Strep II tag onto the solution envelope reconstruction of mSMC2h4h-l. The stalk of the mSMC2h4h-l SAXS envelope is depicted as grey mesh, superimposed with the twenty residue N-terminal Strep II tag and linker region of the crystal structure of the cytochrome OmcF from *Geobacter sulfurreducens* (pdb 3DP5) (294), depicted as stick model in blue, with the Strep II tag residues also present in mSMC2h4h-l (WSHPQFEK) shown in red.

The long construct mSMC2h4h-l, on the other hand, clearly exhibits a different conformational state. The SAXS profiles suggest that this construct has the expected closed conformation, as its scattering profile more closely resembles that of the closed than that of the open conformation (Figure 4.15A). Ten independent *ab initio* envelope reconstructions were calculated of the long construct. Due to the high data quality, there is a hint of the hole in the hinge heterodimer ring even in the averaged low-resolution

envelope (Figure 4.15B). The stalk that sticks out on one side of the globular protein is big enough to contain 20 – 25 residues of an ordered loop or coiled-coil (Figure 4.15C). The construct mSMC2h4h-l is 14 residues longer than mSMC2h4h-s at all ends, and the SMC2 subunit additionally carries an N-terminal Strep II tag (8 residues). It is therefore most likely that the stalk consists of a short stretch of coiled-coil plus the Strep II tag of the SMC2 subunit (see Figure 4.15C for an exemplary superposition of a crystal structure of a Strep II tag onto the stalk), while the ends of the SMC4 subunit are flexible in solution. Docking of the open and closed conformation of mSMC2h4h-s into the SAXS envelope shows a clearly better fit for the closed conformation (Figure 4.15B). The open conformation does not completely fill the envelope whilst still projecting outside it, whereas the closed conformation fills the globular part of the envelope. DNA-binding data also imply that the long construct has two intact dimer interfaces (chapter 4.2.1). Thus, the long construct mSMC2h4h-l adopts the expected closed conformation.
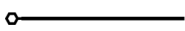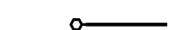
4.2 DNA-Binding Activity of SMC Hinge Domains

4.2.1 DNA-Binding Activity of the Mouse Condensin Hinge Domain

Previous work has demonstrated that the SMC hinge domain can bind DNA (17,31,86,89), but because of the purely qualitative nature of the assays performed in these studies, the specificity for different DNA substrates could not be unambiguously determined. Moreover, the DNA-binding activity of a eukaryotic condensin hinge domain had not been studied before at all. Therefore the binding of different DNA substrates to the mouse condensin hinge domain was analysed both qualitatively and quantitatively. Sequences and structures of the DNA substrates used can be found in Table 4.4.

The short construct mSMC2h4h-s binds DNA only very weakly and nonspecifically (Figure 4.16A and data not shown), probably due to its partially open conformation or the lack of the transition into the coiled-coil region which might harbour additional DNA-binding sites. The long construct mSMC2h4h-l, however, which adopts a closed conformation and contains a short stretch of the coiled-coil regions, binds DNA quite efficiently and shows interesting differential affinity towards different DNA substrates.

Table 4.4. Oligonucleotides used for DNA-binding assays. The 5' end is on the left side for the single-stranded substrates and the top strand(s) of double-stranded substrates. The diamond symbolises the 6-FAM fluorescence label.

Name	Structure	Oligonucleotide sequences
30-mer ssDNA	○—————————	5'-6-FAM-TTTTTTTTTTTTTTTTTTTTTTTTTTTTTT
15-mer ssDNA	○————	5'-6-FAM-TTTTTTTTTTTTTTT
30-mer dsDNA	○══════════	strand 1: 5'-6-FAM-CCGGAAAGCATCTAGCATCCTGTCAGCTGC strand 2: 5'-GCAGCTGACAGGATGCTAGATGCTTTCCGG
30-mer ds-ssDNA-3'	————○══════	strand 1: 5'-6-FAM-CATCCTGTCCGCTGC strand 2: 5'-GCAGCGGACAGGATGTTTTTTTTTTTTTTT
30-mer ds-ssDNA-5'	○══════————	strand 1: 5'-6-FAM-CATCCTGTCCGCTGC strand 2: 5'-TTTTTTTTTTTTTTTGCAGCGGACAGGATG
45-mer ds-ss-dsDNA	══════○══════	strand 1: 5'-6-FAM-CATCCTGTCCGCTGC strand 2: 5'-CCGGAGAGCATCTCG strand 3: 5'-GCAGCGGACAGGATGTTTTTTTTTTTTTTTCGAGATGCTCTCCGG

4.2.1.1 Electrophoretic Mobility Shift Assays

Initially, electrophoretic mobility shift assays (EMSAs) were performed with 6-FAM-labelled DNA substrates (Figure 4.16B). In these assays, the mouse condensin hinge domain showed a qualitatively different binding behaviour towards single-stranded and double-stranded DNA. ssDNA was shifted upwards of the well, that is, the protein-ssDNA complex migrated towards the cathode, suggesting that the protein is so positively charged that even the complex with a 30-mer ssDNA oligonucleotide still has a surplus of positive charge. In fact, the long mouse condensin hinge construct has a theoretical isoelectric point of ~9.3, and positively charged residues are distributed all over the surface of the protein (Figure 4.18). While a 30-mer dsDNA substrate was also bound, EMSAs implied that it was bound much more weakly than the ssDNA substrate of the same length (Figure 4.16B). Also, the protein-dsDNA complex did not migrate towards the cathode, but remained in the wells. Hence EMSAs are not the method of choice to quantitatively analyse DNA binding.
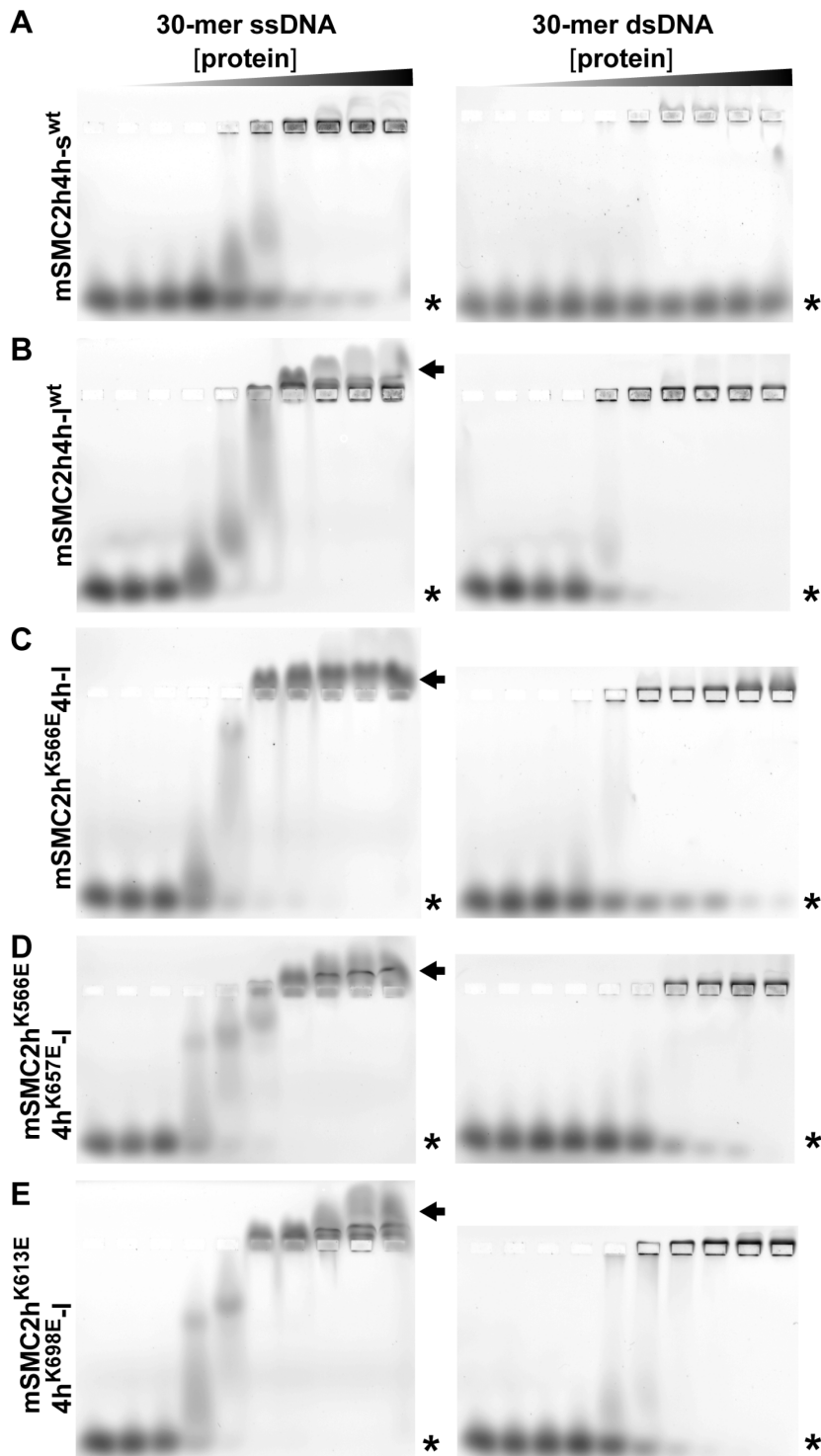
Figure 4.16. Electrophoretic mobility shift assays with the mouse condensin hinge domain. Left panels, titration of the 30-mer ssDNA substrate; right panels, titration of the 30-mer dsDNA substrate. Proteins used for titration are (**A**) mSMC2h4h-s^{wt}; (**B**) mSMC2h4h-l^{wt}; (**C**) mSMC2h^{K566E}4h-l; (**D**) mSMC2h^{K566E}4h^{K657E}-l; (**E**) mSMC2h^{K613E}4h^{K698E}-l. The 6-FAM-labelled DNA substrates at a fixed concentration of 12.5 nM were incubated with increasing concentrations of protein (in a molar excess over the DNA of 0-, 1-, 2-, 10-, 25-, 50-, 100-, 250-, 500-, and 1000-fold) in 1× PBS for 30 min at room temperature. After addition of 10% glycerol, samples were separated on 0.5% agarose gels in 1× TB buffer. Asterisks indicate free DNA, arrows indicate a defined protein-DNA complex.

4.2.1.2 *Quantitative Fluorescence Quenching Titrations*

Fluorescence quenching titrations were performed to better understand the DNA-binding activity of the mouse condensin hinge, exploiting the fact that binding of 6-FAM-labelled DNA to the protein leads to quenching of 6-FAM fluorescence. The resulting titration curves are not only a means to quantify the affinity towards different DNA substrates with great accuracy, but also contain information about the mode of binding.

All measurements were performed at physiological salt concentrations. Inclusion of Mg^{2+} in the assay buffer did not have any influence on DNA binding by the condensin hinge (data not shown).

As can be seen in Figure 4.17A, the binding to dsDNA does not reach saturation even at a 1000-fold excess of protein and cannot be fitted using a simple binding model. This non-saturation behaviour shows that the mouse condensin hinge binds dsDNA nonspecifically. Apparently nonspecific binding produces such large protein-DNA aggregates that they cannot enter the gel matrix and remain in the wells in EMSAs.

On the other hand, the mouse condensin hinge domain binds all DNA substrates tested that are at least partially single-stranded specifically and with high affinity (Figure 4.17A and Table 4.5). Oligo(dT) was used as ssDNA substrate because it does not form intramolecular base pairing or stacking interactions and is a model substrate to study ssDNA-binding specificity (295). All titration curves obtained with partially or completely single-stranded substrates could be fitted using a single-site binding model, meaning that one hinge heterodimer binds one DNA molecule. The 30-mer ssDNA substrate is bound with a dissociation constant of 0.45 ± 0.04 µM. A 15-mer ssDNA substrate is still bound specifically, albeit with an approximately 10-fold higher dissociation constant, suggesting that ~15 nucleotides constitute the minimal binding length. These results led to the hypothesis that the condensin hinge might easily fall off the ends of the short 15-mer oligonucleotide, while it would not so quickly dissociate from the twice as long 30-mer ssDNA substrate. To test this hypothesis, 15-mer ssDNA substrates were designed that are "capped" on one or both ends by a 15-mer dsDNA stretch. Indeed, the 30-mer ds-ssDNA substrate, where one end is capped, is bound twice as strongly as the 15-mer ssDNA. Dissociation constants were found to be the same within the range of error, regardless of whether the ssDNA stretch was a 3' or 5' overhang (Table 4.5). This rules out specific recognition of a particular ssDNA-dsDNA transition by the condensin hinge.
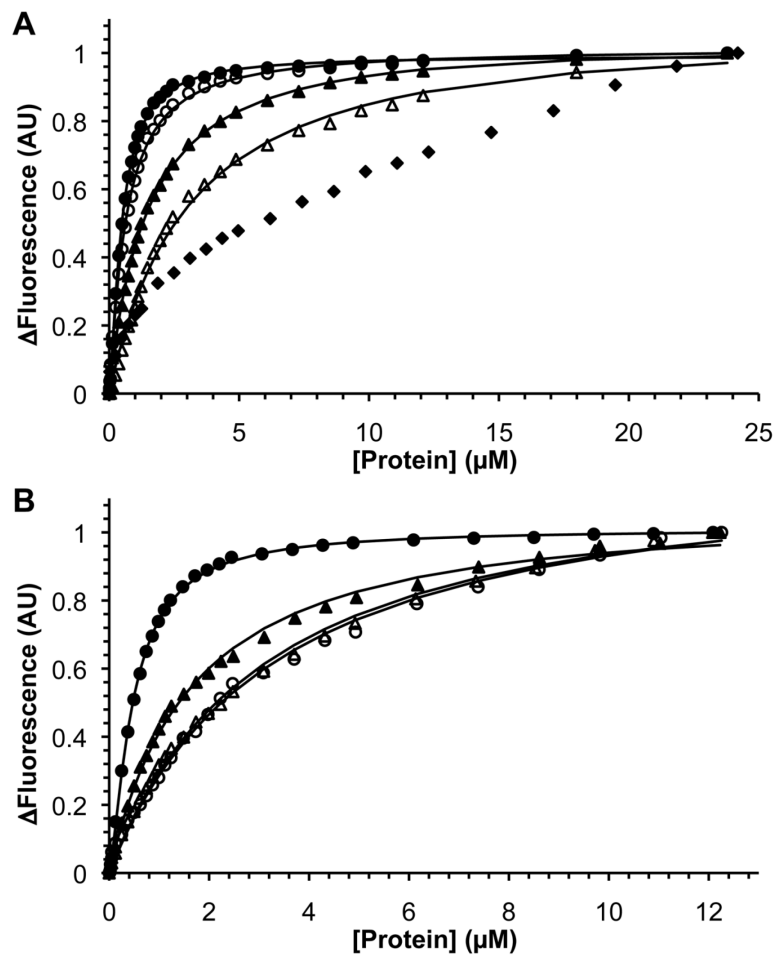
Figure 4.17. Fluorescence quenching titrations with the mouse condensin hinge domain. One representative titration curve of each triplicate measurement is shown. Solid lines represent fits according to a single-site binding model. (**A**) Titrations of different DNA substrates with the long mouse condensin hinge domain construct mSMC2h4h-l^{wt}. DNA substrates are: filled circles, 30-mer ssDNA; open circles, 45-mer ds-ss-dsDNA; filled triangles, 30-mer ds-ssDNA-3'; open triangles, 15-mer ssDNA; filled diamonds, 30-mer dsDNA. The titration with the 30-mer dsDNA substrate could not be fitted with a simple binding model. For clarity, the titration with the 30-mer ds-ssDNA-5' substrate is not shown. For structures and sequences of the DNA substrates see Table 4.4. (**B**) Titrations of the 30-mer ssDNA substrate with mSMC2h4h-l and three point mutants. Proteins are: filled circles, mSMC2h4h-l^{wt}; filled triangles, mSMC2h^{K566E}4h-l; open circles, mSMC2h^{K566E}4h^{K657E}-l; open triangles, mSMC2h^{K613E}4h^{K698E}-l. All titrations were performed with 25 nM of the 6-FAM-labelled DNA substrate in 1× PBS at 20°C in a Horiba Jobin Yvon FluoroMax-P fluorimeter.

Since the fluorescence label is on the 5' end of the short 15-mer strand (see Table 4.4), it is close to the ssDNA stretch in the 30-mer ds-ssDNA-3' substrate and far away from it in the 30-mer ds-ssDNA-5' substrate. Titrations with these two substrates therefore also showed that only the ssDNA stretch is bound by the condensin hinge, as the absolute change in fluorescence intensity during the titration was half as big when the label was far

away from the ssDNA stretch as when it was close to it. Capping both ends of the 15-mer ssDNA results in a five-fold tighter binding with respect to the uncapped 15-mer ssDNA, hence the condensin hinge binds the 45-mer ds-ss-dsDNA substrate almost as tightly as the 30-mer ssDNA substrate.

Table 4.5. Dissociation constants of complexes of the mouse condensin hinge with different DNA substrates. The titration curves from the fluorescence quenching titrations were fitted using a single-site binding model. Dissociation constants K_d are the result of global fits to triplicate measurements, errors are the standard deviations of dissociation constants resulting from independent fits to the three measurements. For structures and sequences of the DNA substrates see Table 4.4. n.d., not determined.

Protein construct	DNA substrate	K_d (µM)
mSMC2h4h-l^{wt}	30-mer ssDNA	0.45 ± 0.04
	15-mer ssDNA	3.21 ± 0.14
	30-mer dsDNA	n.d.
	30-mer ds-ssDNA-3'	1.55 ± 0.05
	30-mer ds-ssDNA-5'	1.77 ± 0.08
	45-mer ds-ss-dsDNA	0.66 ± 0.02
mSMC2h^{K566E}4h-l	30-mer ssDNA	1.80 ± 0.08
mSMC2h^{K566E}4h^{K657E}-l	30-mer ssDNA	3.26 ± 0.58
mSMC2h^{K613E}4h^{K698E}-l	30-mer ssDNA	2.95 ± 0.30

This suggests that the hinge domain is held in place on the ssDNA stretch by the dsDNA caps, making it less likely to dissociate. Although at least two protein molecules should theoretically fit onto the 45-mer ds-ss-dsDNA substrate, data could be fitted very well with a single-site binding model, giving further proof that in partially double-stranded and partially single-stranded DNA substrates only the ssDNA stretch is bound by the condensin hinge.

4.2.1.3 DNA-Binding Activity of Lysine-to-Glutamate Point Mutants

To characterise the DNA-binding activity of the mouse condensin hinge domain more closely, three lysine-to-glutamate point mutants were made of the long construct mSMC2h4h-l: a single mutant mSMC2h^{K566E}4h-l, and two double mutants, mSMC2h^{K566E}4h^{K657E}-l, and mSMC2h^{K613E}4h^{K698E}-l. The first combination of lysine residues (mSMC2-K^{566}/mSMC4-K^{657}) was chosen because this is the only lysine residue

that is highly conserved among SMC proteins from all species (Figure 4.5A, Figure 4.12A). The second combination was chosen due to the position of these lysine residues in the structure. While mSMC2-K^{566}/mSMC4-K^{657} are at the C-terminus of α-helix E, the helix capping off the dimer interface, mSMC2-K^{613}/mSMC4-K^{698} are ~90° removed from the dimer interface, in the short loop connecting helices G and H, on the outside surface of the hinge domain (Figure 4.12A and Figure 4.18). Additionally, they are positioned in a region of the protein where the electrostatic surface potential is almost neutral, whereas there is a cluster of positively charged residues around the dimer interface (Figure 4.18A).
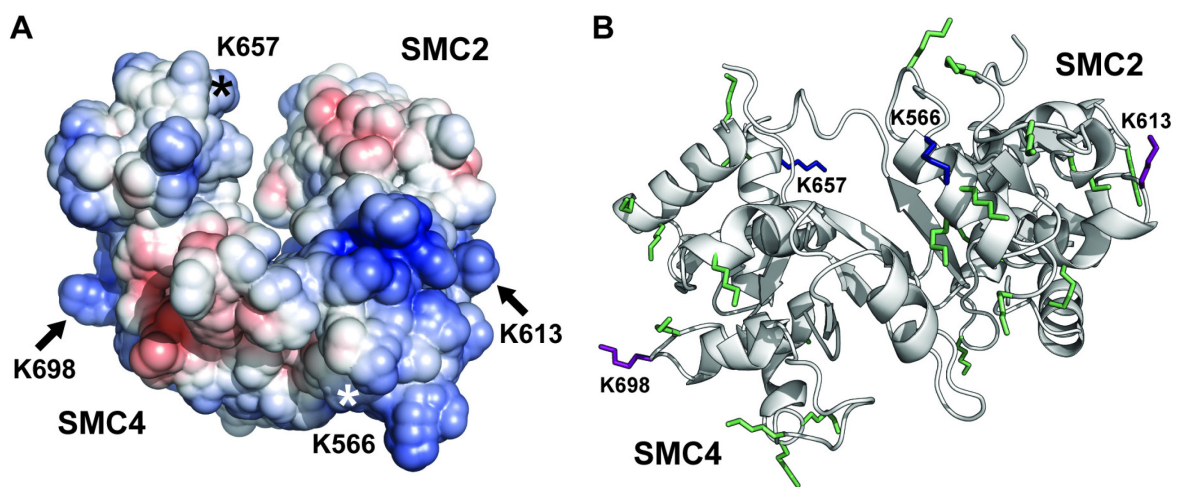
Figure 4.18. Basic regions and residues in the mouse condensin hinge domain. (**A**) Electrostatic surface potential of the mouse condensin hinge domain. Shown is a view onto the top face and side. Positively charged regions are coloured blue, negatively charged regions red, and neutral regions white. Asterisks mark mSMC2-K^{566}/mSMC4-K^{657}, arrows mark mSMC2-K^{613}/mSMC4-K^{698}. (**B**) Lysine residues in the mouse condensin hinge domain. The structure is depicted looking onto the closed interface. The backbone of the condensin hinge is shown in cartoon representation in white, lysines are shown as stick models in green. Lysine residues mutated to glutamate in the point mutants mSMC2-K^{566}E/mSMC4-K^{657}E and mSMC2-K^{613}E/mSMC4-K^{698}E of mSMC2h4h-l are coloured blue and purple, respectively.

All point mutants behaved like the wild-type protein mSMC2h4h-l during purification. As shown in Figure 4.19A, the mutations cause mobility shifts in SDS-PAGE, but the retention volumes of the mutant proteins on an analytical gel filtration column were identical to that of wild-type protein (Figure 4.19B). The multimer/aggregate peak is less pronounced in the mutant preparations, however, the volume of this peak generally varied from batch to batch of wild-type protein as well. The SAXS profiles of all three mutant proteins match the profile of wild-type mSMC2h4h-l, confirming that the mutations do not

disturb the protein fold, although the mutant proteins, especially mSMC2h^{K613E}4h^{K698E}-l, displayed a higher tendency to aggregate than the wild-type protein (Figure 4.19C).
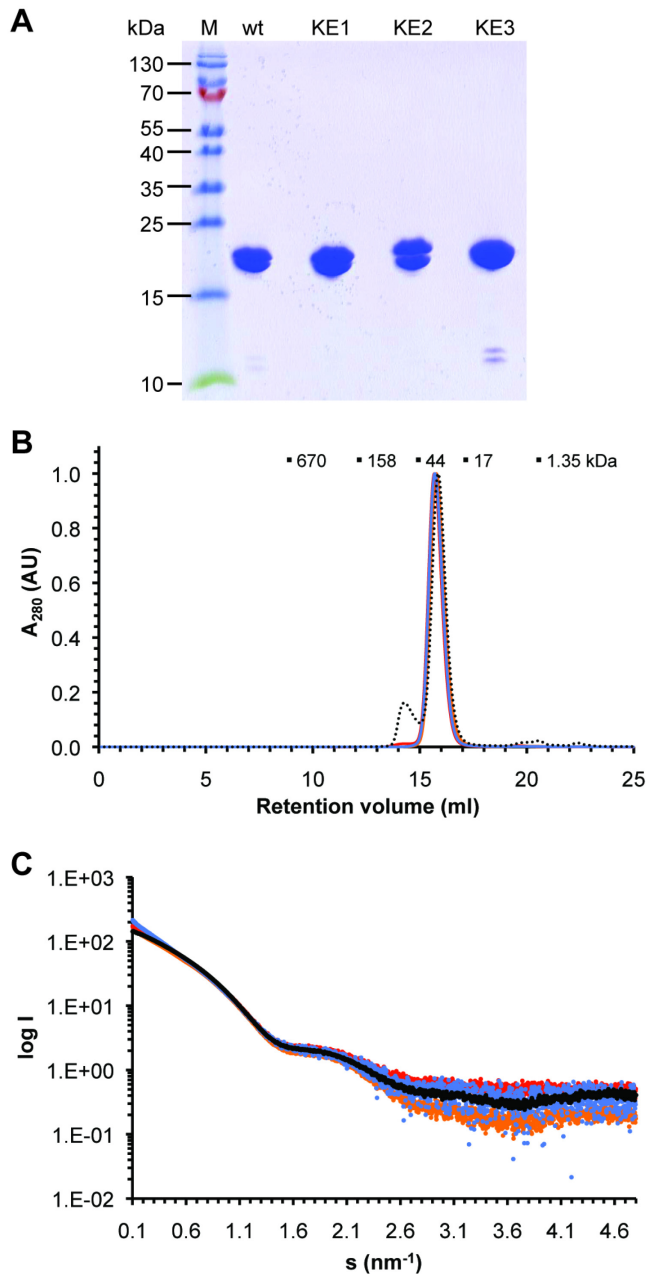
Figure 4.19. Purification of the mouse condensin hinge domain lysine-to-glutamate point mutants. (**A**) SDS-PAGE analysis of the purified proteins. The samples were separated on a 20% SDS polyacrylamide gel and stained with Coomassie Brilliant Blue R-250 (Carl Roth). M, molecular weight marker; wt, mSMC2h4h-l^{wt}; KE1, mSMC2h^{K566E}4h-l; KE2, mSMC2h^{K566E}4h^{K657E}-l; KE3, mSMC2h^{K613E}4h^{K698E}-l. The molecular weight of selected marker bands is indicated. (**B**) Analytical size exclusion chromatograms of the purified proteins mSMC2h^{K566E}4h-l (orange), mSMC2h^{K566E}4h^{K657E}-l (red), mSMC2h^{K613E}4h^{K698E}-l (blue), and mSMC2h4h-l^{wt} (dotted black line). 100 µl of 0.2 mM protein were separated on a Superdex 200 10/300 GL column (GE Healthcare) in 5 mM Tris-HCl pH 8.0, 100 mM NaCl, 0.1 mM EDTA. Above the chromatogram, the elution volumes of standard proteins are indicated with their molecular weights. (**C**) SAXS profiles of the mutant proteins (mSMC2h^{K566E}4h-l, orange; mSMC2h^{K566E}4h^{K657E}-l, red; mSMC2h^{K613E}4h^{K698E}-l, blue) in comparison to wild-type protein (mSMC2h4h-l^{wt}, black).

EMSAs showed a reduction of the nonspecific dsDNA binding for the single mutant and even more dramatically for both double mutants, but results with the 30-mer ssDNA substrate were less clear (Figure 4.16B-E). This is likely to be due to the fact that EMSAs are unsuitable to reveal subtle (10-fold and less) differences in binding strength. Fluorescence quenching titrations of the 30-mer ssDNA substrate with the mutant proteins

clearly demonstrate a reduction in affinity as compared to wild-type (Figure 4.17B and Table 4.5). The effect of the mutations is additive, since the dissociation constant for the single mutant mSMC2h^{K566E}4h-l is half as big as that of the corresponding double mutant. Both double mutants have roughly the same affinity towards the 30-mer ssDNA, it is reduced 7- to 8-fold as compared to wild-type. The mutations also reduce specificity of binding, as the titrations show a contribution of nonspecific interaction. Especially for the double mutants, the binding does not saturate completely, and data could only be fitted up to a 500-fold excess of protein over DNA.

These results imply that ssDNA wraps around the other surface of the hinge domain, and all positively charged residues contribute to binding.

4.2.2 DNA-Binding Activity of the *P. furiosus* SMC Hinge Domain

While the structure of the TmaSMC hinge domain has been solved (15), its DNA-binding activity has not been investigated. Conversely, DNA binding by the BsuSMC hinge domain has been analysed – albeit only in a qualitative manner – (17,31,86), but its structure has not been solved. Therefore the DNA-binding activity of the PfuSMC hinge domain was investigated as well, using the same DNA substrates as for the mouse condensin hinge domain (Table 4.4). Unfortunately, probably due to the relatively low affinity, neither fluorescence quenching nor anisotropy titrations yielded meaningful binding curves, so DNA binding by the PfuSMC hinge domain could only be analysed with EMSAs.

4.2.2.1 Electrophoretic Mobility Shift Assays

In EMSAs, the PfuSMC hinge bound the 30-mer ssDNA substrate relatively well, whereas the dsDNA substrate of the same length was not bound (Figure 4.20A and B). ~50% of the 30-mer ssDNA were bound at a 50 – 100-fold excess of protein over DNA, and at a 250 – 500-fold excess of protein, the ssDNA substrate was completely shifted. In comparison, under the same assay conditions, the same 30-mer ssDNA substrate was shifted completely by the mouse condensin hinge domain at a 100-fold excess of protein over DNA (Figure 4.16B). Hence the PfuSMC hinge domain has a lower affinity for ssDNA than the mouse condensin hinge. The protein concentration at which half the ssDNA bound to the PfuSMC hinge was 0.6 – 1.3 µM, therefore the dissociation constant of the complex should be in this range.
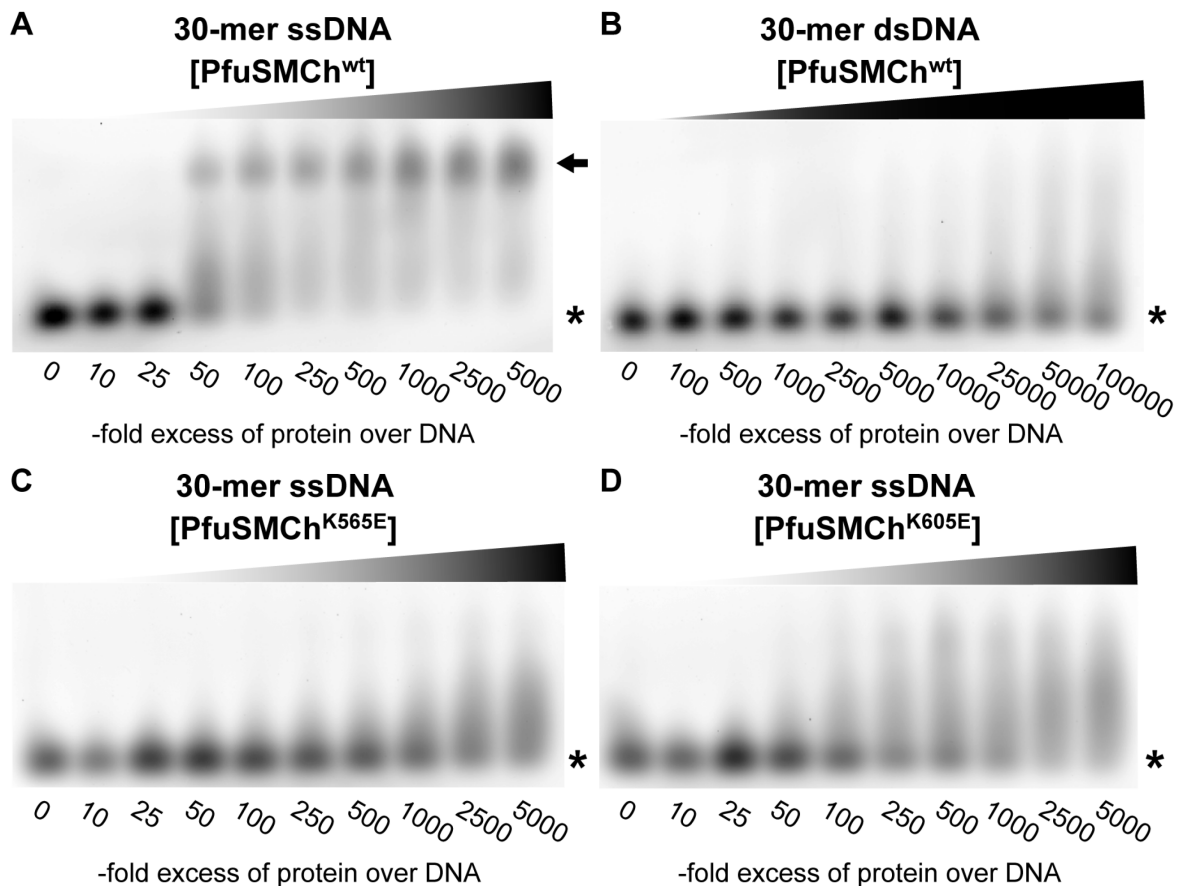
Figure 4.20. Electrophoretic mobility shift assays with the PfuSMC hinge domain. (**A**) Titration of the 30-mer ssDNA substrate with the wild-type PfuSMC hinge domain (PfuSMCh^wt). (**B**) Titration of the 30-mer dsDNA substrate with PfuSMCh^wt. (**C**) Titration of the 30-mer ssDNA substrate with the point mutant PfuSMCh^K565E. (**D**) Titration of the 30-mer ssDNA substrate with the point mutant PfuSMCh^K605E. The 6-FAM-labelled DNA substrates at a fixed concentration of 12.5 nM were incubated with increasing concentrations of protein (in a molar excess over the DNA as detailed underneath each lane) in 1× PBS for 30 min at room temperature. After addition of 10% glycerol, samples were separated on 0.5% agarose gels in 1× TB buffer. Asterisks indicate free DNA, the arrow indicates a defined protein-DNA complex.

The protein-ssDNA complex migrated as a defined band, indicating that a specific complex was formed. With the 30-mer dsDNA, only a smeared shift could be obtained at a very high (25 000 – 100 000-fold) excess of protein (Figure 4.20B). This suggests that the shift was simply caused by the high protein concentration, not by specific binding. Longer DNA substrates essentially yielded the same results, while shorter ssDNA substrates were not bound efficiently (data not shown).

4.2.2.2 DNA-Binding Activity of Lysine-to-Glutamate Point Mutants

In order to more accurately define the DNA-binding interface of the PfuSMC hinge domain, two lysine-to-glutamate point mutants were constructed. The lysines to be mutated were chosen in analogy to the mutations made in the mouse condensin hinge domain (chapter 4.2.1.3), but the choice was based on a tertiary structure rather than a sequence alignment. As mentioned above, while SMC hinge domains generally contain many lysines, there is only one lysine residue that is highly conserved among SMC proteins from all species (PfuSMC-K^{568}, mSMC2-K^{566}/mSMC4-K^{657}) (Figure 4.21A). This residue is located at the C terminus of the α-helix capping the dimer interface in all SMC hinge domain structures solved so far.
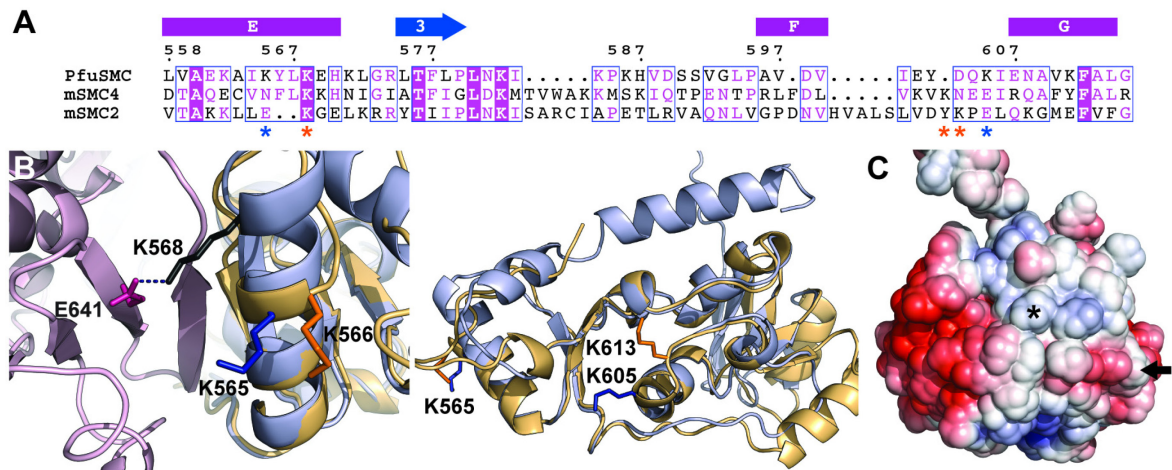
Figure 4.21. Basic regions and residues in the PfuSMC hinge domain. (**A**) Sequence alignment of PfuSMC with mouse SMC2 and SMC4. Shown is only the part of the hinge region containing the lysine residues chosen for mutation to glutamate. The residue numbering is for PfuSMC. The lysine residues mutated in PfuSMC are indicated by blue asterisks, those mutated in mSMC2 and mSMC4 by orange asterisks. The secondary structure of the PfuSMC hinge domain in this region is shown above the alignment, with α-helices displayed as purple rectangles and β-strands as blue arrows. The alignment was generated with MultAlin (249). (**B**) Superposition of the PfuSMC hinge domain (chain A coloured light blue, chain A' light pink) with the mouse SMC2 hinge domain (orange). The lysine residues mutated in the PfuSMC hinge domain are shown as stick models in blue, corresponding lysine residues in the mSMC2 hinge in orange. Note that the conserved residue K^{566} of mSMC2 corresponds to PfuSMC-K^{568} (shown as stick model in black) in a primary sequence alignment, but superimposes with PfuSMC-K^{565} in the tertiary structure. PfuSMC-K^{568} is involved in dimer interactions, forming a hydrogen bond with E^{641} of the other chain (shown as stick model in pink). (**C**) Electrostatic surface potential of the PfuSMC hinge domain, looking onto the dimer interface. Positively charged regions are coloured blue, negatively charged regions red, and neutral regions white. The asterisk marks K^{565}, the arrow marks K^{605}.

In the mSMC2 hinge domain, K^{566} points outwards from the protein surface, whereas the corresponding residue in the PfuSMC hinge domain, K^{568}, is involved in dimer interactions, forming a hydrogen bond with E^{641} of the other chain (Figure 4.21B). PfuSMC-K^{565}, however, is in a similar position in the tertiary structure as mSMC2-K^{566} and was therefore mutated to glutamate instead of the conserved residue PfuSMC-K^{568}. The second residue mutated to glutamate was PfuSMC-K^{605}, located in the same region of the hinge domain as mSMC2-K^{613}/mSMC4-K^{698} (Figure 4.21A). This residue was chosen because, in contrast to PfuSMC-K^{565}, it is distant from the dimer interface and located in an overall negatively charged region (Figure 4.21B and C).

Both point mutants behaved like the wild-type protein during purification. As shown in Figure 4.22A, the mutations cause mobility shifts in SDS-PAGE. The retention volumes of the mutant proteins on an analytical gel filtration column are slightly smaller than that of wild-type protein, but still correspond to the molecular weight of a dimer (Figure 4.22B). The SAXS profiles of both mutant proteins match the profile of the wild-type PfuSMC hinge domain, confirming that the mutations do not disturb the protein fold (Figure 4.22C).

Interestingly, while both mutants displayed reduced affinity towards ssDNA as compared to wild-type, the effect of the $K^{565}E$ mutation was stronger than that of the $K^{605}E$ mutation (Figure 4.20C and D). The $K^{565}E$ mutant protein only started shifting the 30-mer ssDNA at a concentration of 3.1 µM (250-fold excess), whereas the $K^{605}E$ mutant started shifting the DNA substrate at 0.6 µM (50-fold excess), indicating that the affinity of the $K^{565}E$ mutant protein for ssDNA is approximately 5-fold lower than that of the $K^{605}E$ mutant. However, both mutant proteins failed to form a defined protein-DNA complex, instead producing only a smeared shift, and a complete shift was not obtained with either of the two mutant proteins even at high protein concentrations. This suggests that while both the basic patch as well as positively charged residues outside of the basic patch contribute to binding specificity, the binding strength is achieved mostly by the basic patch.
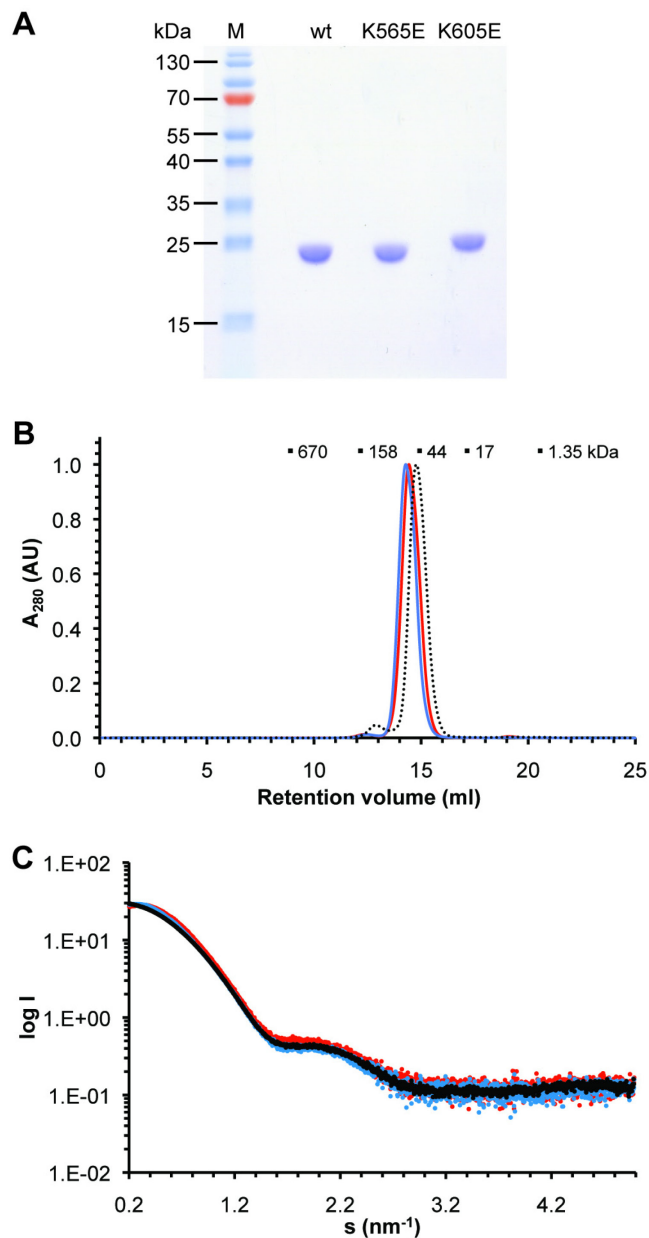
Figure 4.22. Purification of the PfuSMC hinge domain lysine-to-glutamate point mutants. (**A**) SDS-PAGE analysis of the purified proteins. The samples were separated on a 15% SDS polyacrylamide gel and stained with Coomassie Brilliant Blue R-250 (Carl Roth). M, molecular weight marker; wt, PfuSMCh[wt]; K565E, PfuSMCh[K565E]; K605E, PfuSMCh[K605E]. The molecular weight of selected marker bands is indicated. (**B**) Analytical size exclusion chromatograms of the purified proteins PfuSMCh[K565E] (red), PfuSMCh[K605E] (blue), and PfuSMCh[wt] (dotted black line). 100 μl of 1 mM protein were separated on a Superdex 200 10/300 GL column (GE Healthcare) in 5 mM Tris-HCl pH 8.0, 100 mM NaCl, 0.1 mM EDTA. Above the chromatogram, the elution volumes of standard proteins are indicated with their molecular weights. (**C**) SAXS profiles of the mutant proteins in comparison to wild-type protein. The scattering profile of PfuSMCh[wt] is shown in black, the profile of PfuSMCh[K565E] in red, and that of PfuSMCh[K605E] in blue.

5   DISCUSSION

Organisms from all domains of life rely on SMC proteins for the accurate propagation of genetic information. As the core components of the protein complexes named after them, SMC proteins are key players in the control of chromosome structure and dynamics throughout all stages of the cell cycle. SMC proteins consist of N and C-terminal domains that fold back onto each other to create an ATPase head domain, connected to a central hinge domain via long coiled-coils. The hinge domain mediates dimerisation of SMC proteins and binds DNA, but it is not clear to what purpose this activity serves. Therefore the aim of this work was to analyse both prokaryotic and eukaryotic SMC hinge domains, and specifically their DNA-binding activity, in more detail. To this end, the hinge domains of the PfuSMC protein and of mouse condensin were characterised structurally and biochemically.

5.1   The SMC Hinge Domain Fold is Highly Conserved

The primary sequence of SMC hinge domains is strongly conserved: between hinge domains from all three phylogenetic domains, as exemplified by those whose structures have been solved, i.e. the *T. maritima* (15), the *P. furiosus*, and the mouse condensin hinge domain, the sequences are ~30% identical and 50 – 60% similar. Likewise, the tertiary structures of these SMC hinge domains are quite similar, with rms deviations all below 3 Å. The SMC hinge domain comprises two pseudo-two-fold-symmetric subdomains, each consisting of a mixed β-sheet sandwiched between α-helices. The subdomains interact such that a half-ring structure is created with an α-helical core, flanked by the β-sheets and one or two outer helices on both sides. While in prokaryotes the SMC hinge domain homodimerises, the six different eukaryotic hinge domains assemble into specific pseudo-symmetric heterodimers. The characteristic doughnut-shaped dimers are formed by both outermost β-strands on the concave side of the half-ring interacting with those of another subunit to form two continuous β-sheets, so that both coiled-coils emerge from the same face of the dimer.

The SMC proteins of γ-proteobacteria, called MukB, are strongly divergent from those of other species and were initially not recognised as belonging to the SMC family at all (32). MukB proteins are significantly smaller than genuine SMC proteins, and there is no discernible sequence homology. However, despite the substantial difference in size and

large sequence divergence, the structure of the *E. coli* MukB hinge domain is quite similar to that of the PfuSMC and TmaSMC hinge domains (93,94). Interestingly, while the N-terminal subdomains match almost perfectly, only the β-sheet of the C-terminal subdomain is present in the *E. coli* MukB hinge. Apparently, when γ-proteobacteria diverged from other prokaryotes, the sequence encoding the α-helical part of the C-terminal hinge subdomain was deleted from the *smc* gene.

Although the mouse SMC2-SMC4 hinge heterodimer adopts an open conformation in the crystal structure described here, dimerising via only one of the two expected interfaces, the subunit cores themselves closely resemble the prokaryotic SMC hinge domains from *P. furiosus* and *T. maritima* (15). The SMC2 hinge is more similar to the prokaryotic SMC hinges than the SMC4 hinge. The structural features of the SMC4 hinge that are different from its bacterial and archaeal counterparts might be involved in specific functions of the condensin complex which the prokaryotic SMC complex does not have. Since these structural features are exposed on the outer surface of the SMC4 hinge, they could constitute a binding interface for an interaction partner like Cti1/C1D, a protein that was found to interact with the SMC4 hinge domain in fission yeast (90) and is implicated in DNA repair functions (296,297). Further research should clarify whether condensin also interacts with C1D in higher eukaryotes, and if so, whether it does this via the SMC4 hinge domain.

Eukaryotes have six different SMC proteins that form three distinct heterodimeric complexes, pairing SMC1 with SMC3, SMC2 with SMC4, and SMC5 with SMC6. Other dimers do not occur. Only because of this specific heterodimer formation was it possible for the different SMC complexes to specialise and assume different functions. The interface between the SMC2 and SMC4 subunit in the crystal structure offers an explanation as to how dimerisation specificity of eukaryotic SMC proteins is created. Comparing the interacting residues in the SMC2-SMC4 hinge domain with the corresponding residues in SMC1α and SMC3, it becomes apparent that some of these residues would either clash with, or not be able to interact with the interface residues of the "wrong" partners. Thus, although the overall structure of their hinge domains is likely to be very similar, small differences in the primary sequence ensure that only one set of heterodimers can be formed from the six different eukaryotic SMC proteins.

While the overall fold of the SMC hinge domain is conserved from prokaryotes to eukaryotes, functionally relevant structural details have changed, but these changes do not only concern the dimer interface. Most importantly, the surface charge of the hinge domain has been almost reversed throughout evolution. Whereas bacterial and archaeal SMC hinge domains have a quite acidic outer surface with only one basic patch at the dimer interface, the outer surface of the eukaryotic condensin hinge domain is neutral-to-basic, and the positively charged patch at the dimer interface is also much more pronounced. As discussed below, this has implications in the DNA-binding activity and specificity of prokaryotic and eukaryotic SMC hinge domains.

The open conformation of the mouse condensin hinge domain in the crystal structure may have been caused by the construct being too short for the second dimerisation interface to be stable, but it is also possible that it represents a functional intermediate during assembly of SMC complexes or their action on DNA. It would at first glance seem to suggest that the hinge domain could indeed open up to allow DNA to enter into the intra-coiled-coil space, as has been proposed (246). While this possibility cannot be ruled out based on the data presented here, the space between the SMC2 and SMC4 subunits in the crystal structure is not big enough to accomodate a DNA double helix, and the charge distribution on the inner surface of the hinge domain would rather repulse than attract DNA. In fact, the observed charge distribution with only one strongly basic patch argues for a preference for single-stranded over double-stranded DNA (chapter 5.2).

The SMC2-SMC4 hinge heterodimer is stable although one dimer interface is disrupted, indicating that one intact interface suffices for dimerisation. This observation is in close agreement with mutational studies of the bovine and budding yeast cohesin hinge domains (89,298). The interaction between the two subunits is also strong enough to withstand some structural rearrangements, as the interface remains intact despite the hinge being bent open along the interface axis, leading to a wider angle between subunits than in the closed conformation. The data presented in this study therefore provide additional evidence for the structural flexibility of the hinge domain, a quality that is probably very important for the dynamic interactions of SMC proteins with DNA (41,86,246).

It has been demonstrated that the transition into the coiled-coil region is necessary for DNA binding by the cohesin hinge, but not for its dimerisation (89). Similar results were obtained in a previous study of the BsuSMC protein (17), and this was found to be true for the mouse condensin hinge domain as well. In the experiments presented here, the

construct without coiled-coil regions bound to DNA only very weakly and nonspecifically, whereas the construct carrying a short stretch of coiled-coil bound ssDNA strongly and specifically. The structural data show that in the construct without coiled-coil regions only one dimer interface is intact, while the longer construct has both expected dimer interfaces. Taken together, these results suggest that the transition into the coiled-coil region does not directly participate in DNA binding, but rather confers structural stability to the hinge domain, especially to the basic patch at the dimer interface which is essential for DNA binding.

5.2 Condensin SMC Hinge Domains Preferentially Bind Single-Stranded DNA

5.2.1 Localisation of the DNA-Binding Surface

Both prokaryotic and eukaryotic condensin SMC hinge domains bind DNA with medium to high affinity and show a clear preference for single-stranded over double-stranded DNA (but no sequence specificity), as has been demonstrated here for the PfuSMC and the mouse condensin hinge domains, and observed previously with the BsuSMC hinge (17,31,86,91). However, despite the strong structural conservation, the DNA-binding surface of prokaryotic and eukaryotic SMC hinge domains is likely to be different.

The PfuSMC hinge domain displays a marked preference for ssDNA over dsDNA – it binds ssDNA with medium affinity, but does not bind dsDNA at all. The mouse condensin hinge domain, however, binds dsDNA, albeit weakly and non-specifically, whereas its interaction with ssDNA is relatively strong and specific. Interestingly, studies of the BsuSMC protein suggest that the bacterial SMC hinge domain also interacts with dsDNA and ssDNA in mechanistically distinct manners (31,86).

Although the affinity of the PfuSMC hinge domain for ssDNA could not be accurately quantified, it is obviously lower than that of the mouse condensin hinge domain. Thus, the mouse condensin hinge domain has a higher affinity for DNA than the PfuSMC hinge at the cost of a lower specificity for the structure of the DNA bound.

Mutation of a lysine residue in the basic patch of the PfuSMC hinge domain to glutamate caused a stronger reduction of DNA binding than mutation of a lysine residue in the acidic region of the outer hinge domain surface. This suggests that the DNA-binding activity of the PfuSMC hinge domain resides mostly within the basic patch at the dimer

interface. In contrast, in the mouse condensin hinge domain the analogous mutations both had the same quantitative and qualitative effect, reducing affinity as well as specificity, implying that ssDNA wraps around the outer surface of the hinge domain, and all positively charged residues contribute to binding.

As mentioned above, while the outer surface of the condensin hinge domain is neutral-to-positively charged, the PfuSMC hinge domain has a rather acidic outer surface, and only its inner surface – which is, however, not accessible to DNA – is positively charged, with the basic patch at the dimer interface also being less pronounced. Therefore, the effects of the lysine-to-glutamate point mutations confirm what can already be suspected looking at the surface charge distributions, namely that the PfuSMC hinge domain binds DNA only via the basic patch, while in the mouse condensin hinge domain the DNA-binding surface extends further, leading to stronger affinity as well as lower specificity.

Since the surface charge distribution of bacterial SMC hinge domains is similar to that of the archaeal PfuSMC hinge, their DNA-binding surface is likely also confined to the basic patch at the dimer interface. A previous mutational study of the BsuSMC protein supports this conclusion, although residues outside of the basic patch were not mutated in this study (86). However, the authors found that mutation of three consecutive lysine residues in the basic patch of the BsuSMC hinge led to a complete loss of DNA binding (Figure 5.1D). The structure of the BsuSMC hinge domain has not been solved, but is likely to be very similar to the known structures of other genuine SMC hinge domains. Judging from the large number of lysine residues that are clustered around the dimer interface of the BsuSMC hinge domain (Figure 5.1B and D) its basic patch should be more pronounced than that of the PfuSMC hinge, and consequently its affinity for DNA should be higher. Although it has not been quantified accurately, the DNA affinity of the BsuSMC hinge indeed appears to be similar to that of the mouse condensin hinge. The fact that the BsuSMC hinge binds dsDNA also suggests that it behaves more like the mouse condensin hinge domain (17,31,86,91). The DNA-binding activity of the TmaSMC hinge domain has not been investigated, but based on the fact that its surface is slightly more acidic than that of the PfuSMC hinge domain, its affinity for DNA can be expected to be slightly weaker.

Current knowledge suggests that in all genuine SMC hinge domains there is a basic patch at the dimer interface which is (part of) their DNA-binding surface, yet the basic patch is not located in exactly the same position in all SMC hinge domains. There is

always a cluster of basic residues in the region of the dimer interface, but with the exception of one of these residues they are not conserved. In the PfuSMC hinge domain the basic patch is located along the dimer interface, while in the TmaSMC hinge it is shifted more towards the bottom face, and in the BsuSMC hinge domain it is in contrast likely to be shifted more towards the top face of the domain. In the mouse condensin hinge domain the basic patch is much more pronounced and spreads from the top face along the dimer interface to the bottom face (Figure 5.1). The fact that its exact location on the SMC hinge domain varies suggests that the DNA-binding surface has evolved to fulfil different functions (see below).
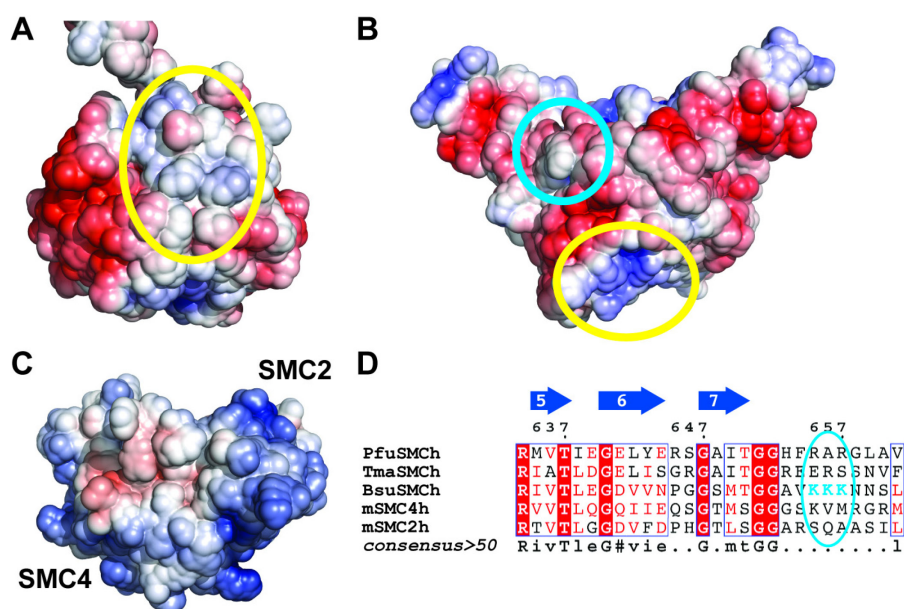
Figure 5.1. Location of the basic patch at the dimer interface in different SMC hinge domains. (**A**) Electrostatic surface potential of the PfuSMC hinge domain, looking onto the dimer interface. The basic patch is circled in yellow. (**B**) Electrostatic surface potential of the TmaSMC hinge domain (pdb 1GXL) (15), looking onto the dimer interface. The basic patch is circled in yellow, the probable location of the basic patch in the BsuSMC hinge domain is circled in cyan. (**C**) Electrostatic surface potential of the mouse condensin hinge domain, looking onto the dimer interface. In (A) – (C), positively charged regions are coloured blue, negatively charged regions red, and neutral regions white. (**D**) Sequence alignment of the C-terminal dimerisation interface residues of the SMC hinge domains of *P. furiosus*, *T. maritima*, *B. subtilis*, and mouse condensin. The cyan circle marks the three consecutive lysine residues in the BsuSMC hinge domain that are required for DNA binding and probably part of the basic patch (86). Numbering of residues is for PfuSMC. The secondary structure of the PfuSMC hinge domain is shown above the alignment, with β-strands displayed as blue arrows. In the consensus sequence, lower case letters are used for ≥50%, upper case letters for ≥90% conservation; # is any one of NDQE. The alignment was generated with MultAlin (249).

The one conserved lysine residue (PfuSMC-K^{568}, mSMC2-K^{566}/mSMC4-K^{657}) is most likely conserved because it participates in the dimer interaction in prokaryotic SMC hinge domains. In mSMC2, this residue points outwards from the protein surface, so that it can assume a different function. Since the dimer interface at which mSMC4-K^{657} is located is open in the crystal structure, it is difficult to say whether or not the same is true for this conserved residue in mSMC4. On the one hand, in the model of the closed conformation, mSMC4-K^{657} points towards mSMC2-D^{655} and could therefore form a similar interaction as PfuSMC-K^{568} does with PfuSMC-E^{641}. On the other hand, its mutation to glutamate in the long mouse condensin hinge domain construct with two intact dimer interfaces did not disturb the protein structure. Hence, it appears that while this lysine residue is conserved throughout evolution due to its participation in the dimer interaction, it can also participate in DNA binding, having a dual or flexible function.

In contrast, MukB has an extensive DNA-binding site on the head domain surface between the coiled-coils (81). No DNA-binding activity was observed with the MukB hinge domain which is even more acidic than genuine prokaryotic SMC hinge domains (93,94). This implies that the DNA-binding activity is a feature acquired by SMC and MukB proteins after γ-proteobacteria diverged from other bacteria.

5.2.2   Functional Implications of the Single-Stranded DNA-Binding Activity

Since SMC hinge domains seem to have acquired the DNA-binding activity quite late during evolution, it is likely that it has developed to support functions that the SMC complex was already fulfilling, and that it therefore supports different functions in different SMC complexes.

The fact that the ssDNA-binding activity appears to have been enhanced in eukaryotic condensin as compared to prokaryotic SMC proteins, while the cohesin hinge domain preferentially binds dsDNA (89), argues that this activity plays a role in a function acquired specifically by the eukaryotic condensin complex. One possibility is that the ssDNA-binding activity of its hinge domain supports the SSB repair function of condensin. Human condensin I is recruited to SSBs by the DNA nick-sensor PARP1 (226). By interacting directly with the ssDNA, the hinge domain might help to tether the condensin complex to the damage site and to organise the DNA structure for repair. The ssDNA-binding activity could also be important during normal DNA replication which transiently produces ssDNA stretches, as suggested by the replication checkpoint defect of condensin

mutants (225), and the accumulation of condensin at stalled replication forks (206). Lower eukaryotes like yeast do not possess PARP1, therefore condensin must have a slightly different function in DNA repair in these organisms (90,225). However, it is likely that condensin participates in SSB repair in lower eukaryotes as well, since budding yeast temperature-sensitive condensin mutants are hypersensitive to SSB damage (Frank Uhlmann, personal communication).

Prokaryotes do not possess PARP1, and the ssDNA-binding activity of the prokaryotic SMC hinge domain is less pronounced than that of its eukaryotic counterpart. Also, while condensin is loaded onto chromosomes in prophase of mitosis (126,194,200,201), the prokaryotic SMC complex appears to be loaded during replication, at the replication fork (30,198,199). The ssDNA-binding activity of its hinge domain might therefore play a role in the DNA-loading process of the prokaryotic SMC complex.

It is conceivable that ssDNA binding has been enhanced during the evolution from prokaryotic SMC proteins to condensin while genome size increased and DNA repair pathways consequently became more and more sophisticated.

5.2.3 Functional Implications of the Double-Stranded DNA-Binding Activity

The weak and nonspecific interaction of the condensin hinge with dsDNA might be involved in the mitotic function of the condensin complex. There is evidence that condensin interacts with mitotic chromosomes in a different manner than cohesin (195). When the coiled-coil region of cohesin is cut at genetically engineered protease cleavage sites, its interaction with chromosomes is lost (172). Cohesin stably bound to a circular minichromosome will also fall off when the DNA is linearised (173). These experiments led to the conclusion that cohesin interacts with DNA in a topological manner, that is that it forms a ring around chromosomes. Due to the structural similarity of SMC proteins it was assumed that they all interact with DNA in this manner. However, when condensin is cut at two protease cleavage sites genetically engineered into the SMC2 coiled-coil region, its association with mitotic chromosomes is not affected (195). Electron micrographs also showed that condensin and cohesin adopt different conformations: while cohesin forms rings that could potentially encircle chromatin, condensin has a rod-like appearance with its two coiled-coil arms juxtaposed (21). In atomic force microscopy images, condensin was observed sitting on DNA with its hinge region (92). Although it is not clear whether these images represent the physiological DNA-bound state of condensin, more and more

results point in this direction. Condensin is therefore more likely to be tethered to chromosomes by interactions with other chromosome-bound proteins, possibly mediated by its regulatory non-SMC subunits. The weak binding to dsDNA via its hinge domain might execute an accessory function.

The cohesin hinge on the other hand seems to interact with DNA in a way quite different to condensin. The bovine cohesin hinge domain preferentially binds dsDNA and DNA rich in secondary structures (89). This points to a role of the hinge domain in the DNA-loading process or the DSB repair function of cohesin. In comparison with the data presented in this study, it also shows once more that of all three eukaryotic SMC complexes, the condensin complex is most closely related to prokaryotic SMC proteins not only in sequence, but also in function.

5.3 Conclusion

With more and more data on structure and activity of SMC hinge domains being available, it is becoming increasingly clear that while the SMC hinge domain fold has been strongly conserved throughout evolution, its function has diversified. Although the precise role of its DNA-binding activity is still unclear, the hinge domain is obviously much more than just a simple dimerisation domain.

This work has unambiguously demonstrated that both prokaryotic and eukaryotic condensin hinge domains preferentially and specifically bind ssDNA, while their interaction with dsDNA is weak and nonspecific. The ssDNA-binding activity of condensin hinge domains should therefore no longer be regarded as unphysiological and therefore meaningless. On the contrary, the results presented here are a clear indication that this activity should be investigated *in vivo*.

6 REFERENCES

1. Flemming, W. (1880) Beiträge zur Kenntnis der Zelle und ihrer Lebenserscheinungen. *Arch. Mikrosk. Anat.*, **18**, 151-259.
2. Flemming, W. (1882) *Zellsubstanz, Kern und Zelltheilung.* F.C.W. Vogel, Leipzig.
3. Waldeyer, H.W. (1888) Über Karyokinese und ihre Beziehungen zu den Befruchtungsvorgängen. *Arch. Mikrosk. Anat.*, **32**, 1-22.
4. Hirano, T. (2006) At the heart of the chromosome: SMC proteins in action. *Nat. Rev. Mol. Cell Biol.*, **7**, 311-322.
5. Graumann, P.L. and Knust, T. (2009) Dynamics of the bacterial SMC complex and SMC-like proteins involved in DNA repair. *Chromosome Res.*, **17**, 265-275.
6. Hudson, D.F., Marshall, K.M. and Earnshaw, W.C. (2009) Condensin: architect of mitotic chromosomes. *Chromosome Res.*, **17**, 131-144.
7. Nasmyth, K. and Haering, C.H. (2009) Cohesin: its roles and mechanisms. *Annu. Rev. Genet.*, **43**, 525-558.
8. De Piccoli, G., Torres-Rosell, J. and Aragon, L. (2009) The unnamed complex: what do we know about Smc5-Smc6? *Chromosome Res.*, **17**, 251-263.
9. Donze, D., Adams, C.R., Rine, J. and Kamakaka, R.T. (1999) The boundaries of the silenced HMR domain in *Saccharomyces cerevisiae. Genes Dev.*, **13**, 698-708.
10. Lupo, R., Breiling, A., Bianchi, M.E. and Orlando, V. (2001) *Drosophila* chromosome condensation proteins Topoisomerase II and Barren colocalize with Polycomb and maintain *Fab-7* PRE silencing. *Mol. Cell*, **7**, 127-136.
11. Bhalla, N., Biggins, S. and Murray, A.W. (2002) Mutation of YCS4, a budding yeast condensin subunit, affects mitotic and nonmitotic chromosome behavior. *Mol. Biol. Cell*, **13**, 632-645.
12. Lara-Pezzi, E., Pezzi, N., Prieto, I., Barthelemy, I., Carreiro, C., Martinez, A., Maldonado-Rodriguez, A., Lopez-Cabrera, M. and Barbero, J.L. (2004) Evidence of a transcriptional co-activator function of cohesin STAG/SA/Scc3. *J. Biol. Chem.*, **279**, 6553-6559.
13. Rollins, R.A., Korom, M., Aulner, N., Martens, A. and Dorsett, D. (2004) *Drosophila* nipped-B protein supports sister chromatid cohesion and opposes the stromalin/Scc3 cohesion factor to facilitate long-range activation of the *cut* gene. *Mol. Cell. Biol.*, **24**, 3100-3111.
14. Horsfield, J.A., Anagnostou, S.H., Hu, J.K., Cho, K.H., Geisler, R., Lieschke, G., Crosier, K.E. and Crosier, P.S. (2007) Cohesin-dependent regulation of Runx genes. *Development*, **134**, 2639-2649.
15. Haering, C.H., Lowe, J., Hochwagen, A. and Nasmyth, K. (2002) Molecular architecture of SMC proteins and the yeast cohesin complex. *Mol. Cell*, **9**, 773-788.
16. Hirano, M., Anderson, D.E., Erickson, H.P. and Hirano, T. (2001) Bimodal activation of SMC ATPase by intra- and inter-molecular interactions. *EMBO J.*, **20**, 3238-3250.
17. Hirano, M. and Hirano, T. (2002) Hinge-mediated dimerization of SMC protein is essential for its dynamic interaction with DNA. *EMBO J.*, **21**, 5733-5744.
18. Kinoshita, E., van der Linden, E., Sanchez, H. and Wyman, C. (2009) RAD50, an SMC family member with multiple roles in DNA break repair: how does ATP affect function? *Chromosome Res.*, **17**, 277-288.
19. Hopfner, K.P., Craig, L., Moncalian, G., Zinkel, R.A., Usui, T., Owen, B.A., Karcher, A., Henderson, B., Bodmer, J.L., McMurray, C.T. *et al.* (2002) The

Rad50 zinc-hook is a structure joining Mre11 complexes in DNA recombination and repair. *Nature*, **418**, 562-566.

20. Melby, T.E., Ciampaglio, C.N., Briscoe, G. and Erickson, H.P. (1998) The symmetrical structure of structural maintenance of chromosomes (SMC) and MukB proteins: long, antiparallel coiled coils, folded at a flexible hinge. *J. Cell Biol.*, **142**, 1595-1604.

21. Anderson, D.E., Losada, A., Erickson, H.P. and Hirano, T. (2002) Condensin and cohesin display different arm conformations with characteristic hinge angles. *J. Cell Biol.*, **156**, 419-424.

22. Haering, C.H., Schoffnegger, D., Nishino, T., Helmhart, W., Nasmyth, K. and Lowe, J. (2004) Structure and stability of cohesin's Smc1-kleisin interaction. *Mol. Cell*, **15**, 951-964.

23. Nasmyth, K. and Haering, C.H. (2005) The structure and function of SMC and kleisin complexes. *Annu. Rev. Biochem.*, **74**, 595-648.

24. Britton, R.A., Lin, D.C. and Grossman, A.D. (1998) Characterization of a prokaryotic SMC protein involved in chromosome partitioning. *Genes Dev.*, **12**, 1254-1259.

25. Graumann, P.L., Losick, R. and Strunnikov, A.V. (1998) Subcellular localization of *Bacillus subtilis* SMC, a protein involved in chromosome condensation and segregation. *J. Bacteriol.*, **180**, 5749-5755.

26. Moriya, S., Tsujikawa, E., Hassan, A.K., Asai, K., Kodama, T. and Ogasawara, N. (1998) A *Bacillus subtilis* gene-encoding protein homologous to eukaryotic SMC motor protein is necessary for chromosome partition. *Mol. Microbiol.*, **29**, 179-187.

27. Mascarenhas, J., Soppa, J., Strunnikov, A.V. and Graumann, P.L. (2002) Cell cycle-dependent localization of two novel prokaryotic chromosome segregation and condensation proteins in *Bacillus subtilis* that interact with SMC protein. *EMBO J.*, **21**, 3108-3118.

28. Soppa, J., Kobayashi, K., Noirot-Gros, M.F., Oesterhelt, D., Ehrlich, S.D., Dervyn, E., Ogasawara, N. and Moriya, S. (2002) Discovery of two novel families of proteins that are proposed to interact with prokaryotic SMC proteins, and characterization of the *Bacillus subtilis* family members ScpA and ScpB. *Mol. Microbiol.*, **45**, 59-71.

29. Volkov, A., Mascarenhas, J., Andrei-Selmer, C., Ulrich, H.D. and Graumann, P.L. (2003) A prokaryotic condensin/cohesin-like complex can actively compact chromosomes from a single position on the nucleoid and binds to DNA as a ring-like structure. *Mol. Cell. Biol.*, **23**, 5638-5650.

30. Mascarenhas, J., Volkov, A.V., Rinn, C., Schiener, J., Guckenberger, R. and Graumann, P.L. (2005) Dynamic assembly, localization and proteolysis of the *Bacillus subtilis* SMC complex. *BMC Cell Biol.*, **6**, 28.

31. Hirano, M. and Hirano, T. (2004) Positive and negative regulation of SMC-DNA interactions by ATP and accessory proteins. *EMBO J.*, **23**, 2664-2673.

32. Niki, H., Jaffe, A., Imamura, R., Ogura, T. and Hiraga, S. (1991) The new gene *mukB* codes for a 177 kd protein with coiled-coil domains involved in chromosome partitioning of *E. coli*. *EMBO J.*, **10**, 183-193.

33. Yamanaka, K., Ogura, T., Niki, H. and Hiraga, S. (1996) Identification of two new genes, *mukE* and *mukF*, involved in chromosome partitioning in *Escherichia coli*. *Mol. Gen. Genet.*, **250**, 241-251.

34. Fennell-Fezzie, R., Gradia, S.D., Akey, D. and Berger, J.M. (2005) The MukF subunit of *Escherichia coli* condensin: architecture and functional relationship to kleisins. *EMBO J.*, **24**, 1921-1930.

35. Matoba, K., Yamazoe, M., Mayanagi, K., Morikawa, K. and Hiraga, S. (2005) Comparison of MukB homodimer versus MukBEF complex molecular architectures by electron microscopy reveals a higher-order multimerization. *Biochem. Biophys. Res. Commun.*, **333**, 694-702.

36. Petrushenko, Z.M., Lai, C.H. and Rybenkov, V.V. (2006) Antagonistic interactions of kleisins and DNA with bacterial Condensin MukB. *J. Biol. Chem.*, **281**, 34208-34217.

37. Yamazoe, M., Onogi, T., Sunako, Y., Niki, H., Yamanaka, K., Ichimura, T. and Hiraga, S. (1999) Complex formation of MukB, MukE and MukF proteins involved in chromosome partitioning in *Escherichia coli. EMBO J.*, **18**, 5873-5884.

38. Palecek, J., Vidot, S., Feng, M., Doherty, A.J. and Lehmann, A.R. (2006) The Smc5-Smc6 DNA repair complex. bridging of the Smc5-Smc6 heads by the KLEISIN, Nse4, and non-Kleisin subunits. *J. Biol. Chem.*, **281**, 36952-36959.

39. Duan, X., Yang, Y., Chen, Y.H., Arenz, J., Rangi, G.K., Zhao, X. and Ye, H. (2009) Architecture of the Smc5/6 Complex of *Saccharomyces cerevisiae* Reveals a Unique Interaction between the Nse5-6 Subcomplex and the Hinge Regions of Smc5 and Smc6. *J. Biol. Chem.*, **284**, 8507-8515.

40. Hirano, T., Kobayashi, R. and Hirano, M. (1997) Condensins, chromosome condensation protein complexes containing XCAP-C, XCAP-E and a *Xenopus* homolog of the *Drosophila* Barren protein. *Cell*, **89**, 511-521.

41. Onn, I., Aono, N., Hirano, M. and Hirano, T. (2007) Reconstitution and subunit geometry of human condensin complexes. *EMBO J.*, **26**, 1024-1034.

42. Schleiffer, A., Kaitna, S., Maurer-Stroh, S., Glotzer, M., Nasmyth, K. and Eisenhaber, F. (2003) Kleisins: a superfamily of bacterial and eukaryotic SMC protein partners. *Mol. Cell*, **11**, 571-575.

43. Strunnikov, A.V., Larionov, V.L. and Koshland, D. (1993) SMC1: an essential yeast gene encoding a putative head-rod-tail protein is required for nuclear division and defines a new ubiquitous protein family. *J. Cell Biol.*, **123**, 1635-1648.

44. Guacci, V., Koshland, D. and Strunnikov, A. (1997) A direct link between sister chromatid cohesion and chromosome condensation revealed through the analysis of MCD1 in *S. cerevisiae. Cell*, **91**, 47-57.

45. Michaelis, C., Ciosk, R. and Nasmyth, K. (1997) Cohesins: chromosomal proteins that prevent premature separation of sister chromatids. *Cell*, **91**, 35-45.

46. Losada, A., Hirano, M. and Hirano, T. (1998) Identification of *Xenopus* SMC protein complexes required for sister chromatid cohesion. *Genes Dev.*, **12**, 1986-1997.

47. Toth, A., Ciosk, R., Uhlmann, F., Galova, M., Schleiffer, A. and Nasmyth, K. (1999) Yeast cohesin complex requires a conserved protein, Eco1p(Ctf7), to establish cohesion between sister chromatids during DNA replication. *Genes Dev.*, **13**, 320-333.

48. Tomonaga, T., Nagao, K., Kawasaki, Y., Furuya, K., Murakami, A., Morishita, J., Yuasa, T., Sutani, T., Kearsey, S.E., Uhlmann, F. *et al.* (2000) Characterization of fission yeast cohesin: essential anaphase proteolysis of Rad21 phosphorylated in the S phase. *Genes Dev.*, **14**, 2757-2770.

49. Losada, A., Yokochi, T., Kobayashi, R. and Hirano, T. (2000) Identification and characterization of SA/Scc3p subunits in the Xenopus and human cohesin complexes. *J. Cell Biol.*, **150**, 405-416.

50. Panizza, S., Tanaka, T., Hochwagen, A., Eisenhaber, F. and Nasmyth, K. (2000) Pds5 cooperates with cohesin in maintaining sister chromatid cohesion. *Curr. Biol.*, **10**, 1557-1564.

51. Sumara, I., Vorlaufer, E., Gieffers, C., Peters, B.H. and Peters, J.M. (2000) Characterization of vertebrate cohesin complexes and their regulation in prophase. *J. Cell Biol.*, **151**, 749-762.

52. Mc Intyre, J., Muller, E.G., Weitzer, S., Snydsman, B.E., Davis, T.N. and Uhlmann, F. (2007) In vivo analysis of cohesin architecture using FRET in the budding yeast *Saccharomyces cerevisiae*. *EMBO J.*, **26**, 3783-3793.

53. Revenkova, E., Eijpe, M., Heyting, C., Gross, B. and Jessberger, R. (2001) Novel meiosis-specific isoform of mammalian SMC1. *Mol. Cell. Biol.*, **21**, 6984-6998.

54. Revenkova, E., Eijpe, M., Heyting, C., Hodges, C.A., Hunt, P.A., Liebe, B., Scherthan, H. and Jessberger, R. (2004) Cohesin SMC1 beta is required for meiotic chromosome dynamics, sister chromatid cohesion and DNA recombination. *Nat. Cell Biol.*, **6**, 555-562.

55. Molnar, M., Bahler, J., Sipiczki, M. and Kohli, J. (1995) The *rec8* gene of *Schizosaccharomyces pombe* is involved in linear element formation, chromosome pairing and sister-chromatid cohesion during meiosis. *Genetics*, **141**, 61-73.

56. Kitajima, T.S., Yokobayashi, S., Yamamoto, M. and Watanabe, Y. (2003) Distinct cohesin complexes organize meiotic chromosome domains. *Science*, **300**, 1152-1155.

57. Klein, F., Mahr, P., Galova, M., Buonomo, S.B., Michaelis, C., Nairz, K. and Nasmyth, K. (1999) A central role for cohesins in sister chromatid cohesion, formation of axial elements, and recombination during yeast meiosis. *Cell*, **98**, 91-103.

58. Parisi, S., McKay, M.J., Molnar, M., Thompson, M.A., van der Spek, P.J., van Drunen-Schoenmaker, E., Kanaar, R., Lehmann, E., Hoeijmakers, J.H. and Kohli, J. (1999) Rec8p, a meiotic recombination and sister chromatid cohesion phosphoprotein of the Rad21p family conserved from fission yeast to humans. *Mol. Cell. Biol.*, **19**, 3515-3528.

59. Prieto, I., Suja, J.A., Pezzi, N., Kremer, L., Martinez, A.C., Rufas, J.S. and Barbero, J.L. (2001) Mammalian STAG3 is a cohesin specific to sister chromatid arms in meiosis I. *Nat. Cell Biol.*, **3**, 761-766.

60. Pasierbek, P., Jantsch, M., Melcher, M., Schleiffer, A., Schweizer, D. and Loidl, J. (2001) A *Caenorhabditis elegans* cohesion protein with functions in meiotic chromosome pairing and disjunction. *Genes Dev.*, **15**, 1349-1360.

61. Saitoh, N., Goldberg, I.G., Wood, E.R. and Earnshaw, W.C. (1994) ScII: an abundant chromosome scaffold protein is a member of a family of putative ATPases with an unusual predicted tertiary structure. *J. Cell Biol.*, **127**, 303-318.

62. Hirano, T. and Mitchison, T.J. (1994) A heterodimeric coiled-coil protein required for mitotic chromosome condensation *in vitro*. *Cell*, **79**, 449-458.

63. Ono, T., Losada, A., Hirano, M., Myers, M.P., Neuwald, A.F. and Hirano, T. (2003) Differential contributions of condensin I and condensin II to mitotic chromosome architecture in vertebrate cells. *Cell*, **115**, 109-121.

64. Kimura, K. and Hirano, T. (2000) Dual roles of the 11S regulatory subcomplex in condensin functions. *Proc. Natl. Acad. Sci. USA*, **97**, 11972-11977.

65. Lehmann, A.R., Walicka, M., Griffiths, D.J., Murray, J.M., Watts, F.Z., McCready, S. and Carr, A.M. (1995) The *rad18* gene of *Schizosaccharomyces pombe* defines a new subgroup of the SMC superfamily involved in DNA repair. *Mol. Cell. Biol.*, **15**, 7067-7080.

66. Fousteri, M.I. and Lehmann, A.R. (2000) A novel SMC protein complex in *Schizosaccharomyces pombe* contains the Rad18 DNA repair protein. *EMBO J.*, **19**, 1691-1702.

67. Taylor, E.M., Moghraby, J.S., Lees, J.H., Smit, B., Moens, P.B. and Lehmann, A.R. (2001) Characterization of a novel human SMC heterodimer homologous to the *Schizosaccharomyces pombe* Rad18/Spr18 complex. *Mol. Biol. Cell*, **12**, 1583-1594.

68. Fujioka, Y., Kimata, Y., Nomaguchi, K., Watanabe, K. and Kohno, K. (2002) Identification of a novel non-structural maintenance of chromosomes (SMC) component of the SMC5-SMC6 complex involved in DNA repair. *J. Biol. Chem.*, **277**, 21585-21591.

69. McDonald, W.H., Pavlova, Y., Yates, J.R., 3rd and Boddy, M.N. (2003) Novel essential DNA repair proteins Nse1 and Nse2 are subunits of the fission yeast Smc5-Smc6 complex. *J. Biol. Chem.*, **278**, 45460-45467.

70. Hazbun, T.R., Malmstrom, L., Anderson, S., Graczyk, B.J., Fox, B., Riffle, M., Sundin, B.A., Aranda, J.D., McDonald, W.H., Chiu, C.H. *et al.* (2003) Assigning function to yeast proteins by integration of technologies. *Mol. Cell*, **12**, 1353-1365.

71. Pebernard, S., McDonald, W.H., Pavlova, Y., Yates, J.R., 3rd and Boddy, M.N. (2004) Nse1, Nse2, and a novel subunit of the Smc5-Smc6 complex, Nse3, play a crucial role in meiosis. *Mol. Biol. Cell*, **15**, 4866-4876.

72. Sergeant, J., Taylor, E., Palecek, J., Fousteri, M., Andrews, E.A., Sweeney, S., Shinagawa, H., Watts, F.Z. and Lehmann, A.R. (2005) Composition and architecture of the *Schizosaccharomyces pombe* Rad18 (Smc5-6) complex. *Mol. Cell. Biol.*, **25**, 172-184.

73. Zhao, X. and Blobel, G. (2005) A SUMO ligase is part of a nuclear multiprotein complex that affects DNA repair and chromosomal organization. *Proc. Natl. Acad. Sci. USA*, **102**, 4777-4782.

74. Pebernard, S., Wohlschlegel, J., McDonald, W.H., Yates, J.R., 3rd and Boddy, M.N. (2006) The Nse5-Nse6 dimer mediates DNA repair roles of the Smc5-Smc6 complex. *Mol. Cell. Biol.*, **26**, 1617-1630.

75. Taylor, E.M., Copsey, A.C., Hudson, J.J., Vidot, S. and Lehmann, A.R. (2008) Identification of the proteins, including MAGEG1, that make up the human SMC5-6 protein complex. *Mol. Cell. Biol.*, **28**, 1197-1206.

76. Pebernard, S., Perry, J.J., Tainer, J.A. and Boddy, M.N. (2008) Nse1 RING-like domain supports functions of the Smc5-Smc6 holocomplex in genome stability. *Mol. Biol. Cell*, **19**, 4099-4109.

77. Andrews, E.A., Palecek, J., Sergeant, J., Taylor, E., Lehmann, A.R. and Watts, F.Z. (2005) Nse2, a component of the Smc5-6 complex, is a SUMO ligase required for the response to DNA damage. *Mol. Cell. Biol.*, **25**, 185-196.

78. Potts, P.R. and Yu, H. (2005) Human MMS21/NSE2 is a SUMO ligase required for DNA repair. *Mol. Cell. Biol.*, **25**, 7021-7032.

79. Lammens, A., Schele, A. and Hopfner, K.P. (2004) Structural biochemistry of ATP-driven dimerization and DNA-stimulated activation of SMC ATPases. *Curr. Biol.*, **14**, 1778-1782.

80. Lowe, J., Cordell, S.C. and van den Ent, F. (2001) Crystal structure of the SMC head domain: an ABC ATPase with 900 residues antiparallel coiled-coil inserted. *J. Mol. Biol.*, **306**, 25-35.

81. Woo, J.S., Lim, J.H., Shin, H.C., Suh, M.K., Ku, B., Lee, K.H., Joo, K., Robinson, H., Lee, J., Park, S.Y. *et al.* (2009) Structural studies of a bacterial condensin complex reveal ATP-dependent disruption of intersubunit interactions. *Cell*, **136**, 85-96.

82. Hopfner, K.P., Karcher, A., Shin, D.S., Craig, L., Arthur, L.M., Carney, J.P. and Tainer, J.A. (2000) Structural biology of Rad50 ATPase: ATP-driven conformational control in DNA double-strand break repair and the ABC-ATPase superfamily. *Cell*, **101**, 789-800.

83. Hung, L.W., Wang, I.X., Nikaido, K., Liu, P.Q., Ames, G.F. and Kim, S.H. (1998) Crystal structure of the ATP-binding subunit of an ABC transporter. *Nature*, **396**, 703-707.

84. Kimura, K. and Hirano, T. (1997) ATP-dependent positive supercoiling of DNA by 13S condensin: a biochemical implication for chromosome condensation. *Cell*, **90**, 625-634.

85. Hirano, T. (1998) SMC protein complexes and higher-order chromosome dynamics. *Curr. Opin. Cell Biol.*, **10**, 317-322.

86. Hirano, M. and Hirano, T. (2006) Opening closed arms: long-distance activation of SMC ATPase by hinge-DNA interactions. *Mol. Cell*, **21**, 175-186.

87. Lengronne, A., McIntyre, J., Katou, Y., Kanoh, Y., Hopfner, K.P., Shirahige, K. and Uhlmann, F. (2006) Establishment of sister chromatid cohesion at the *S. cerevisiae* replication fork. *Mol. Cell*, **23**, 787-799.

88. Arumugam, P., Nishino, T., Haering, C.H., Gruber, S. and Nasmyth, K. (2006) Cohesin's ATPase activity is stimulated by the C-terminal Winged-Helix domain of its kleisin subunit. *Curr. Biol.*, **16**, 1998-2008.

89. Chiu, A., Revenkova, E. and Jessberger, R. (2004) DNA interaction and dimerization of eukaryotic SMC hinge domains. *J. Biol. Chem.*, **279**, 26233-26242.

90. Chen, E.S., Sutani, T. and Yanagida, M. (2004) Cti1/C1D interacts with condensin SMC hinge and supports the DNA repair function of condensin. *Proc. Natl. Acad. Sci. USA*, **101**, 8078-8083.

91. Hirano, M. and Hirano, T. (1998) ATP-dependent aggregation of single-stranded DNA by a bacterial SMC homodimer. *EMBO J.*, **17**, 7139-7148.

92. Yoshimura, S.H., Hizume, K., Murakami, A., Sutani, T., Takeyasu, K. and Yanagida, M. (2002) Condensin architecture and interaction with DNA: regulatory non-SMC subunits bind to the head of SMC heterodimer. *Curr. Biol.*, **12**, 508-513.

93. Ku, B., Lim, J.H., Shin, H.C., Shin, S.Y. and Oh, B.H. (2010) Crystal structure of the MukB hinge domain with coiled-coil stretches and its functional implications. *Proteins: Struct. Funct. Bioinform.*, **78**, 1483-1490.

94. Li, Y., Schoeffler, A.J., Berger, J.M. and Oakley, M.G. (2010) The crystal structure of the hinge domain of the *Escherichia coli* structural maintenance of chromosomes protein MukB. *J. Mol. Biol.*, **395**, 11-19.

95. Dorsett, D. (2007) Roles of the sister chromatid cohesion apparatus in gene expression, development, and human syndromes. *Chromosoma*, **116**, 1-13.

96. Darwiche, N., Freeman, L.A. and Strunnikov, A. (1999) Characterization of the components of the putative mammalian sister chromatid cohesion complex. *Gene*, **233**, 39-47.

97. Ciosk, R., Shirayama, M., Shevchenko, A., Tanaka, T., Toth, A. and Nasmyth, K. (2000) Cohesin's binding to chromosomes depends on a separate complex consisting of Scc2 and Scc4 proteins. *Mol. Cell*, **5**, 243-254.
98. Takahashi, T.S., Yiu, P., Chou, M.F., Gygi, S. and Walter, J.C. (2004) Recruitment of *Xenopus* Scc2 and cohesin to chromatin requires the pre-replication complex. *Nat. Cell Biol.*, **6**, 991-996.
99. Gillespie, P.J. and Hirano, T. (2004) Scc2 couples replication licensing to sister chromatid cohesion in *Xenopus* egg extracts. *Curr. Biol.*, **14**, 1598-1603.
100. Bernard, P., Drogat, J., Maure, J.F., Dheur, S., Vaur, S., Genier, S. and Javerzat, J.P. (2006) A screen for cohesion mutants uncovers Ssl3, the fission yeast counterpart of the cohesin loading factor Scc4. *Curr. Biol.*, **16**, 875-881.
101. Seitan, V.C., Banks, P., Laval, S., Majid, N.A., Dorsett, D., Rana, A., Smith, J., Bateman, A., Krpic, S., Hostert, A. *et al.* (2006) Metazoan Scc4 homologs link sister chromatid cohesion to cell and axon migration guidance. *PLoS Biol.*, **4**, e242.
102. Watrin, E., Schleiffer, A., Tanaka, K., Eisenhaber, F., Nasmyth, K. and Peters, J.M. (2006) Human Scc4 is required for cohesin binding to chromatin, sister-chromatid cohesion, and mitotic progression. *Curr. Biol.*, **16**, 863-874.
103. Uhlmann, F. and Nasmyth, K. (1998) Cohesion between sister chromatids must be established during DNA replication. *Curr. Biol.*, **8**, 1095-1101.
104. Lengronne, A., Katou, Y., Mori, S., Yokobayashi, S., Kelly, G.P., Itoh, T., Watanabe, Y., Shirahige, K. and Uhlmann, F. (2004) Cohesin relocation from sites of chromosomal loading to places of convergent transcription. *Nature*, **430**, 573-578.
105. Blat, Y. and Kleckner, N. (1999) Cohesins bind to preferential sites along yeast chromosome III, with differential regulation along arms versus the centric region. *Cell*, **98**, 249-259.
106. Megee, P.C., Mistrot, C., Guacci, V. and Koshland, D. (1999) The centromeric sister chromatid cohesion site directs Mcd1p binding to adjacent sequences. *Mol. Cell*, **4**, 445-450.
107. Laloraya, S., Guacci, V. and Koshland, D. (2000) Chromosomal addresses of the cohesin component Mcd1p. *J. Cell Biol.*, **151**, 1047-1056.
108. Tanaka, T., Cosma, M.P., Wirth, K. and Nasmyth, K. (1999) Identification of cohesin association sites at centromeres and along chromosome arms. *Cell*, **98**, 847-858.
109. Weber, S.A., Gerton, J.L., Polancic, J.E., DeRisi, J.L., Koshland, D. and Megee, P.C. (2004) The kinetochore is an enhancer of pericentric cohesin binding. *PLoS Biol.*, **2**, E260.
110. Eckert, C.A., Gravdahl, D.J. and Megee, P.C. (2007) The enhancement of pericentromeric cohesin association by conserved kinetochore components promotes high-fidelity chromosome segregation and is sensitive to microtubule-based tension. *Genes Dev.*, **21**, 278-291.
111. Arumugam, P., Gruber, S., Tanaka, K., Haering, C.H., Mechtler, K. and Nasmyth, K. (2003) ATP hydrolysis is required for cohesin's association with chromosomes. *Curr. Biol.*, **13**, 1941-1953.
112. Weitzer, S., Lehane, C. and Uhlmann, F. (2003) A model for ATP hydrolysis-dependent binding of cohesin to DNA. *Curr. Biol.*, **13**, 1930-1940.
113. Heidinger-Pauli, J.M., Onn, I. and Koshland, D. (2010) Genetic Evidence that the Acetylation of the Smc3p Subunit of Cohesin Modulates its ATP-bound State to Promote Cohesion Establishment in *Saccharomyces cerevisiae*. *Genetics*.

114. Skibbens, R.V., Corson, L.B., Koshland, D. and Hieter, P. (1999) Ctf7p is essential for sister chromatid cohesion and links mitotic chromosome structure to the DNA replication machinery. *Genes Dev.*, **13**, 307-319.

115. Rolef Ben-Shahar, T., Heeger, S., Lehane, C., East, P., Flynn, H., Skehel, M. and Uhlmann, F. (2008) Eco1-dependent cohesin acetylation during establishment of sister chromatid cohesion. *Science*, **321**, 563-566.

116. Unal, E., Heidinger-Pauli, J.M., Kim, W., Guacci, V., Onn, I., Gygi, S.P. and Koshland, D.E. (2008) A molecular determinant for the establishment of sister chromatid cohesion. *Science*, **321**, 566-569.

117. Zhang, J., Shi, X., Li, Y., Kim, B.J., Jia, J., Huang, Z., Yang, T., Fu, X., Jung, S.Y., Wang, Y. *et al.* (2008) Acetylation of Smc3 by Eco1 is required for S phase sister chromatid cohesion in both human and yeast. *Mol. Cell*, **31**, 143-151.

118. Rowland, B.D., Roig, M.B., Nishino, T., Kurze, A., Uluocak, P., Mishra, A., Beckouet, F., Underwood, P., Metson, J., Imre, R. *et al.* (2009) Building sister chromatid cohesion: smc3 acetylation counteracts an antiestablishment activity. *Mol. Cell*, **33**, 763-774.

119. Sutani, T., Kawaguchi, T., Kanno, R., Itoh, T. and Shirahige, K. (2009) Budding yeast Wpl1(Rad61)-Pds5 complex counteracts sister chromatid cohesion-establishing reaction. *Curr. Biol.*, **19**, 492-497.

120. Hanna, J.S., Kroll, E.S., Lundblad, V. and Spencer, F.A. (2001) *Saccharomyces cerevisiae* CTF18 and CTF4 are required for sister chromatid cohesion. *Mol. Cell. Biol.*, **21**, 3144-3158.

121. Mayer, M.L., Gygi, S.P., Aebersold, R. and Hieter, P. (2001) Identification of RFC(Ctf18p, Ctf8p, Dcc1p): an alternative RFC complex required for sister chromatid cohesion in *S. cerevisiae*. *Mol. Cell*, **7**, 959-970.

122. Bermudez, V.P., Maniwa, Y., Tappin, I., Ozato, K., Yokomori, K. and Hurwitz, J. (2003) The alternative Ctf18-Dcc1-Ctf8-replication factor C complex required for sister chromatid cohesion loads proliferating cell nuclear antigen onto DNA. *Proc. Natl. Acad. Sci. USA*, **100**, 10237-10242.

123. Sumara, I., Vorlaufer, E., Stukenberg, P.T., Kelm, O., Redemann, N., Nigg, E.A. and Peters, J.M. (2002) The dissociation of cohesin from chromosomes in prophase is regulated by Polo-like kinase. *Mol. Cell*, **9**, 515-525.

124. Losada, A., Hirano, M. and Hirano, T. (2002) Cohesin release is required for sister chromatid resolution, but not for condensin-mediated compaction, at the onset of mitosis. *Genes Dev.*, **16**, 3004-3016.

125. Hauf, S., Roitinger, E., Koch, B., Dittrich, C.M., Mechtler, K. and Peters, J.M. (2005) Dissociation of cohesin from chromosome arms and loss of arm cohesion during early mitosis depends on phosphorylation of SA2. *PLoS Biol.*, **3**, e69.

126. Hirota, T., Gerlich, D., Koch, B., Ellenberg, J. and Peters, J.M. (2004) Distinct functions of condensin I and II in mitotic chromosome assembly. *J. Cell Sci.*, **117**, 6435-6445.

127. Gandhi, R., Gillespie, P.J. and Hirano, T. (2006) Human Wapl is a cohesin-binding protein that promotes sister-chromatid resolution in mitotic prophase. *Curr. Biol.*, **16**, 2406-2417.

128. Kueng, S., Hegemann, B., Peters, B.H., Lipp, J.J., Schleiffer, A., Mechtler, K. and Peters, J.M. (2006) Wapl controls the dynamic association of cohesin with chromatin. *Cell*, **127**, 955-967.

129. Salic, A., Waters, J.C. and Mitchison, T.J. (2004) Vertebrate shugoshin links sister centromere cohesion and kinetochore microtubule stability in mitosis. *Cell*, **118**, 567-578.

130. Kitajima, T.S., Hauf, S., Ohsugi, M., Yamamoto, T. and Watanabe, Y. (2005) Human Bub1 defines the persistent cohesion site along the mitotic chromosome by affecting Shugoshin localization. *Curr. Biol.*, **15**, 353-359.

131. McGuinness, B.E., Hirota, T., Kudo, N.R., Peters, J.M. and Nasmyth, K. (2005) Shugoshin prevents dissociation of cohesin from centromeres during mitosis in vertebrate cells. *PLoS Biol.*, **3**, e86.

132. Kitajima, T.S., Sakuno, T., Ishiguro, K., Iemura, S., Natsume, T., Kawashima, S.A. and Watanabe, Y. (2006) Shugoshin collaborates with protein phosphatase 2A to protect cohesin. *Nature*, **441**, 46-52.

133. Tang, Z., Shu, H., Qi, W., Mahmood, N.A., Mumby, M.C. and Yu, H. (2006) PP2A is required for centromeric localization of Sgo1 and proper chromosome segregation. *Dev. Cell*, **10**, 575-585.

134. Rivera, T. and Losada, A. (2009) Shugoshin regulates cohesion by driving relocalization of PP2A in Xenopus extracts. *Chromosoma*, **118**, 223-233.

135. Kawashima, S.A., Tsukahara, T., Langegger, M., Hauf, S., Kitajima, T.S. and Watanabe, Y. (2007) Shugoshin enables tension-generating attachment of kinetochores by loading Aurora to centromeres. *Genes Dev.*, **21**, 420-435.

136. Jager, H., Herzig, A., Lehner, C.F. and Heidmann, S. (2001) *Drosophila* separase is required for sister chromatid separation and binds to PIM and THR. *Genes Dev.*, **15**, 2572-2584.

137. Kudo, N.R., Wassmann, K., Anger, M., Schuh, M., Wirth, K.G., Xu, H., Helmhart, W., Kudo, H., McKay, M., Maro, B. *et al.* (2006) Resolution of chiasmata in oocytes requires separase-mediated proteolysis. *Cell*, **126**, 135-146.

138. Kumada, K., Yao, R., Kawaguchi, T., Karasawa, M., Hoshikawa, Y., Ichikawa, K., Sugitani, Y., Imoto, I., Inazawa, J., Sugawara, M. *et al.* (2006) The selective continued linkage of centromeres from mitosis to interphase in the absence of mammalian separase. *J. Cell Biol.*, **172**, 835-846.

139. Liu, Z. and Makaroff, C.A. (2006) *Arabidopsis* separase AESP is essential for embryo development and the release of cohesin during meiosis. *Plant Cell*, **18**, 1213-1225.

140. Siomos, M.F., Badrinath, A., Pasierbek, P., Livingstone, D., White, J., Glotzer, M. and Nasmyth, K. (2001) Separase is required for chromosome segregation during meiosis I in *Caenorhabditis elegans*. *Curr. Biol.*, **11**, 1825-1835.

141. Wirth, K.G., Wutz, G., Kudo, N.R., Desdouets, C., Zetterberg, A., Taghybeeglu, S., Seznec, J., Ducos, G.M., Ricci, R., Firnberg, N. *et al.* (2006) Separase: a universal trigger for sister chromatid disjunction but not chromosome cycle progression. *J. Cell Biol.*, **172**, 847-860.

142. Hauf, S., Waizenegger, I.C. and Peters, J.M. (2001) Cohesin cleavage by separase required for anaphase and cytokinesis in human cells. *Science*, **293**, 1320-1323.

143. Uhlmann, F., Lottspeich, F. and Nasmyth, K. (1999) Sister-chromatid separation at anaphase onset is promoted by cleavage of the cohesin subunit Scc1. *Nature*, **400**, 37-42.

144. Uhlmann, F., Wernic, D., Poupart, M.A., Koonin, E.V. and Nasmyth, K. (2000) Cleavage of cohesin by the CD clan protease separin triggers anaphase in yeast. *Cell*, **103**, 375-386.

145. Cohen-Fix, O., Peters, J.M., Kirschner, M.W. and Koshland, D. (1996) Anaphase initiation in *Saccharomyces cerevisiae* is controlled by the APC-dependent degradation of the anaphase inhibitor Pds1p. *Genes Dev.*, **10**, 3081-3093.

146. Funabiki, H., Yamano, H., Kumada, K., Nagao, K., Hunt, T. and Yanagida, M. (1996) Cut2 proteolysis required for sister-chromatid seperation in fission yeast. *Nature*, **381**, 438-441.

147. Funabiki, H., Kumada, K. and Yanagida, M. (1996) Fission yeast Cut1 and Cut2 are essential for sister chromatid separation, concentrate along the metaphase spindle and form large complexes. *EMBO J.*, **15**, 6617-6628.

148. Ciosk, R., Zachariae, W., Michaelis, C., Shevchenko, A., Mann, M. and Nasmyth, K. (1998) An ESP1/PDS1 complex regulates loss of sister chromatid cohesion at the metaphase to anaphase transition in yeast. *Cell*, **93**, 1067-1076.

149. Kumada, K., Nakamura, T., Nagao, K., Funabiki, H., Nakagawa, T. and Yanagida, M. (1998) Cut1 is loaded onto the spindle by binding to Cut2 and promotes anaphase spindle movement upon Cut2 proteolysis. *Curr. Biol.*, **8**, 633-641.

150. Gorr, I.H., Boos, D. and Stemmann, O. (2005) Mutual inhibition of separase and Cdk1 by two-step complex formation. *Mol. Cell*, **19**, 135-141.

151. Stemmann, O., Zou, H., Gerber, S.A., Gygi, S.P. and Kirschner, M.W. (2001) Dual inhibition of sister chromatid separation at metaphase. *Cell*, **107**, 715-726.

152. Musacchio, A. and Salmon, E.D. (2007) The spindle-assembly checkpoint in space and time. *Nat. Rev. Mol. Cell Biol.*, **8**, 379-393.

153. Nasmyth, K. (2005) How do so few control so many? *Cell*, **120**, 739-746.

154. Irniger, S., Piatti, S., Michaelis, C. and Nasmyth, K. (1995) Genes involved in sister chromatid separation are needed for B-type cyclin proteolysis in budding yeast. *Cell*, **81**, 269-278.

155. Yamamoto, A., Guacci, V. and Koshland, D. (1996) Pds1p, an inhibitor of anaphase in budding yeast, plays a critical role in the APC and checkpoint pathway(s). *J. Cell Biol.*, **133**, 99-110.

156. Waizenegger, I.C., Hauf, S., Meinke, A. and Peters, J.M. (2000) Two distinct pathways remove mammalian cohesin from chromosome arms in prophase and from centromeres in anaphase. *Cell*, **103**, 399-410.

157. Sun, Y., Kucej, M., Fan, H.Y., Yu, H., Sun, Q.Y. and Zou, H. (2009) Separase is recruited to mitotic chromosomes to dissolve sister chromatid cohesion in a DNA-dependent manner. *Cell*, **137**, 123-132.

158. Alexandru, G., Uhlmann, F., Mechtler, K., Poupart, M.A. and Nasmyth, K. (2001) Phosphorylation of the cohesin subunit Scc1 by Polo/Cdc5 kinase regulates sister chromatid separation in yeast. *Cell*, **105**, 459-472.

159. Hornig, N.C. and Uhlmann, F. (2004) Preferential cleavage of chromatin-bound cohesin after targeted phosphorylation by Polo-like kinase. *EMBO J.*, **23**, 3144-3153.

160. Goldstein, L.S. (1980) Mechanisms of chromosome orientation revealed by two meiotic mutants in *Drosophila melanogaster*. *Chromosoma*, **78**, 79-111.

161. Kerrebrock, A.W., Moore, D.P., Wu, J.S. and Orr-Weaver, T.L. (1995) Mei-S332, a *Drosophila* protein required for sister-chromatid cohesion, can localize to meiotic centromere regions. *Cell*, **83**, 247-256.

162. Kitajima, T.S., Kawashima, S.A. and Watanabe, Y. (2004) The conserved kinetochore protein shugoshin protects centromeric cohesion during meiosis. *Nature*, **427**, 510-517.

163. Marston, A.L., Tham, W.H., Shah, H. and Amon, A. (2004) A genome-wide screen identifies genes required for centromeric cohesion. *Science*, **303**, 1367-1370.

164. Rabitsch, K.P., Gregan, J., Schleiffer, A., Javerzat, J.P., Eisenhaber, F. and Nasmyth, K. (2004) Two fission yeast homologs of *Drosophila* Mei-S332 are required for chromosome segregation during meiosis I and II. *Curr. Biol.*, **14**, 287-301.

165. Llano, E., Gomez, R., Gutierrez-Caballero, C., Herran, Y., Sanchez-Martin, M., Vazquez-Quinones, L., Hernandez, T., de Alava, E., Cuadrado, A., Barbero, J.L. *et al.* (2008) Shugoshin-2 is essential for the completion of meiosis but not for mitotic cell division in mice. *Genes Dev.*, **22**, 2400-2413.

166. Buonomo, S.B., Clyne, R.K., Fuchs, J., Loidl, J., Uhlmann, F. and Nasmyth, K. (2000) Disjunction of homologous chromosomes in meiosis I depends on proteolytic cleavage of the meiotic cohesin Rec8 by separin. *Cell*, **103**, 387-398.

167. Kitajima, T.S., Miyazaki, Y., Yamamoto, M. and Watanabe, Y. (2003) Rec8 cleavage by separase is required for meiotic nuclear divisions in fission yeast. *EMBO J.*, **22**, 5643-5653.

168. Terret, M.E., Wassmann, K., Waizenegger, I., Maro, B., Peters, J.M. and Verlhac, M.H. (2003) The meiosis I-to-meiosis II transition in mouse oocytes requires separase activity. *Curr. Biol.*, **13**, 1797-1802.

169. Kudo, N.R., Anger, M., Peters, A.H., Stemmann, O., Theussl, H.C., Helmhart, W., Kudo, H., Heyting, C. and Nasmyth, K. (2009) Role of cleavage by separase of the Rec8 kleisin subunit of cohesin during mammalian meiosis I. *J. Cell Sci.*, **122**, 2686-2698.

170. Brar, G.A., Kiburz, B.M., Zhang, Y., Kim, J.E., White, F. and Amon, A. (2006) Rec8 phosphorylation and recombination promote the step-wise loss of cohesins in meiosis. *Nature*, **441**, 532-536.

171. Riedel, C.G., Katis, V.L., Katou, Y., Mori, S., Itoh, T., Helmhart, W., Galova, M., Petronczki, M., Gregan, J., Cetin, B. *et al.* (2006) Protein phosphatase 2A protects centromeric sister chromatid cohesion during meiosis I. *Nature*, **441**, 53-61.

172. Gruber, S., Haering, C.H. and Nasmyth, K. (2003) Chromosomal cohesin forms a ring. *Cell*, **112**, 765-777.

173. Ivanov, D. and Nasmyth, K. (2005) A topological interaction between cohesin rings and a circular minichromosome. *Cell*, **122**, 849-860.

174. Birkenbihl, R.P. and Subramani, S. (1992) Cloning and characterization of *rad21* an essential gene of *Schizosaccharomyces pombe* involved in DNA double-strand-break repair. *Nucleic Acids Res.*, **20**, 6605-6611.

175. Sjogren, C. and Nasmyth, K. (2001) Sister chromatid cohesion is required for postreplicative double-strand break repair in *Saccharomyces cerevisiae*. *Curr. Biol.*, **11**, 991-995.

176. Kim, J.S., Krasieva, T.B., LaMorte, V., Taylor, A.M. and Yokomori, K. (2002) Specific recruitment of human cohesin to laser-induced DNA damage. *J. Biol. Chem.*, **277**, 45149-45153.

177. Kim, S.T., Xu, B. and Kastan, M.B. (2002) Involvement of the cohesin protein, Smc1, in Atm-dependent and independent responses to DNA damage. *Genes Dev.*, **16**, 560-570.

178. Cortes-Ledesma, F. and Aguilera, A. (2006) Double-strand breaks arising by replication through a nick are repaired by cohesin-dependent sister-chromatid exchange. *EMBO Rep.*, **7**, 919-926.

179. van Heemst, D., James, F., Poggeler, S., Berteaux-Lecellier, V. and Zickler, D. (1999) Spo76p is a conserved chromosome morphogenesis protein that links the mitotic and meiotic programs. *Cell*, **98**, 261-271.

180. Ellermeier, C. and Smith, G.R. (2005) Cohesins are required for meiotic DNA breakage and recombination in *Schizosaccharomyces pombe*. *Proc. Natl. Acad. Sci. USA*, **102**, 10952-10957.

181. Strom, L., Lindroos, H.B., Shirahige, K. and Sjogren, C. (2004) Postreplicative recruitment of cohesin to double-strand breaks is required for DNA repair. *Mol. Cell*, **16**, 1003-1015.

182. Unal, E., Arbel-Eden, A., Sattler, U., Shroff, R., Lichten, M., Haber, J.E. and Koshland, D. (2004) DNA damage response pathway uses histone modification to assemble a double-strand break-specific cohesin domain. *Mol. Cell*, **16**, 991-1002.

183. Hartlerode, A.J. and Scully, R. (2009) Mechanisms of double-strand break repair in somatic mammalian cells. *Biochem. J.*, **423**, 157-168.

184. Strom, L., Karlsson, C., Lindroos, H.B., Wedahl, S., Katou, Y., Shirahige, K. and Sjogren, C. (2007) Postreplicative formation of cohesion is required for repair and induced by a single DNA break. *Science*, **317**, 242-245.

185. Unal, E., Heidinger-Pauli, J.M. and Koshland, D. (2007) DNA double-strand breaks trigger genome-wide sister-chromatid cohesion through Eco1 (Ctf7). *Science*, **317**, 245-248.

186. Heidinger-Pauli, J.M., Unal, E., Guacci, V. and Koshland, D. (2008) The kleisin subunit of cohesin dictates damage-induced cohesion. *Mol. Cell*, **31**, 47-56.

187. Heidinger-Pauli, J.M., Unal, E. and Koshland, D. (2009) Distinct targets of the Eco1 acetyltransferase modulate cohesion in S phase and in response to DNA damage. *Mol. Cell*, **34**, 311-321.

188. Saka, Y., Sutani, T., Yamashita, Y., Saitoh, S., Takeuchi, M., Nakaseko, Y. and Yanagida, M. (1994) Fission yeast cut3 and cut14, members of a ubiquitous protein family, are required for chromosome condensation and segregation in mitosis. *EMBO J.*, **13**, 4938-4952.

189. Strunnikov, A.V., Hogan, E. and Koshland, D. (1995) SMC2, a *Saccharomyces cerevisiae* gene essential for chromosome segregation and condensation, defines a subgroup within the SMC family. *Genes Dev.*, **9**, 587-599.

190. Bhat, M.A., Philp, A.V., Glover, D.M. and Bellen, H.J. (1996) Chromatid segregation at anaphase requires the *barren* product, a novel chromosome-associated protein that interacts with Topoisomerase II. *Cell*, **87**, 1103-1114.

191. Hagstrom, K.A., Holmes, V.F., Cozzarelli, N.R. and Meyer, B.J. (2002) *C. elegans* condensin promotes mitotic chromosome architecture, centromere organization, and sister chromatid segregation during mitosis and meiosis. *Genes Dev.*, **16**, 729-742.

192. Hudson, D.F., Vagnarelli, P., Gassmann, R. and Earnshaw, W.C. (2003) Condensin is required for nonhistone protein assembly and structural integrity of vertebrate mitotic chromosomes. *Dev. Cell*, **5**, 323-336.

193. Vagnarelli, P., Hudson, D.F., Ribeiro, S.A., Trinkle-Mulcahy, L., Spence, J.M., Lai, F., Farr, C.J., Lamond, A.I. and Earnshaw, W.C. (2006) Condensin and Repo-Man-PP1 co-operate in the regulation of chromosome architecture during mitosis. *Nat. Cell Biol.*, **8**, 1133-1142.

194. Gerlich, D., Hirota, T., Koch, B., Peters, J.M. and Ellenberg, J. (2006) Condensin I stabilizes chromosomes mechanically through a dynamic interaction in live cells. *Curr. Biol.*, **16**, 333-344.

195. Hudson, D.F., Ohta, S., Freisinger, T., Macisaac, F., Sennels, L., Alves, F., Lai, F., Kerr, A., Rappsilber, J. and Earnshaw, W.C. (2008) Molecular and genetic analysis of condensin function in vertebrate cells. *Mol. Biol. Cell*, **19**, 3070-3079.

196. Oliveira, R.A., Coelho, P.A. and Sunkel, C.E. (2005) The condensin I subunit Barren/CAP-H is essential for the structural integrity of centromeric heterochromatin during mitosis. *Mol. Cell. Biol.*, **25**, 8971-8984.

197. Ribeiro, S.A., Gatlin, J.C., Dong, Y., Joglekar, A., Cameron, L., Hudson, D.F., Farr, C.J., McEwen, B.F., Salmon, E.D., Earnshaw, W.C. *et al.* (2009) Condensin regulates the stiffness of vertebrate centromeres. *Mol. Biol. Cell*, **20**, 2371-2380.

198. Gruber, S. and Errington, J. (2009) Recruitment of condensin to replication origin regions by ParB/SpoOJ promotes chromosome segregation in B. subtilis. *Cell*, **137**, 685-696.

199. Sullivan, N.L., Marquis, K.A. and Rudner, D.Z. (2009) Recruitment of SMC by ParB-parS organizes the origin region and promotes efficient chromosome segregation. *Cell*, **137**, 697-707.

200. Ono, T., Fang, Y., Spector, D.L. and Hirano, T. (2004) Spatial and temporal regulation of Condensins I and II in mitotic chromosome assembly in human cells. *Mol. Biol. Cell*, **15**, 3296-3308.

201. Oliveira, R.A., Heidmann, S. and Sunkel, C.E. (2007) Condensin I binds chromatin early in prophase and displays a highly dynamic association with *Drosophila* mitotic chromosomes. *Chromosoma*, **116**, 259-274.

202. Eide, T., Carlson, C., Tasken, K.A., Hirano, T., Tasken, K. and Collas, P. (2002) Distinct but overlapping domains of AKAP95 are implicated in chromosome condensation and condensin targeting. *EMBO Rep.*, **3**, 426-432.

203. Longworth, M.S., Herr, A., Ji, J.Y. and Dyson, N.J. (2008) RBF1 promotes chromatin condensation through a conserved interaction with the Condensin II protein dCAP-D3. *Genes Dev.*, **22**, 1011-1024.

204. Lipp, J.J., Hirota, T., Poser, I. and Peters, J.M. (2007) Aurora B controls the association of condensin I but not condensin II with mitotic chromosomes. *J. Cell Sci.*, **120**, 1245-1255.

205. Wang, B.D., Eyre, D., Basrai, M., Lichten, M. and Strunnikov, A. (2005) Condensin binding at distinct and specific chromosomal sites in the *Saccharomyces cerevisiae* genome. *Mol. Cell. Biol.*, **25**, 7216-7225.

206. D'Ambrosio, C., Schmidt, C.K., Katou, Y., Kelly, G., Itoh, T., Shirahige, K. and Uhlmann, F. (2008) Identification of cis-acting sites for condensin loading onto budding yeast chromosomes. *Genes Dev.*, **22**, 2215-2227.

207. Gerlich, D., Koch, B., Dupeux, F., Peters, J.M. and Ellenberg, J. (2006) Live-cell imaging reveals a stable cohesin-chromatin interaction after but not before DNA replication. *Curr. Biol.*, **16**, 1571-1578.

208. Stray, J.E. and Lindsley, J.E. (2003) Biochemical analysis of the yeast condensin Smc2/4 complex: an ATPase that promotes knotting of circular DNA. *J. Biol. Chem.*, **278**, 26238-26248.

209. Takemoto, A., Kimura, K., Yanagisawa, J., Yokoyama, S. and Hanaoka, F. (2006) Negative regulation of condensin I by CK2-mediated phosphorylation. *EMBO J.*, **25**, 5339-5348.

210. Kimura, K., Cuvier, O. and Hirano, T. (2001) Chromosome condensation by a human condensin complex in *Xenopus* egg extracts. *J. Biol. Chem.*, **276**, 5417-5420.

211. Kimura, K., Hirano, M., Kobayashi, R. and Hirano, T. (1998) Phosphorylation and activation of 13S condensin by Cdc2 in vitro. *Science*, **282**, 487-490.

212. Yeong, F.M., Hombauer, H., Wendt, K.S., Hirota, T., Mudrak, I., Mechtler, K., Loregger, T., Marchler-Bauer, A., Tanaka, K., Peters, J.M. *et al.* (2003) Identification of a subunit of a novel Kleisin-beta/SMC complex as a potential substrate of protein phosphatase 2A. *Curr. Biol.*, **13**, 2058-2064.

213. Wang, Q., Mordukhova, E.A., Edwards, A.L. and Rybenkov, V.V. (2006) Chromosome condensation in the absence of the non-SMC subunits of MukBEF. *J. Bacteriol.*, **188**, 4431-4441.

214. She, W., Wang, Q., Mordukhova, E.A. and Rybenkov, V.V. (2007) MukEF Is required for stable association of MukB with the chromosome. *J. Bacteriol.*, **189**, 7062-7068.

215. Cui, Y., Petrushenko, Z.M. and Rybenkov, V.V. (2008) MukB acts as a macromolecular clamp in DNA condensation. *Nat. Struct. Mol. Biol.*, **15**, 411-418.

216. Kimura, K., Rybenkov, V.V., Crisona, N.J., Hirano, T. and Cozzarelli, N.R. (1999) 13S condensin actively reconfigures DNA by introducing global positive writhe: implications for chromosome condensation. *Cell*, **98**, 239-248.

217. Bazett-Jones, D.P., Kimura, K. and Hirano, T. (2002) Efficient supercoiling of DNA by a single condensin complex as revealed by electron spectroscopic imaging. *Mol. Cell*, **9**, 1183-1190.

218. Stray, J.E., Crisona, N.J., Belotserkovskii, B.P., Lindsley, J.E. and Cozzarelli, N.R. (2005) The *Saccharomyces cerevisiae* Smc2/4 condensin compacts DNA into (+) chiral structures without net supercoiling. *J. Biol. Chem.*, **280**, 34723-34734.

219. Strick, T.R., Kawaguchi, T. and Hirano, T. (2004) Real-time detection of single-molecule DNA compaction by condensin I. *Curr. Biol.*, **14**, 874-880.

220. Petrushenko, Z.M., Lai, C.H., Rai, R. and Rybenkov, V.V. (2006) DNA reshaping by MukB. Right-handed knotting, left-handed supercoiling. *J. Biol. Chem.*, **281**, 4606-4615.

221. Chen, N., Zinchenko, A.A., Yoshikawa, Y., Araki, S., Adachi, S., Yamazoe, M., Hiraga, S. and Yoshikawa, K. (2008) ATP-induced shrinkage of DNA with MukB protein and the MukBEF complex of *Escherichia coli*. *J. Bacteriol.*, **190**, 3731-3737.

222. Sawitzke, J.A. and Austin, S. (2000) Suppression of chromosome segregation defects of *Escherichia coli muk* mutants by mutations in topoisomerase I. *Proc. Natl. Acad. Sci. USA*, **97**, 1671-1676.

223. Lindow, J.C., Britton, R.A. and Grossman, A.D. (2002) Structural maintenance of chromosomes protein of *Bacillus subtilis* affects supercoiling *in vivo*. *J. Bacteriol.*, **184**, 5317-5322.

224. Tadesse, S., Mascarenhas, J., Kosters, B., Hasilik, A. and Graumann, P.L. (2005) Genetic interaction of the SMC complex with topoisomerase IV in *Bacillus subtilis*. *Microbiology*, **151**, 3729-3737.

225. Aono, N., Sutani, T., Tomonaga, T., Mochida, S. and Yanagida, M. (2002) Cnd2 has dual roles in mitotic condensation and interphase. *Nature*, **417**, 197-202.

226. Heale, J.T., Ball, A.R., Jr., Schmiesing, J.A., Kim, J.S., Kong, X., Zhou, S., Hudson, D.F., Earnshaw, W.C. and Yokomori, K. (2006) Condensin I interacts with the PARP-1-XRCC1 complex and functions in DNA single-strand break repair. *Mol. Cell*, **21**, 837-848.

227. Caldecott, K.W. (2008) Single-strand break repair and genetic disease. *Nat. Rev. Genet.*, **9**, 619-631.

228. Prakash, L. and Prakash, S. (1977) Isolation and characterization of MMS-sensitive mutants of *Saccharomyces cerevisiae*. *Genetics*, **86**, 33-55.

229. Prakash, S. and Prakash, L. (1977) Increased spontaneous mitotic segregation in MMS-sensitive mutants of *Saccharomyces cerevisiae*. *Genetics*, **87**, 229-236.

230. Verkade, H.M., Bugg, S.J., Lindsay, H.D., Carr, A.M. and O'Connell, M.J. (1999) Rad18 is required for DNA repair and checkpoint responses in fission yeast. *Mol. Biol. Cell*, **10**, 2905-2918.

231. Hu, B., Liao, C., Millson, S.H., Mollapour, M., Prodromou, C., Pearl, L.H., Piper, P.W. and Panaretou, B. (2005) Qri2/Nse4, a component of the essential Smc5/6 DNA repair complex. *Mol. Microbiol.*, **55**, 1735-1750.

232. Onoda, F., Takeda, M., Seki, M., Maeda, D., Tajima, J., Ui, A., Yagi, H. and Enomoto, T. (2004) SMC6 is required for MMS-induced interchromosomal and sister chromatid recombinations in *Saccharomyces cerevisiae*. *DNA Repair*, **3**, 429-439.

233. Ampatzidou, E., Irmisch, A., O'Connell, M.J. and Murray, J.M. (2006) Smc5/6 is required for repair at collapsed replication forks. *Mol. Cell. Biol.*, **26**, 9387-9401.

234. Harvey, S.H., Sheedy, D.M., Cuddihy, A.R. and O'Connell, M.J. (2004) Coordination of DNA damage responses via the Smc5/Smc6 complex. *Mol. Cell. Biol.*, **24**, 662-674.

235. Montelone, B.A. and Koelliker, K.J. (1995) Interactions among mutations affecting spontaneous mutation, mitotic recombination, and DNA repair in yeast. *Curr. Genet.*, **27**, 102-109.

236. Morikawa, H., Morishita, T., Kawane, S., Iwasaki, H., Carr, A.M. and Shinagawa, H. (2004) Rad62 protein functionally and physically associates with the smc5/smc6 protein complex and is required for chromosome integrity and recombination repair in fission yeast. *Mol. Cell. Biol.*, **24**, 9401-9413.

237. Torres-Rosell, J., Machin, F., Farmer, S., Jarmuz, A., Eydmann, T., Dalgaard, J.Z. and Aragon, L. (2005) SMC5 and SMC6 genes are required for the segregation of repetitive chromosome regions. *Nat. Cell Biol.*, **7**, 412-419.

238. Branzei, D., Sollier, J., Liberi, G., Zhao, X., Maeda, D., Seki, M., Enomoto, T., Ohta, K. and Foiani, M. (2006) Ubc9- and mms21-mediated sumoylation counteracts recombinogenic events at damaged replication forks. *Cell*, **127**, 509-522.

239. Lindroos, H.B., Strom, L., Itoh, T., Katou, Y., Shirahige, K. and Sjogren, C. (2006) Chromosomal association of the Smc5/6 complex reveals that it functions in differently regulated pathways. *Mol. Cell*, **22**, 755-767.

240. Tsuyama, T., Inou, K., Seki, M., Seki, T., Kumata, Y., Kobayashi, T., Kimura, K., Hanaoka, F., Enomoto, T. and Tada, S. (2006) Chromatin loading of Smc5/6 is induced by DNA replication but not by DNA double-strand breaks. *Biochem. Biophys. Res. Commun.*, **351**, 935-939.

241. Torres-Rosell, J., De Piccoli, G., Cordon-Preciado, V., Farmer, S., Jarmuz, A., Machin, F., Pasero, P., Lisby, M., Haber, J.E. and Aragon, L. (2007) Anaphase onset before complete DNA replication with intact checkpoint responses. *Science*, **315**, 1411-1415.

242. De Piccoli, G., Cortes-Ledesma, F., Ira, G., Torres-Rosell, J., Uhle, S., Farmer, S., Hwang, J.Y., Machin, F., Ceschia, A., McAleenan, A. *et al.* (2006) Smc5-Smc6 mediate DNA double-strand-break repair by promoting sister-chromatid recombination. *Nat. Cell Biol.*, **8**, 1032-1034.

243. Potts, P.R., Porteus, M.H. and Yu, H. (2006) Human SMC5/6 complex promotes sister chromatid homologous recombination by recruiting the SMC1/3 cohesin complex to double-strand breaks. *EMBO J.*, **25**, 3377-3388.

244. Potts, P.R. and Yu, H. (2007) The SMC5/6 complex maintains telomere length in ALT cancer cells through SUMOylation of telomere-binding proteins. *Nat. Struct. Mol. Biol.*, **14**, 581-590.

245. Chavez, A., George, V., Agrawal, V. and Johnson, F.B. (2010) Sumoylation and the structural maintenance of chromosomes (Smc) 5/6 complex slow senescence through recombination intermediate resolution. *J. Biol. Chem.*, **285**, 11922-11930.

246. Gruber, S., Arumugam, P., Katou, Y., Kuglitsch, D., Helmhart, W., Shirahige, K. and Nasmyth, K. (2006) Evidence that loading of cohesin onto chromosomes involves opening of its SMC hinge. *Cell*, **127**, 523-537.

247. Shintomi, K. and Hirano, T. (2007) How are cohesin rings opened and closed? *Trends Biochem. Sci.*, **32**, 154-157.

248. Sambrook, J. and Russell, D.W. (2001) *Molecular Cloning: A Laboratory Manual.* 3rd ed. Cold Spring Harbor Laboratory Press, New York.

249. Corpet, F. (1988) Multiple sequence alignment with hierarchical clustering. *Nucleic Acids Res.*, **16**, 10881-10890.

250. Larkin, M.A., Blackshields, G., Brown, N.P., Chenna, R., McGettigan, P.A., McWilliam, H., Valentin, F., Wallace, I.M., Wilm, A., Lopez, R. *et al.* (2007) Clustal W and Clustal X version 2.0. *Bioinformatics*, **23**, 2947-2948.

251. Lupas, A., Van Dyke, M. and Stock, J. (1991) Predicting coiled coils from protein sequences. *Science*, **252**, 1162-1164.

252. Bryson, K., McGuffin, L.J., Marsden, R.L., Ward, J.J., Sodhi, J.S. and Jones, D.T. (2005) Protein structure prediction servers at University College London. *Nucleic Acids Res.*, **33**, W36-38.

253. Jones, D.T. (1999) Protein secondary structure prediction based on position-specific scoring matrices. *J. Mol. Biol.*, **292**, 195-202.

254. Bates, P.A. and Sternberg, M.J. (1999) Model building by comparison at CASP3: using expert knowledge and computer automation. *Proteins*, **Suppl 3**, 47-54.

255. Bates, P.A., Kelley, L.A., MacCallum, R.M. and Sternberg, M.J. (2001) Enhancement of protein modeling by human intervention in applying the automatic programs 3D-JIGSAW and 3D-PSSM. *Proteins*, **Suppl 5**, 39-46.

256. Contreras-Moreira, B. and Bates, P.A. (2002) Domain fishing: a first step in protein comparative modelling. *Bioinformatics*, **18**, 1141-1142.

257. Kibbe, W.A. (2007) OligoCalc: an online oligonucleotide properties calculator. *Nucleic Acids Res.*, **35**, W43-46.

258. Hanahan, D. (1983) Studies on transformation of Escherichia coli with plasmids. *J. Mol. Biol.*, **166**, 557-580.

259. Bertani, G. (1951) Studies on lysogenesis. I. The mode of phage liberation by lysogenic Escherichia coli. *J. Bacteriol.*, **62**, 293-300.

260. LeMaster, D.M. and Richards, F.M. (1985) 1H-15N heteronuclear NMR studies of *Escherichia coli* thioredoxin in samples isotopically labeled by residue type. *Biochemistry*, **24**, 7263-7268.

261. Gasteiger, E., Hoogland, C., Gattiker, A., Duvaud, S., Wilkins, M.R., Appel, R.D. and Bairoch, A. (2005) In Walker, J. M. (ed.), *The Proteomics Protocols Handbook*. Humana Press, pp. 571-607.

262. Laemmli, U.K. (1970) Cleavage of structural proteins during the assembly of the head of bacteriophage T4. *Nature*, **227**, 680-685.

263. Drenth, J. (2007) *Principles of protein X-ray crystallography*. 3rd ed. Springer-Verlag, New York.

264. Giacovazzo, C., Monaco, H.L., Artioli, G., Viterbo, D., Ferraris, G., Gilli, G., Zanotti, G. and Catti, M. (2002) *Fundamentals of Crystallography*. Oxford University Press, Oxford.

265. Putnam, C.D., Hammel, M., Hura, G.L. and Tainer, J.A. (2007) X-ray solution scattering (SAXS) combined with crystallography and computation: defining accurate macromolecular structures, conformations and assemblies in solution. *Q. Rev. Biophys.*, **40**, 191-285.

266. Rhodes, G. (2006) *Crystallography made crystal clear*. 3rd ed. Academic Press, San Diego.

267. Leslie, A.G.W. (1992) Recent changes to the MOSFLM package for processing film and image plate data. *Joint CCP4 + ESF-EAMCB Newsletter on Protein Crystallography*, **26**.

268. Kabsch, W. (1993) Automatic processing of rotation diffraction data from crystals of initially unknown symmetry and cell constants. *J. Appl. Crystallogr.*, **26**, 795-800.

269. Vonrhein, C., Blanc, E., Roversi, P. and Bricogne, G. (2007) Automated structure solution with autoSHARP. *Methods Mol. Biol.*, **364**, 215-230.

270. Emsley, P., Lohkamp, B., Scott, W.G. and Cowtan, K. (2010) Features and development of Coot. *Acta Cryst. D*, **66**, 486-501.

271. Collaborative Computational Project, N. (1994) The CCP4 suite: programs for protein crystallography. *Acta Cryst. D*, **50**, 760-763.

272. McCoy, A.J., Grosse-Kunstleve, R.W., Storoni, L.C. and Read, R.J. (2005) Likelihood-enhanced fast translation functions. *Acta Cryst. D*, **61**, 458-464.

273. Brunger, A.T., Adams, P.D., Clore, G.M., DeLano, W.L., Gros, P., Grosse-Kunstleve, R.W., Jiang, J.S., Kuszewski, J., Nilges, M., Pannu, N.S. *et al.* (1998) Crystallography & NMR system: a new software suite for macromolecular structure determination. *Acta Cryst. D*, **54**, 905-921.

274. Afonine, P.V., Grosse-Kunstleve, R.W., Adams, P.D. (2005) The Phenix refinement framework. *CCP4 Newsletter*, **42**, contribution 8.

275. Davis, I.W., Leaver-Fay, A., Chen, V.B., Block, J.N., Kapral, G.J., Wang, X., Murray, L.W., Arendall, W.B., 3rd, Snoeyink, J., Richardson, J.S. *et al.* (2007) MolProbity: all-atom contacts and structure validation for proteins and nucleic acids. *Nucleic Acids Res.*, **35**, W375-383.

276. Lovell, S.C., Davis, I.W., Adrendall, W.B., de Bakker, P.I.W., Word, J.M., Prisant, M.G., Richardson, J.S. and Richardson, D.C. (2003) Structure validation by C alpha geometry: phi, psi and C beta deviation. *Proteins: Struct. Funct. Genet.*, **50**, 437-450.

277. Laskowski, R.A., Macarthur, M.W., Moss, D.S. and Thornton, J.M. (1993) Procheck - a program to check the stereochemical quality of protein structures. *J. Appl. Crystallogr.*, **26**, 283-291.

278. Baker, N.A., Sept, D., Joseph, S., Holst, M.J. and McCammon, J.A. (2001) Electrostatics of nanosystems: application to microtubules and the ribosome. *Proc. Natl. Acad. Sci. USA*, **98**, 10037-10041.

279. DeLano, W.L., DeLano Scientific LLC, Palo Alto, CA, USA. (2008).

280. Murshudov, G.N., Vagin, A.A. and Dodson, E.J. (1997) Refinement of macromolecular structures by the maximum-likelihood method. *Acta Cryst. D*, **53**, 240-255.

281. Perrakis, A., Morris, R. and Lamzin, V.S. (1999) Automated protein model building combined with iterative structure refinement. *Nat. Struct. Biol.*, **6**, 458-463.

282. Konarev, P.V., Petoukhov, M.V., Volkov, V.V. and Svergun, D.I. (2006) ATSAS 2.1, a program package for small-angle scattering data analysis. *J. Appl. Crystallogr.*, **39**, 277-286.

283. Konarev, P.V., Volkov, V.V., Sokolova, A.V., Koch, M.H.J. and Svergun, D.I. (2003) PRIMUS: a Windows PC-based system for small-angle scattering data analysis. *J. Appl. Crystallogr.*, **36**, 1277-1282.

284. Svergun, D.I. (1992) Determination of the Regularization Parameter in Indirect-Transform Methods Using Perceptual Criteria. *J. Appl. Crystallogr.*, **25**, 495-503.

285. Svergun, D., Barberato, C. and Koch, M.H.J. (1995) CRYSOL - A program to evaluate x-ray solution scattering of biological macromolecules from atomic coordinates. *J. Appl. Crystallogr.*, **28**, 768-773.

286. Svergun, D.I., Petoukhov, M.V. and Koch, M.H. (2001) Determination of domain structure of proteins from X-ray solution scattering. *Biophys. J.*, **80**, 2946-2953.

287. Kozin, M.B. and Svergun, D.I. (2001) Automated matching of high- and low-resolution structural models. *J. Appl. Crystallogr.*, **34**, 33-41.

288. Volkov, V.V. and Svergun, D.I. (2003) Uniqueness of *ab initio* shape determination in small-angle scattering. *J. Appl. Crystallogr.*, **36**, 860-864.

289. Wriggers, W., Milligan, R.A. and McCammon, J.A. (1999) Situs: a package for docking crystal structures into low-resolution maps from electron microscopy. *J. Struct. Biol.*, **125**, 185-195.

290. Wriggers, W. and Chacon, P. (2001) Using Situs for the registration of protein structures with low-resolution bead models from X-ray solution scattering. *J. Appl. Crystallogr.*, **34**, 773-776.

291. Bond, C.S. (2003) TopDraw: a sketchpad for protein structure topology cartoons. *Bioinformatics*, **19**, 311-312.

292. Walter, T.S., Meier, C., Assenberg, R., Au, K.F., Ren, J., Verma, A., Nettleship, J.E., Owens, R.J., Stuart, D.I. and Grimes, J.M. (2006) Lysine methylation as a routine rescue strategy for protein crystallization. *Structure*, **14**, 1617-1622.

293. Cobbe, N. and Heck, M.M. (2004) The evolution of SMC proteins: phylogenetic analysis and structural implications. *Mol. Biol. Evol.*, **21**, 332-347.

294. Lukat, P., Hoffmann, M. and Einsle, O. (2008) Crystal packing of the c(6)-type cytochrome OmcF from *Geobacter sulfurreducens* is mediated by an N-terminal Strep-tag II. *Acta Cryst. D*, **64**, 919-926.

295. Overman, L.B., Bujalowski, W. and Lohman, T.M. (1988) Equilibrium binding of *Escherichia coli* single-strand binding protein to single-stranded nucleic acids in the (SSB)65 binding mode. Cation and anion effects and polynucleotide specificity. *Biochemistry*, **27**, 456-471.

296. Erdemir, T., Bilican, B., Cagatay, T., Goding, C.R. and Yavuzer, U. (2002) *Saccharomyces cerevisiae* C1D is implicated in both non-homologous DNA end joining and homologous recombination. *Mol. Microbiol.*, **46**, 947-957.

297. Yavuzer, U., Smith, G.C., Bliss, T., Werner, D. and Jackson, S.P. (1998) DNA end-independent activation of DNA-PK mediated via association with the DNA-binding protein C1D. *Genes Dev.*, **12**, 2188-2199.

298. Mishra, A., Hu, B., Kurze, A., Beckouet, F., Farcas, A.M., Dixon, S.E., Katou, Y., Khalid, S., Shirahige, K. and Nasmyth, K. (2010) Both interaction surfaces within

cohesin's hinge domain are essential for its stable chromosomal association. *Curr. Biol.*, **20**, 279-289.

299.   Dong, X., Stothard, P., Forsythe, I.J. and Wishart, D.S. (2004) PlasMapper: a web server for drawing and auto-annotating plasmid maps. *Nucleic Acids Res.*, **32**, W660-664.

7   APPENDIX

7.1   The Bicistronic Vector for Heterodimeric Expression Constructs
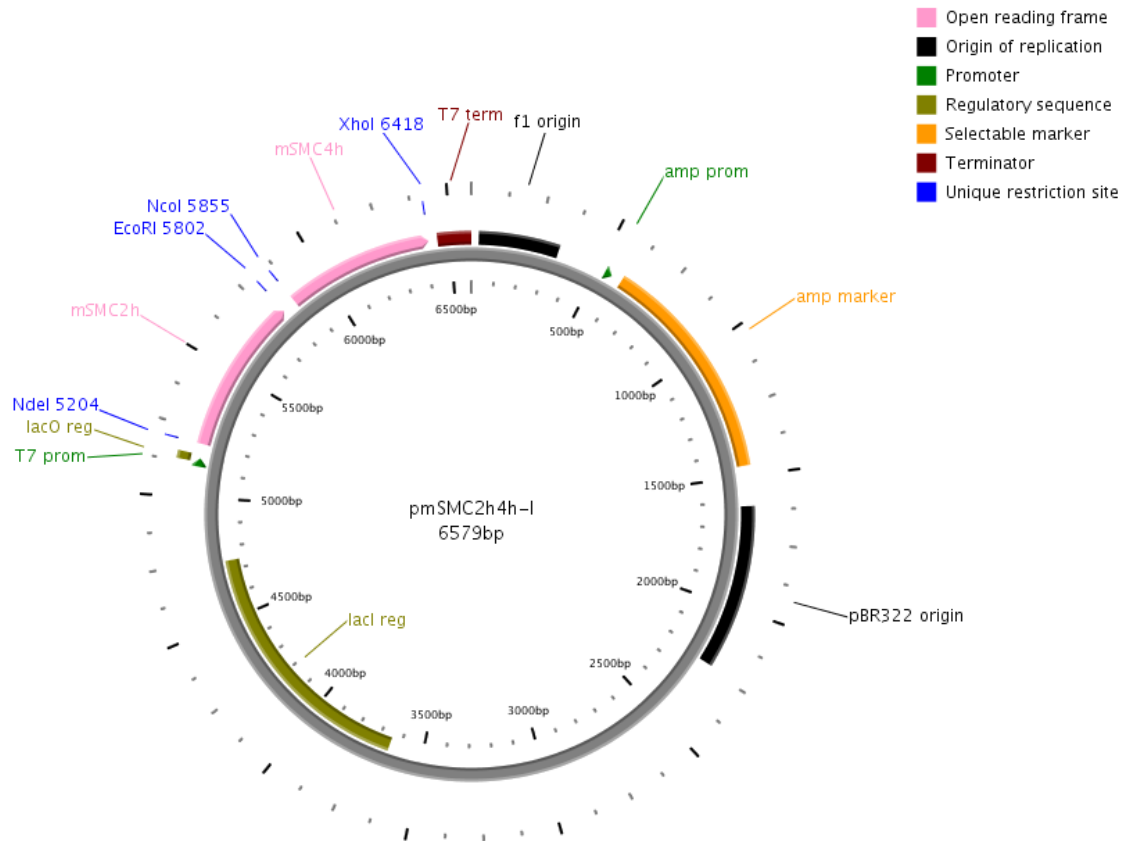
Figure 7.1. Map of the modified bicistronic pET-21b vector containing the construct mSMC2h4h-l. Only the restriction sites used for cloning are shown. The map was generated with PlasMapper (299).

```
NdeI    NheI         EcoRI SacI    SalI                                    RBS
CATATGGCTAGCgene1GAATTCGAGCTCCGTCGACAATAATTTTGTTTAACTTTAAGAAGGAGATATA

 NcoI        NotI     XhoI        His6        STOP
CCATGGgene2GCGGCCGCACTCGAGCACCACCACCACCACCACTGA
```

Figure 7.2. Multiple cloning site of the modified bicistronic pET-21b vector. The vector was generated by inserting a second ribosome binding site between the SalI and NotI sites of pET-21b (Novagen).

7.2 Amino Acid Sequences and Physico-Chemical Parameters of Proteins

Table 7.1. Amino acid sequences of protein constructs used in this study. The sequences of affinity tags are printed in bold letters.

Name	Amino acid sequence
PfuSMC hinge	MELESSERELIAAEAQREVRGNRAAEELKRSGIGGIYGTLAELIKVKDEAYALAIEVALG NRADNVVVEDELVAEKAIKYLKEHKLGRLTFLPLNKIKPKHVDSSVGLPAVDVIEYDQKI ENAVKFALGDTVIVNSMEEARPHIGKVRMVTIEGELYERSGAITGGHFRARGLAVDTTKL R**LEHHHHHH**
mSMC2h-l	**MWSHPQFEK**LKGKHEALLAKFPNLQFAYKDPEKNWNRNSVKGLVASLINVKDNSTATALE VVAGERLYNVVVDTEVTAKKLLEKGELKRRYTIIPLNKISARCIAPETLRVAQNLVGPDN VHVALSLVDYKPELQKGMEFVFGTTFVCNNMDNAKKVAFDKRIMTRTVTLGGDVFDPHGT LSGGARSQAASILTKFQE
mSMC4h-l	MVEEAKSSLAMNRSRGKVLDAIIQEKKSGRIPGIYGRLGDLGAIDEKYDIAISSCCHALD YIVVDSIDTAQECVNFLKKHNIGIATFIGLDKMTVWAKKMSKIQTPENTPRLFDLVKVKN EEIRQAFYFALRDTLVANNLDQATRVAYQRDRRWRVVTLQGQIIEQSGTMSGGGSKVMRG RMGSSVI**LEHHHHHH**
mSMC2h-s	MLQFAYKDPEKNWNRNSVKGLVASLINVKDNSTATALEVVAGERLYNVVVDTEVTAKKLL EKGELKRRYTIIPLNKISARCIAPETLRVAQNLVGPDNVHVALSLVDYKPELQKGMEFVF GTTFVCNNMDNAKKVAFDKRIMTRTVTLGGDVFDPHGTLSGG
mSMC4h-s	MGKVLDAIIQEKKSGRIPGIYGRLGDLGAIDEKYDIAISSCCHALDYIVVDSIDTAQECV NFLKKHNIGIATFIGLDKMTVWAKKMSKIQTPENTPRLFDLVKVKNEEIRQAFYFALRDT LVANNLDQATRVAYQRDRRWRVVTLQGQIIEQSGTMSGG**LEHHHHHH**

Table 7.2. Physico-chemical parameters of protein constructs used in this study, as determined by ProtParam (261).

Name	Residues of full length protein	Affinity tag	Molecular weight (Da)	Number of residues	Theoretical isoelectric point	Calculated extinction coefficient at 280 nm (M^{-1}cm^{-1})
PfuSMC hinge	488-667	C-His$_6$	20 986.0	189	6.21	7450
mSMC2h4h-l			43 984.6	393	9.34	35 410
mSMC2h-l	492-680	N-Strep II	22 032.4	198	9.39	16 960
mSMC4h-l	581-766	C-His$_6$	21 952.2	195	9.28	18 450
mSMC2h4h-s			36 858.4	329	8.75	29 910
mSMC2h-s	506-666		17 912.7	162	9.08	11 460
mSMC4h-s	595-752	C-His$_6$	18 945.7	167	8.42	18 450

7.3 Abbreviations

aa	amino acid
ABC	ATP-binding cassette
ADP	adenosine diphosphate
AKAP95	A kinase-anchoring protein 95
APC	anaphase-promoting complex
APE1	apurinic-apyrimidinic endonuclease 1
APS	ammonium persulfate
ARM	Armadillo (repeat)
ATM	ataxia telangiectasia mutated
ATP	adenosine triphosphate
BER	base-excision repair
Bsu	*Bacillus subtilis*
CAP	chromosome-associated protein
Cdc	cell-division cycle
Cdk	cyclin-dependent kinase
Chk	checkpoint kinase
CK2	casein kinase 2
CPS	counts per second
Ctf	chromosome transmission fidelity
C-WHD	C-terminal winged-helix domain
DLS	dynamic light scattering
DNA	deoxyribonucleic acid
DSB	DNA double-strand break
dsDNA	double-stranded DNA
DTT	dithiothreitol
Eco	establishment of cohesion
EDTA	ethylenediaminetetraacetic acid
EMSA	electrophoretic mobility shift assay
6-FAM	6-carboxyfluorescein
FEN1	flap endonuclease 1
FRET	Förster resonance energy transfer

HEAT	Huntingtin, elongation factor 3, the A subunit of protein phosphatase 2A, TOR lipid kinase
HPSF	high purity salt free
HR	homologous recombination
IPTG	isopropyl ®-D-1-thiogalactopyranoside
LB	lysogeny broth
MAD	multiple-wavelength anomalous dispersion
Mad2	mitotic arrest-deficient
MAGE	melanoma-antigen encoding gene
Mre11	meiotic recombination 11
MRN	Mre11-Rad50-Nbs1
m(SMC)	mouse (SMC)
Muk	from Japanese *mukaku*, meaning "anucleate"
Nbs	Nijmegen breakage syndrome
NEBD	nuclear envelope breakdown
Nse	non-SMC element
OD_{600}	optical density at 600 nm
ORF	open reading frame
PAGE	polyacrylamide gel electrophoresis
PARP1	poly(ADP-ribose) polymerase 1
PBS	phosphate buffered saline
PCNA	proliferating cell nuclear antigen
PCR	polymerase chain reaction
PDB	protein data bank
Pds	precocious dissociation of sisters
PEG	polyethylene glycol
Pfu	*Pyrococcus furiosus*
Plk1	Polo-like kinase 1
PP2A	protein phosphatase 2A
Rad	radiation sensitive
Rbf1	RPG-box-binding factor 1
rDNA	ribosomal DNA
Rec	recombination

RFC	replication factor C
RING	really interesting new gene
rms	root mean square
RPA	replication protein A
RP-HPLC	reversed phase high performance liquid chromatography
SAD	single-wavelength anomalous dispersion
SAXS	small-angle X-ray Scattering
Sc	*Saccharomyces cerevisiae*
Scc	sister chromatid cohesion (protein)
Scp	segregation and condensation protein
SDS	sodium dodecyl sulfate
SLS	Swiss Light Source
SMC	Structural Maintenance of Chromosomes
SSB	DNA single-strand break
ssDNA	single-stranded DNA
SUMO	small ubiquitin-like modifier
TB	Tris-borate
TCEP	tris(2-carboxyethyl)phosphine
TEMED	*N,N,N′,N′*-tetramethylethylenediamine
TfB	transformation buffer
TFIIIC	transcription factor IIIC
Tma	*Thermotoga maritima*
Tris	tris(hydroxymethyl)aminomethane
Wapl	wings apart-like
WHD	winged-helix domain
wt	wild-type
XRCC1	X-ray repair cross-complementing protein 1

8 CURRICULUM VITAE

Personal details

Name	Julia Johanna Griese
Date of birth	March 1, 1982
Place of birth	Erbach im Odenwald, Germany
Nationality	German
Marital status	single

Education

1988 – 1992	Grundschule in Vielbrunn, Germany
1992 – 2001	Gymnasium in Michelstadt, Germany
09/1997 – 02/1998	Poway High School, Poway, California, USA

Academic Training

2001 – 2005	Studies of Biochemistry (Diploma) at the University of Bayreuth, Germany
06/2005 – 12/2005	Diploma thesis in the group of Dr. Holger Dobbek, Department of Biochemistry, University of Bayreuth, Germany
03/2006 – 02/2007	Research assistant in the group of Prof. Dr. Ilme Schlichting, Department of Biomolecular Mechanisms, Max Planck Institute for Medical Research, Heidelberg, Germany
since 03/2007	PhD thesis in the group of Prof. Dr. Karl-Peter Hopfner, Gene Center, Department of Biochemistry, University of Munich, Germany
01/2007 – 10/2009	PhD fellowship of the Boehringer Ingelheim Fonds

9 ACKNOWLEDGEMENTS

I would like to thank all the people who have contributed to this work in one way or another.

First of all, I want to thank Karl-Peter Hopfner for taking me in, for allowing me the freedom to develop my own ideas, and for helping me see things more positively than I tend to.

I want to thank all the members of the Happy Hopfners, past and present, for everything I learned from them, for all the little things they helped me out with, for all the cakes, and for making this lab a good place to work in. In particular I would like to thank:

Gregor Witte for teaching me (almost) everything I now know about fluorescence, SAXS, and Äktas, and most of all for all the long discussions about my work that helped me find the right way to continue;

Alfred Lammens for introducing me to the project, Katja and Alfred Lammens for showing me how to solve crystal structures, and Sophia Hartung for showing me how to deal with SAXS data;

Matthew Bennett for teaching me a lot about crystallography and showing me all the cool tricks in PyMOL, and of course for all the proofreading;

Alexandra Schele for keeping the lab running and always helping me out with whatever I happened to need;

and my practical and bachelor students Florian Priller and Nils Kulak for their good work.

I would like to thank Frank Uhlmann and the members of his lab, especially Chris Lehane, for taking me in for a while and showing me how to work with yeast. I also want to thank Frank for the interest he showed in my work and all the helpful discussions.

I can't thank the Boehringer Ingelheim Fonds enough for their generous support – not only for all the money they spent on me, but also for all the great workshops (not to mention the parties), and the opportunity to meet so many interesting people, and most of all for supporting my decision to change labs and start again from scratch. I especially want to thank Hermann Fröhlich and Monika Beutelspacher for their wise and caring support, and for making BIF feel like a big family. I am grateful to have known you.

Nicht zuletzt möchte ich meinen Eltern für ihre immerwährende Unterstützung danken, und vor allem dafür, daß sie nie an mir gezweifelt und selbst meine Entscheidung aufzugeben und von vorne anzufangen nie in Frage gestellt haben.

Lastly, I want to thank Matt for his love and support and for making me see reason whenever I had lost sight of it.